

University of Louisville

ThinkIR: The University of Louisville's Institutional Repository

Electronic Theses and Dissertations

5-2019

Glycine receptor expression across identified retinal ganglion cell types.

Ian Scot Pyle
University of Louisville

Follow this and additional works at: <https://ir.library.louisville.edu/etd>



Part of the [Medicine and Health Sciences Commons](#), [Molecular and Cellular Neuroscience Commons](#), [Molecular Biology Commons](#), and the [Other Neuroscience and Neurobiology Commons](#)

Recommended Citation

Pyle, Ian Scot, "Glycine receptor expression across identified retinal ganglion cell types." (2019). *Electronic Theses and Dissertations*. Paper 3187.
<https://doi.org/10.18297/etd/3187>

This Doctoral Dissertation is brought to you for free and open access by ThinkIR: The University of Louisville's Institutional Repository. It has been accepted for inclusion in Electronic Theses and Dissertations by an authorized administrator of ThinkIR: The University of Louisville's Institutional Repository. This title appears here courtesy of the author, who has retained all other copyrights. For more information, please contact thinkir@louisville.edu.

GLYCINE RECEPTOR EXPRESSION ACROSS IDENTIFIED
RETINAL GANGLION CELL TYPES

By

Ian Scot Pyle

B.A., Hanover College (Hanover, IN), 2008

M.S., University of Louisville (Louisville, KY), 2013

M.S., University of Louisville (Louisville, KY), 2016

A Dissertation

Submitted to the Faculty of the
School of Medicine of the University of Louisville
in Partial Fulfillment of the Requirements
for the Degree of

Doctor of Philosophy

in Anatomical Sciences and Neurobiology

Department of Anatomical Sciences and Neurobiology
University of Louisville School of Medicine
Louisville, KY

May 2019

Copyright 2019 by Ian Scot Pyle

All rights reserved

GLYCINE RECEPTOR EXPRESSION ACROSS IDENTIFIED
RETINAL GANGLION CELL TYPES

By

Ian Scot Pyle

B.A., Hanover College (Hanover, IN), 2008

M.S., University of Louisville (Louisville, KY), 2013

M.S., University of Louisville (Louisville, KY), 2016

A Dissertation Approved on

April 9, 2019

by the following Dissertation Committee:

Maureen McCall, Ph.D.

Bart Borghuis, Ph.D.

Ron Gregg, Ph.D.

William Guido, Ph.D.

Jeffrey Petruska, Ph.D.

DEDICATION

I dedicate this dissertation to my two lovely daughters Ella and Lilia and to my beautiful wife Miki whose unconditional love and fervent support was my reprieve during this time in my life.

ACKNOWLEDGMENTS

Foremost, I thank my mentor, Dr. Maureen McCall. She is the epitome of work ethic; a passionate and professional scientist whose wisdom and attention to detail is consistent while she leads by example and demonstrates the most diligent work hours among her students and colleagues. Intentionally or unintentionally, Maureen constantly pushed me to think harder, work smarter, be more skeptical, and trust my data. Also, my research and success were only possible with help from: Drs. Gobinda Pangen, Chi Zhang, James Fransen, Katie Fransen, Jennifer Noel, Archana Jalligampala, Aaron Rising, Nazarul Hasan, Sean Masterson, Rui Ji and Ms. Madeline Mitchell and Ms. Maha Jabbar. Furthermore, I thank my committee members, Drs. Bart Borghuis, Ron Gregg, Bill Guido, and Jeffrey Petruska.

I thank my parents for their love and support. I would not be successful today if it weren't for their philosophy of raising a lifelong learner and assert independence. They were gracious in providing me with exceptional educational opportunities both in the classroom and via traveling the world. Finally, I thank my beautiful, loving and gracious wife, Miki. The journey of graduate school is challenging, arduous, time-consuming, and outright brutal. Miki supported me during this time with unconditional love while simultaneously raising our two daughters Ella and Lilia, a feat unsurpassed by any human. Ultimately, both of us accomplished this journey together, and I will forever be in her gratitude.

ABSTRACT

GLYCINE RECEPTOR EXPRESSION ACROSS IDENTIFIED
RETINAL GANGLION CELL TYPES

Ian Scot Pyle

April 9, 2019

Retinal ganglion cells (RGCs) represent the culmination of all retinal signaling and their output forms the substrate for vision throughout the rest of the brain. About 40 different RGC types have been defined by differences in their visually evoked responses, morphology, and genetic makeup. These responses arise from interactions between inhibition and excitation throughout the retinal circuit (Franke et al., 2017; Masland, 2012; Sanes & Masland, 2015; Werblin, 2011). Unlike most other areas of the central nervous system (CNS), the retina utilizes both GABA and glycine inhibitory neurotransmitters to refine glutamatergic excitatory signals (Franke & Baden, 2017; Werblin, 2011; C. Zhang, Nobles, & McCall, 2015). Glycine receptors (GlyRs) are heteromers composed of a single β subunit and one of four α subunits, with a stoichiometry of $3\beta:2\alpha$ (Grudzinska et al., 2005; Heinze, Harvey, Haverkamp, & Wässle, 2007; Lynch, 2004). All four GlyR α subunits ($\alpha1$, $\alpha2$, $\alpha3$, or $\alpha4$) are differentially expressed in the retina and subunit specific expression has been defined for bipolar, some amacrine cells and

RGCs (Haverkamp, Muller, Zeilhofer, Harvey, & Wassle, 2004; Heinze et al., 2007). The roles for GlyR α subunit specific inhibition are unknown, although glycinergic input is generally linked to temporal response tuning (Murphy & Rieke, 2006; Nobles, Zhang, Muller, Betz, & McCall, 2012; van Wyk, Wassle, & Taylor, 2009; Wassle et al., 2009; Werblin, 2010). We have surveyed GlyR α subunit expression in a variety of identified RGC types, using GlyR α knockout mice and an rAAV-mediated RNAi to knockdown GlyR α subunit specific expression. We find that the four α RGCs only express GlyR α 1. All of the other RGCs we studied express at least two GlyR α subunits. In some RGCs, the GlyR kinetics are similar, whereas in others the kinetics differs. We propose that this diversity will contribute to the richness of retinal inhibitory processing.

TABLE OF CONTENTS

ABSTRACT	v
LIST OF FIGURES	ix
LIST OF TABLES	xi
CHAPTER I	1
INTRODUCTION	1
1.1 The Visual system.....	1
1.2 The Retina	2
1.3 Photoreceptors.....	4
1.4 Photoisomerization.....	5
1.5 Bipolar Cells.....	6
1.6 Horizontal Cells	8
1.7 Amacrine Cells.....	8
1.8 Inhibitory Circuits	9
1.9 Retinal Ganglion Cells.....	12
1.10 Neurotransmission	13
1.11 Synaptic Release	14
1.12 Inhibitory Receptors in the Retina	16
1.13 Glycine Receptors.....	17
1.14 Glycine Receptor Kinetics	19
1.15 Differential Expression of GlyR α Subunits in the IPL of the retina	22
II. SPECIFIC AIMS	24
Aim 1 – Identify Glycinergic Expression on a Subset of Retinal Ganglion Cells.....	25
Aim 2 - Examine the GlyR α Expression of ooDS RGCs using an rAAV- <i>Gira4</i> shRNA.....	26
CHAPTER II	27
EXPERIMENTAL MATERIALS AND METHODS	27
2.1 Animals	27

2.2 Viral Vector Construction and Packaging.....	29
2.3 rAAV injection into Major Optic Nerve Targets of the Brain.....	32
2.4 Tissue Dissection and Preparation	33
2.5 Electrophysiology Recording of Retinal Ganglion Cells	34
2.6 Pharmacological Manipulations of sIPSCs.....	35
2.7 Light Stimulation	35
2.8 Immunohistochemistry	36
2.9 Electrophysiology Recording Analysis	38
CHAPTER III	40
EXPRESSION OF DISTINCT GLYCINE RECEPTOR SUBUNITS IS FOUND ACROSS IDENTIFIED RETINAL GANGLION CELL TYPES.....	40
INTRODUCTION.....	40
MATERIALS AND METHODS	43
RESULTS.....	52
DISCUSSION.....	86
CHAPTER IV	92
GLYCINE RECEPTOR SUBUNIT EXPRESSION IN MOUSE RETINAL ON-OFF DIRECTION SELECTIVE GANGLION CELLS	92
INTRODUCTION.....	92
MATERIALS AND METHODS	94
RESULTS.....	103
DISCUSSION.....	116
CHAPTER V	122
DISCUSSION	122
I. GENERAL DISCUSSION.....	122
II. FURTHER DIRECTIONS	126
REFERENCES	129
CURRICULUM VITAE	138

LIST OF FIGURES

FIGURE	PAGE
1.1 Schematic of the retina	3
1.2 Absorbance Spectrum of trivariant color vision from three different cones	5
1.3 Schematic Representations of Different Forms of Inhibition.	11
1.4 Schematics of glycine receptors	18
1.5 Representative examples of an IPSC waveform demonstrating both rise time and τ_{decay}	22
1.6 Representative confocal images of transverse wild type sections stained for glycine receptor subunit expression (green) across the IPL.	23
2.1. <i>Gla4</i> _{KD-D} chosen among four different shRNA candidates.....	31
3.1. WT big soma RGC Glycinergic sIPSCs are fast and mediated by GlyR α 1..	53
3.2. Big Soma GCs Express GlyR α 1	55
3.3. AAV- <i>Gla1</i> -shRNA knocks down GlyR α 1 expression in alpha RGCs.....	57
3.4. GlyR α 1 puncta expression is knocked down in AAV- <i>Gla1</i> -shRNA infected ON α , ON τ , and OFF δ RGCs	59
3.5. W3 RGCs appear to have GlyR α 3-mediated sIPSCs.....	61
3.6. AAV-mediated RNAi to <i>Gla1</i> eliminates GlyR α 1 sIPSC activity; <i>Gla3</i> ^{-/-} eliminates GlyR α 3 sIPSC activity, in W3 RGCs	65
3.7. W3 GCs do not express GlyR α 1 and GlyR α 3 puncta.....	67
3.8. F-mini RGCs appear to have GlyR α 3-mediated sIPSCs	69
3.9. <i>Gla2</i> ^{-/-} / <i>Gla3</i> ^{-/-} eliminates glycinergic sIPSC activity in F-mini RGCs.	72
3.10. F-mini GCs Express GlyR α 2 and GlyR α 3.....	74
3.11. J-RGCs appear to have GlyR α 2 or GlyR α 4-mediated sIPSCs	76
3.12. <i>Gla2</i> ^{-/-} / <i>Gla4</i> ^{-/-} eliminates glycinergic sIPSC activity in J-RGCs	79
3.13. ON SAC glycinergic sIPSCs are slow and mediated by either GlyR α 2 or GlyR α 4	81
3.14. ON SAC glycinergic sIPSCs are slow and mediated by GlyR α 2.	83

3.15. ON SACs Express GlyR α 2 and GlyR α 4 puncta.	85
4.1. Schematic diagram of plasmid delivered via AAV, used to change the expression of GlyR α 4 in ooDS GCs.	96
4.2. WT ooDS GC Glycinergic sIPSCs are Slow and are Likely Mediated by GlyR α 4.	105
4.3. ooDS RGCs Express GlyR α 4 Puncta.	106
4.4. ooDS GCs express both GlyR α 2 and GlyR α 4.	109
4.5. AAV- <i>Glr4</i> _{KD} -shRNA reduces the frequency of glycinergic sIPSCs in ooDS GCs	114
Supplemental Figure 1. No difference observed among W3 RGC sIPSC characteristics.	137

LIST OF TABLES

TABLE	PAGE
1.1 (τ_{decay} of GlyR α subtypes).....	21
2.1 List of Animal Lines Used for Experiments	28
2.2 List of Antibodies Used for Immunohistochemistry Experiments	37
3.1 List of Animal Lines and their Labeled Cells Used for Experiments.....	44
3.2 Primary and Secondary Antibodies used for Immunohistochemistry	47
4.1 Primary and Secondary Antibodies used for Immunohistochemistry	101

CHAPTER I

INTRODUCTION

1.1 The Visual system

Critical to an organism's proliferation and survival is its ability to interact with its environment. More than 500 million years ago, organisms developed rudimentary photoreceptors to convert energy (light) into information to understand their surroundings and improve survival outcome. Throughout evolution, the mammalian visual system became a complex arrangement of neurons and developed the ability to filter and interpret an ever-changing visual scene. This process of filtering and interpreting occurs in neural tissue in the eye, called the retina, and happens rapidly, on the order of tens of milliseconds. In the initial stages of processing, a diverse array of circuits segregate information into distinct channels even before transmission to the brain. The parsing of information makes the visual system more efficient at transmitting signals and interpreting the visual scene. The retina utilizes complex interactions between inhibitory and excitatory neurons that are specialized within their particular circuit to create these channels. Excitatory neurons typically release neurotransmitter onto post-synaptic cells which bind to excitatory receptors allowing an influx of sodium or potassium ions to depolarize the post-synaptic cell membrane

Conversely, inhibitory neurons typically release neurotransmitters, which bind to inhibitory receptors on post-synaptic cells allowing an influx of chloride ions into the cell. These ions hyperpolarize the membrane and reduce the probability of an action potential or help modulate excitatory output. Our understanding of the interplay of the visual excitatory and inhibitory circuits requires systematic study of the receptors and their ligands that shape neuronal responses within the retina. My dissertation will focus on one class of inhibitory receptors that are sensitive to the neurotransmitter glycine.

1.2 The Retina

The retina is a thin piece of neural tissue (approximately 150 to 400 μm thick depending on species and the position of the retina measured), located at the back of the eye, where phototransduction first occurs (Ferguson, Dominguez, Balaiya, Grover, & Chalam, 2013; Yamada, 1969). The retina is a laminar structure consisting of five different classes of neurons and two synaptic layers. These cells classes include the photoreceptors, horizontal cells, bipolar cells, amacrine cells, and ganglion cells (Figure 1.1). Retinal neuron somas reside in three nuclear layers: the outer nuclear layer (ONL) contains photoreceptors; the inner nuclear layer (INL) contains bipolar cells, horizontal cells, and amacrine cells; the ganglion cell layer (GCL) contains ganglion cells and displaced amacrine cells (Figure 1.1). In between the cellular layers are two synaptic layers called plexiform layers. The photoreceptors, horizontal cells, and bipolar cells synapse in the outer plexiform layer (OPL) while the bipolar cells, amacrine cells, and ganglion cells synapse in the inner plexiform layer (IPL, Figure 1.1). These retinal cells synapse together and

form the parallel circuits, which parse, filter, and process visual input and transmit interpretable visual signals to the brain such as the ONset and OFFset of light, direction selectivity, and edge detection.

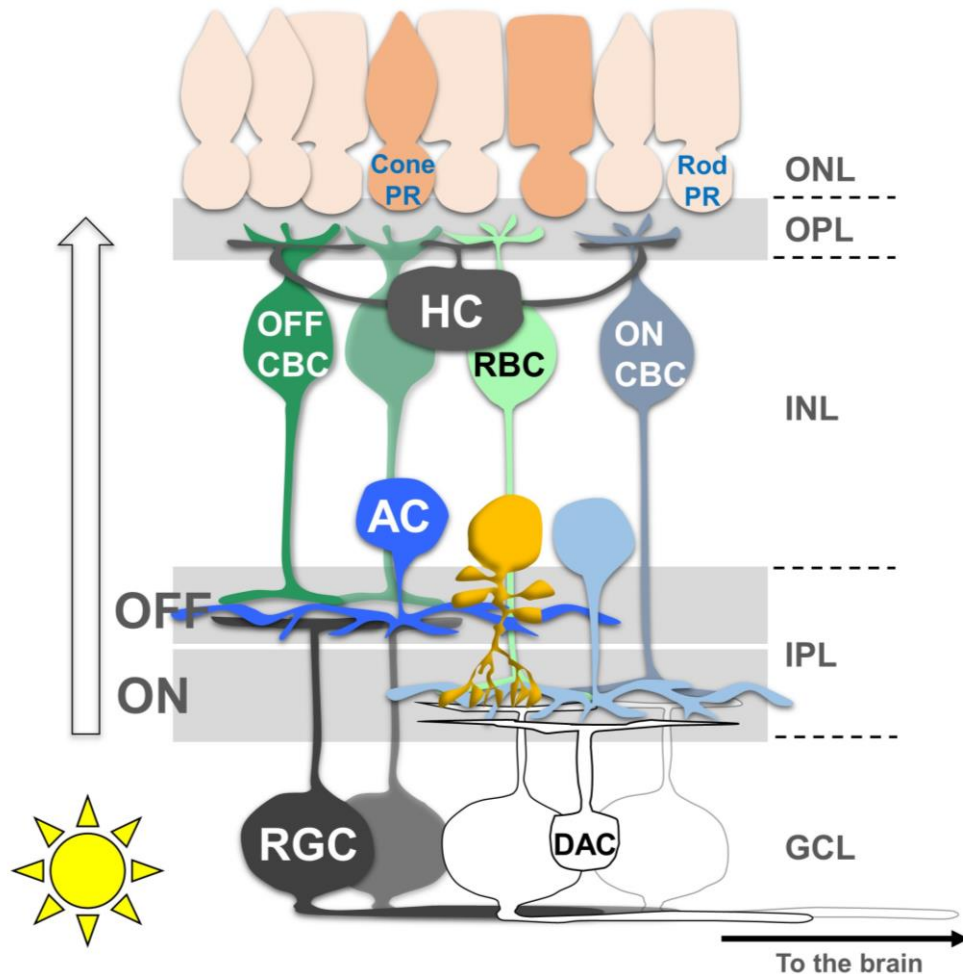


Figure 1.1 Schematic of the retina. Source: modified figure from (C. Zhang, 2015). The retina contains five unique classes of cells: photoreceptors (PR), horizontal cells (HC) bipolar cells (BC), amacrine cells (AC) and ganglion cells (GC). The cell somas are found in the nuclear layers: the outer nuclear layer (ONL), the inner nuclear layer (INL), and the ganglion cell layer (GCL). Retinal cell dendrites connect via synapses in the plexiform layers: the outer plexiform layer (OPL) and the inner plexiform layer (INL). Light passes through the retina before falling upon the photoreceptor outer segments. Some amacrine cell somas are found in the GCL and are called displaced amacrine cells (DAC).

1.3 Photoreceptors

The photoreceptors are comprised of two major classes: rods and cones. Rods are more sensitive to light at the cost of visual acuity. One rod cell can detect a single photon, which allows them to function in scotopic, or dim light, conditions (a luminance of 10^{-6} to 10^{-2} cd/m²) (Hecht, Schlaer, & Pirenne, 1941; Tinsley et al., 2016). Rods transmit lower visual acuity because of the signal convergence of multiple rods to single bipolar cell targets. Conversely, cone cells are less sensitive to light, but have greater visual acuity. This increased visual acuity is due to less signal convergence of cones to their bipolar cell targets; in some cases, only one cone makes synapses with one bipolar cell target. They primarily function in photopic or sunlit conditions (a luminance of 1 to 10^6 cd/m²). With two different classes of photoreceptors, a mammal, for instance, can interact in an environment consisting of wider ranges of light diversity. Similarly, most human retinas have three different types of cone photoreceptors, each being stimulated by a specific wavelength of light within the visible spectrum. These three cone types allow the brain to perceive color, again widening the range of environmental interpretation. Light in the 400-500nm wavelength range is on the lower end of the detectable range and is coded by cones called short wavelength (S) cones. Medium wavelength (M) cones detect light in the 500-600nm range, and long (L) cones

detect light in the 550-650nm wavelength range (Figure 1.2) (Bowmaker & Dartnall, 1980).

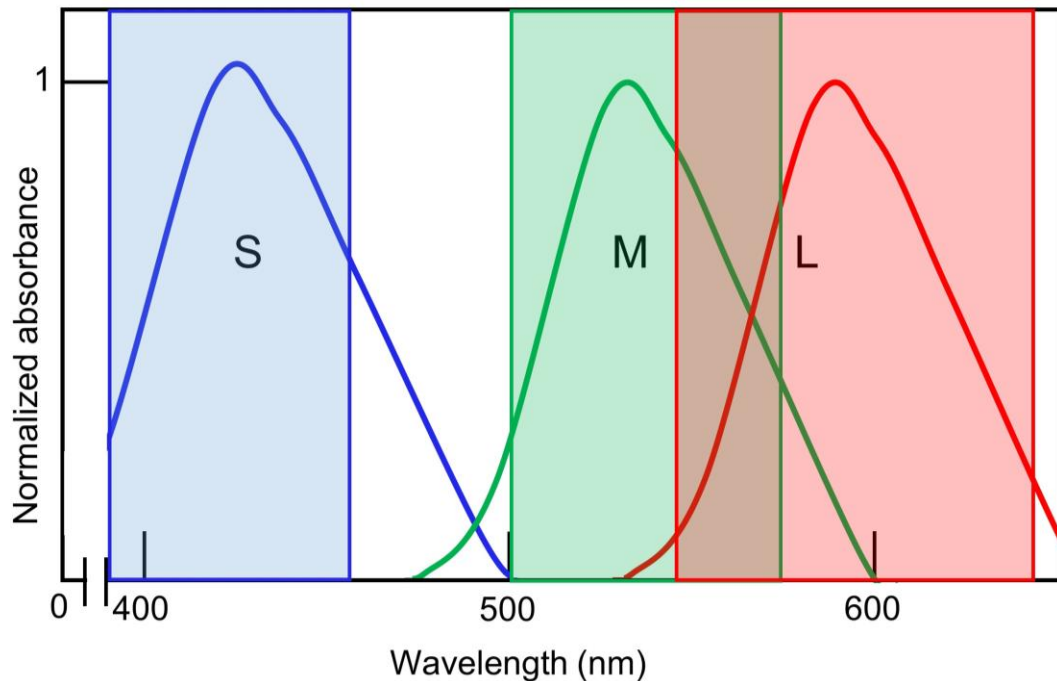


Figure 1.2 Absorbance Spectrum of trivariant color vision from three different cones. A short (S) cone has an absorbance around 400-450nm wavelength (blue). A medium (M) cone has an absorbance around 500-575nm wavelength (green). A long (L) cone has an absorbance around 550-650nm wavelength (red).

1.4 Photoisomerization

Photopigments called opsins are light-sensitive proteins that reside in the outer segment discs of photoreceptors and begin the conversion of light energy into neural information. There are two types of opsins, one for rods called rhodopsin, and one for cones called cone opsin (Lamb, 2013). While a photoreceptor is in the dark, (or photons have not activated an opsin), photoreceptor membrane-bound cGMP-gated cation channels are open, Na^{2+} and Ca^{2+} enter the cell, which causes the photoreceptor cell to depolarize and release glutamate (Dowling & Ripps, 1973; Suryanarayanan & Slaughter, 2006; Trifonov,

1968). This results in a constant depolarizing current in the dark (called the dark current), and it leads to sustained glutamate release in the absence of photon activation. However, once an opsin absorbs a photon, which causes photoisomerization, the membrane-bound cGMP-gated cation channels close, causing the photoreceptor cell membrane to hyperpolarize (Morgans, 2000). This reduces glutamate release from the photoreceptor proportionally to the intensity of light (i.e., the number of photons absorbed in the photoreceptor). The light-evoked signal is then transmitted through parallel circuits formed by the bipolar cells, amacrine cells, and ganglion cells and sent to the brain.

1.5 Bipolar Cells

Bipolar cells are the major excitatory interneurons in the retina. The bipolar cells form synaptic connections with the photoreceptors in the OPL and with the amacrine cells and ganglion cells in the IPL (Figure 1.1). At least fourteen different types of bipolar cells are found in the mammalian retina (Euler, Haverkamp, Schubert, & Baden, 2014; Greene, Kim, Seung, & EyeWriters, 2016). Bipolar cells fit into two major classes based on their presynaptic photoreceptor partner. Rod bipolar cells are postsynaptic to rods and cone bipolar cells are postsynaptic to cones. However, there are instances where cones make synapses on rod bipolar cells, so a general characterization is not entirely accurate (Pang, Yang, Jacoby, & Wu, 2018).

Cone bipolar cells can be further divided into two major varieties, OFF and ON. These two major varieties are the bases for the OFF and ON pathways within the retina (Ghosh, Bujan, Haverkamp, Feigenspan, & Wassle, 2004). While in the

dark, both OFF and ON cone bipolar cells continually receive tonic glutamate from cone photoreceptors. However, in the dark, the OFF cone bipolar cells are depolarized and release glutamate in the IPL whereas the ON cone bipolar cells are hyperpolarized and do not release glutamate. Hence, at the bipolar cell level, the OFF pathway is more excited in the dark with little inhibition, and the ON pathway is tonically inhibited. Conversely, when photons activate photoreceptors, glutamate release is interrupted, so both OFF and ON cone bipolar cells receive less glutamate. In the light, OFF cone bipolar cells hyperpolarize and stop releasing glutamate into the IPL, while ON cone bipolar cells depolarize and release glutamate into the IPL. Therefore, the ON pathway is excited in the presence of light, while the OFF pathway receives more inhibition.

To maintain the division between the OFF and ON pathways, OFF cone bipolar cells form synaptic connections with OFF ganglion cells in the upper region of the IPL (Figure 1.1). This region is called the OFF sublamina of the IPL. Similarly, the ON cone bipolar cells form synaptic connections with ON ganglion cells in the lower region of the IPL called the ON sublamina (Figure 1.1). Though the cone bipolar cells help define these pathways, the rod bipolar cells indirectly connect to both of these major parallel pathways. In contrast to the cone bipolar cells, the rod bipolar cells form synaptic connections with bistratified All amacrine cells but not retinal ganglion cells (RGCs) (Bloomfield & Dacheux, 2001; Demb & Singer, 2012) (Figure 1.1). In turn, the All amacrine cell forms gap junctions with the ON cone bipolar cells where an excitatory signal can transmit onto the ON ganglion cells (Demb & Singer, 2012). Additionally, the All amacrine cell is

bistratified and also forms inhibitory synaptic connections with the OFF cone bipolar cells, which in turn are synaptically coupled to OFF ganglion cells (Demb & Singer, 2012). These three different functional types of bipolar cells are the foundation for the major parallel pathways in the retina: the ON pathway, the OFF pathway, and the rod bipolar cell pathway.

1.6 Horizontal Cells

Horizontal cells are one of the major inhibitory neurons in the retina. Located in the INL, their dendrites innervate the OPL where they form synapses with photoreceptors. The primary role of horizontal cells is they form a negative feedback loop to the photoreceptors, utilizing either with a hemichannel-mediated ephaptic mechanism, and/or Na/HCO_3 transporters modulating the local pH of photoreceptor cell and bipolar cell synapses (Byzov & Shura-Bura, 1986; Fahrenfort et al., 2009; Kamermans et al., 2001). These cells also release γ -Aminobutyric acid (GABA), but the role of this neurotransmitter is unclear (Fahrenfort et al., 2009; Kamermans & Werblin, 1992). This feedback loop has been shown to have an essential role in color constancy and opponency, contrast enhancement, and forming center-surround receptive fields of cones (Chapot, Euler, & Schubert, 2017; Kamermans & Werblin, 1992). Horizontal cells are connected to each other via gap junctions to form an interconnected network (Kamermans & Werblin, 1992).

1.7 Amacrine Cells

To date, there are approximately forty known types of amacrine cells (Akrouh & Kerschensteiner, 2015; Helmstaedter et al., 2013; Masland, 2012). The primary function of amacrine cells is to release neurotransmitter (GABA or glycine) into the inhibitory synapses of ganglion cells or bipolar cells or both to integrate and modulate these cells excitatory output (Park et al., 2018; C. Zhang & McCall, 2012). Some amacrine cells also release less conventional neurotransmitters, including acetylcholine (S. Lee et al., 2014; Park et al., 2018). The somas of amacrine cells can occupy either the INL where the bipolar cell somas reside or the ganglion cell layer where amacrine cells are called displaced amacrine cells (Figure 1.1). The location of the IPL where amacrine cell dendrites ramify and whether these dendrites are monostратified, bistratified, or diffuse are the two major factors that determine the type of circuit with which the amacrine cell is involved. To date, only narrow-field amacrine cells release glycine and wide-field amacrine cells release GABA. Co-release of GABA and glycine in a synapse is observed in regions such as the lateral superior olive, the medial nucleus of the trapezoid body, and a variety of locations in the spinal cord (Gamlin, Yu, Wong, & Hoon, 2018; Moore & Trussell, 2017). However, co-release of GABA and glycine has yet to be observed in the retina. By releasing neurotransmitter into inhibitory synapses of bipolar cells or RGCs, amacrine cells facilitate the function of four major types of inhibitory circuits.

1.8 Inhibitory Circuits

The four important inhibitory circuits involving amacrine cells are: feedforward and feedback, which provide direct inhibition onto their postsynaptic

targets and crossover and serial circuits, which provide disinhibition onto their postsynaptic targets.

An inhibitory feedforward circuit consists of a neuron, which depolarizes and excites an inhibitory neuron to release neurotransmitter onto the inhibitory receptors of a third neuron (Figure 1.3A). Succinctly, the excitatory output of the first neuron causes the second neuron to inhibit the third neuron (Figure 1.3A). An example of a feedforward circuit is that of a bipolar cell, which excites an amacrine cell to release inhibitory neurotransmitter onto a ganglion cell (Chen, Hsueh, Greenberg, & Werblin, 2010).

An inhibitory feedback circuit consists of a neuron, which depolarizes and excites an inhibitory neuron to release neurotransmitters onto the inhibitory receptors of the first neuron, thus inhibiting first cell (Figure 1.3B). An example of a feedback circuit is that of a rod bipolar cell, which releases glutamate (an excitatory neurotransmitter) onto A17 amacrine cells, which in turn release inhibitory neurotransmitter (GABA) back onto the rod bipolar cell (Hartveit, 1999). In addition, a feedback inhibitory circuit can be half of a reciprocal circuit where the inhibitory component helps enhance the excitatory component of the antagonist (in relevance to the inhibitory) target (Grimes, Zhang, Graydon, Kachar, & Diamond, 2010; Nobles et al., 2012).

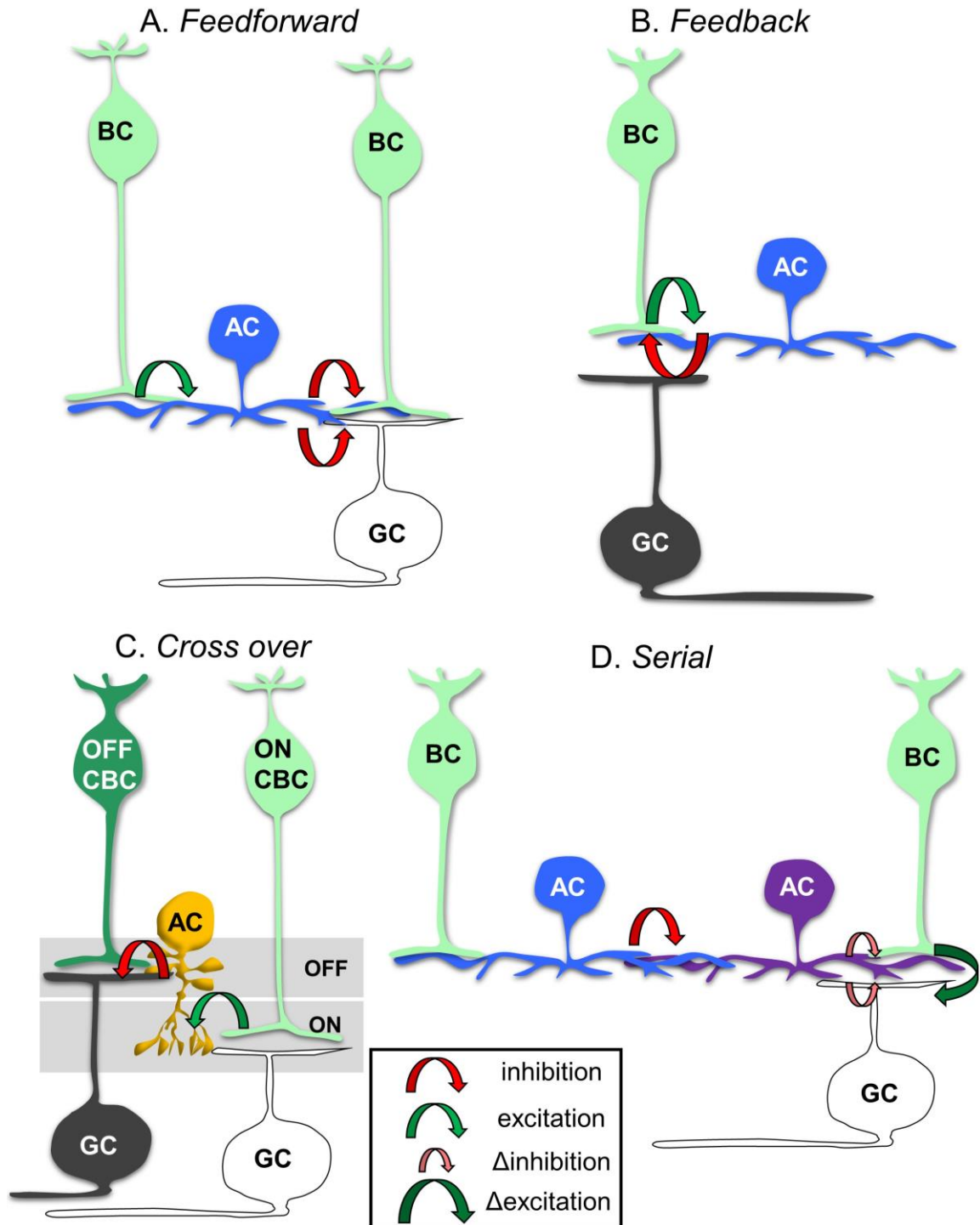


Figure 1.3 Schematic Representations of Different Forms of Inhibition. Source: modified from (C. Zhang, 2015). A) Feedforward inhibition - excitation of an amacrine cell initiates inhibition of a bipolar cell or retinal ganglion cell B) Feedback inhibition - excitation of an amacrine cell starts feedback into the initial excitatory cell reducing further excitation. C) Crossover inhibition – excitation

from one pathway of a bistratified amacrine cell initiates inhibition of a bipolar cell or retinal ganglion cell of a different pathway D) Serial inhibition – excitation of an amacrine cell leads to the inhibition of another amacrine cell, which reduces its inhibitory output resulting in enhanced excitation of the final retinal ganglion cell target. This type of inhibition is disinhibition.

An inhibitory crossover circuit consists of a neuron, which depolarizes and excites a bistratified inhibitory neuron to release neurotransmitter onto the inhibitory receptors of a third neuron, which receives excitatory input from a different pathway (Figure 1.3C). The bistratified neuron is a crucial component of crossover inhibition as it facilitates the signal transfer from one major pathway to another based on dendritic morphology. An example of this circuit is an ON cone bipolar cell excites an AII amacrine cell, which then inhibits an OFF ganglion cell (Demb & Singer, 2012).

A serial inhibitory circuit consists of a neuron, which depolarizes and excites an inhibitory neuron, which releases neurotransmitter onto the inhibitory receptors of a second inhibitory neuron, which in turn stops releasing neurotransmitter onto the inhibitory receptors of a fourth cell (Figure 1.3D). The result in an enhancement of excitatory release to the fourth cell, otherwise known as disinhibition. An example of a serial inhibitory circuit is a rod bipolar cell stimulates a GABAergic amacrine cell, which then inhibits a second GABAergic amacrine cell. The second GABAergic amacrine cell then reduces the inhibition onto a second bipolar cell (Eggers et al. 2010).

1.9 Retinal Ganglion Cells

Retinal ganglion cells, the feature detectors of the visual scene, transmit information about our rich and complex visual environment using spiking signals to the rest of the brain. The retinal ganglion cell somas reside in the retinal ganglion cell layer, and their dendrites stratify in the IPL and make synaptic connections with both bipolar cells and amacrine cells. The forty retinal ganglion cell types found in the mouse retina are defined by their: morphology, visual response properties, and genetic profiles (Baden et al., 2016; Bae et al., 2018; Rockhill, Daly, MacNeil, Brown, & Masland, 2002; Sanes & Masland, 2015). The circuits formed in the IPL between the excitatory output of the bipolar cells and inhibitory input of the amacrine cells onto the ganglion cells help complete the retina's interpretation, filtration, and feature detection of the signal of the visual scene. The axons of the retinal ganglion cells form the optic nerve and these axons innervate roughly twenty different areas in the brain; largely the superior colliculus, the lateral geniculate nucleus, and the suprachiasmatic nucleus of the hypothalamus (Canteras, Ribeiro-Barbosa, Goto, Cipolla-Neto, & Swanson, 2011; Ellis, Gauvain, Sivyer, & Murphy, 2016).

1.10 Neurotransmission

Neurons form synapses with each other to orchestrate the transmission of these different modes of communication. Individual neurons can have as many as 10,000 synaptic connections (Kandel, Schwartz, & Jessell, 2000). Both chemical and electrical synapses are found in the retina (Kuo, Schwartz, & Rieke, 2016). Electrical synapses, known as gap junctions are formed by twelve connexins that bridge between two cells and serve as a low resistance channel, which allows ions

to pass between them, effectively transferring charges between cells (Brink, Cronin, & Ramanan, 1996).

Similarly, chemical synapses form between two cells (a pre-synaptic cell and a post-synaptic cell). However, chemical synapses form between a presynaptic bouton and either a small region of a dendrite or the soma of the post-synaptic cell (Figure 1.4). In a chemical synapse, the presynaptic cell releases neurotransmitters, which are small peptides that act as ligands on the post-synaptic cell receptors. Once a ligand binds to the post-synaptic cell receptor, the receptor responds by either opening an ionic channel to allow ions to flow across the membrane (ionotropic) or initiating a signal transduction cascade (metabotropic). The diversity of transferring information via a chemical synapse is staggering because of all of the different components at play. A number of different neurotransmitters have been identified in the retina. They include: glutamate, acetylcholine, GABA, glycine, and dopamine. Each appears to be stored in synaptic vesicles, when released bind to their respective excitatory or inhibitory postsynaptic receptors. The neurotransmitter release properties and the receptor kinetics differ and can have a major impact on the volume or quanta of neurotransmitter release and its uptake. Understanding these factors is critical to our interpretation of how circuits in the retina function and unveiling their roles in vision.

1.11 Synaptic Release

In preparation for release, neurotransmitters are packaged in synaptic vesicles in the presynaptic bouton and reside in one of three groups: the readily

releasable pool (there might be two of these, one for driven release, and one for spontaneous release), the reserve, or in the vesicle recycling pathway (Smith et al., 2012). Vesicle release can be either spontaneous or elicited by an action potential or graded electrical potential. Synaptic vesicles release their contents into the synaptic cleft via different mechanisms. A vesicle can fuse with the cell membrane and release all of its content via exocytosis; a method called full collapse. Or, vesicles can fuse with the cell membrane and release a portion of their contents, called partial collapse or fuse-pinch-linger. In a third mechanism, called kiss-and-run, a vesicle docks with a membrane pore, release a fraction of its contents, and then undocks from the pore. After a neurotransmitter enters the synapse, it can bind to a receptor, it can be taken up by a transporter, or if the concentration is high enough, it can diffuse out of the synapse.

The release of vesicles can be spontaneous, or driven by input to the cell. Driven release is caused by excitation of the pre-synaptic cell and most or all vesicles from the readily releasable pool empty their contents into the synapse. Driven release can occur either synchronously, or asynchronously. Synchronous release is fast and clearance of the synapses happens rapidly (Eggers & Lukasiewicz, 2006b). Contrarily, Asynchronous release is slow, and neurotransmitter concentration remains high in the synapse, long enough to “spillover” and out of the synapse (Eggers & Lukasiewicz, 2006b; Keros & Hablitz, 2005; Smith et al., 2012). Spillover often results in neurotransmitter binding to extrasynaptic receptors or receptors in a different synapse. (Eggers & Lukasiewicz, 2006b; Keros & Hablitz, 2005).

The spontaneous release of the vesicles is stochastic, likely dependent on the extracellular calcium concentration of the presynaptic cell, and the spontaneously released vesicles come from a vesicle pool other than the readily releasable pool (Smith et al., 2012). Moreover, spontaneous release can involve a single vesicle release (univesicular) or multivesicular release. Univesicular release involves only one vesicle releasing its contents at a time; the spontaneous post-synaptic currents that result from univesicular release are called “minis.” Minis also demonstrate the release of a single quantum of vesicle contents (Eggers & Lukasiewicz, 2006b; Moore-Dotson, Klein, Mazade, & Eggers, 2015). Multivesicular release comprises of multiple vesicles releasing their contents into the synapse simultaneously. The simultaneous release of multiple vesicle contents results in larger post-synaptic current amplitude. Spontaneous release can be measured by recording the change in postsynaptic current via whole cell patch clamping. To isolate inhibitory inputs, the cell’s membrane potential is held at the reversal potential for cations (C. Zhang, Rompani, Roska, & McCall, 2014). These currents are then analyzed to answer questions related to spontaneous release.

1.12 Inhibitory Receptors in the Retina

In the central nervous system, inhibition shapes excitatory neurotransmission (Eggers, McCall, & Lukasiewicz, 2007). GABA receptors predominately mediate inhibition in the brain, whereas; glycine receptors predominately mediate inhibition in the spinal cord (Haverkamp, 1995; Haverkamp et al., 2004; Legendre, 2001). In addition to the spinal cord, glycine receptors are found in the brain stem, cerebellum, hippocampus, calyx of Held, and in the retina

(Hruskova et al., 2012; Manzke et al., 2010). Interestingly, both GABA and glycine receptors are expressed throughout the retina (Haverkamp et al., 2004; Nobles et al., 2012).

In the retina, GABA_ARs expressed on retinal ganglion cells detect GABA release from wide field ACs, which mediate spatial properties of center and receptive field surround (Manookin, Beaudoin, Ernst, Flagel, & Demb, 2008; O'Brien, Richardson, & Berson, 2003). The GABAergic amacrine cells innervate either the ON or the OFF sublamina of the IPL to form serial inhibitory circuits or reciprocal inhibitory circuits (Veruki, Gill, & Hartveit, 2007). Small dendritic field bistratified or diffuse amacrine cells release glycine at their synapses with bipolar cells or RGCs within the IPL (Haverkamp, 1995; Haverkamp et al., 2004; Veruki et al., 2007; Weiss et al., 2008). Frequently, these amacrine cells cross over the ON and OFF sublamina of the IPL to facilitate crossover inhibition (MacNeil & Masland, 1998; Nobles et al., 2012). My dissertation focuses on the expression of glycine receptors in the retinal ganglion cells.

1.13 Glycine Receptors

Glycine receptors are heteropentameric ligand-gated chloride ion channels. Figure 1.4A illustrates a typical glycine receptor containing one type of GlyR β subunit and one of four different types of GlyR α -subunits (Fig1.5B) (GlyR α 1, GlyR α 2, GlyR α 3, and GlyR α 4; (Cascio, 2006; Dutertre, Drwal, Laube, & Betz, 2012; Lynch, 2004, 2009; Wassle et al., 2009). The most predominant glycine receptors are heteromeric and are composed of three GlyR β subunits and two GlyR α subunits (Figure 1.4C). Heteromeric expression of two different GlyR α

subunits within one GlyR has only been observed only in heterologous systems (e.g., *Xenopus oocytes*) (Figure 1.4C); (Kuhse, Laube, Magalei, & Betz, 1993). Homomeric GlyRs, made of five of the same GlyR α subunits, are rare but have been found *in situ*, for instance at the calyx of held (Figure 1.4C) (Hruskova et al., 2012). To date, all four heteromeric GlyRs (GlyR α 1, GlyR α 2, GlyR α 3, and GlyR α 4) have been found in the mouse retina (Heinze et al., 2007; Veruki et al., 2007; Wassle et al., 2009; Y. Zhang, Dixon, Keramidas, & Lynch, 2015).

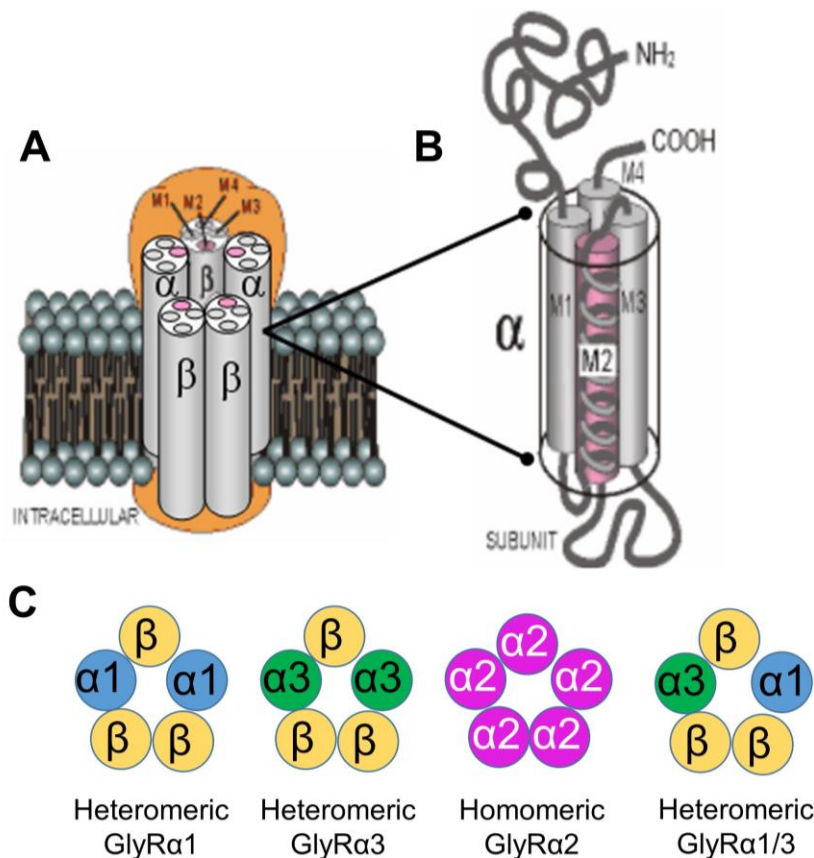


Figure 1.4 Schematics of glycine receptors. Illustration sourced from the Australian Society for Biophysics. A) Illustration of the transmembrane heteropentameric chloride ion channel glycine made of three β subunits and two of the same α subunits. B) Illustration of a single α subunit of a glycine receptor. Each α subunit is made from four major transmembrane domains and both the N and C terminuses are on the extracellular portion of the subunit. The M2 domain of the α and β subunits face the interior of the channel pore. C) Illustration of a

heteromeric GlyR α 1, heteromeric GlyR α 3, and homomeric GlyR α 2 glycine receptors. Notice the lack of β subunit in the homomeric GlyR α 2 glycine receptor.

1.14 Glycine Receptor Kinetics

Receptor channel current kinetics are either derived from the subunit structure of the receptor, which can be influenced by auxiliary protein modulation such as phosphorylation. The receptor kinetics are measurable based on the current fluctuations they produce when opening and closing. These fluctuations are called postsynaptic currents. A current is evoked when a ligand binds to the postsynaptic receptor and opens the channel. In the case of glycine receptor channels, chloride ions flow into the cell until: a) the ligand dissociates from the receptor, which closes the channel or b) the channel desensitizes and closes after a certain timecourse. Current research suggests glycine receptors do not desensitize (Singer & Berger, 1999). While the glycine receptor channel is open, the inward flow of chloride ions hyperpolarizes the postsynaptic cell, which leads to inhibition. The timing of these glycinergic currents appears to depend primarily on the receptor alpha subunit, as the binding characteristics are similar for each subunit specific alpha receptor class. In addition, ligand concentration at the receptor, temperature, receptor expression density at the synapse, and phosphorylation of the glycine receptors also can modify the basic alpha receptor based current kinetics (Beato, 2008; Lynch, 2004; Maksay, 1996). Typical glycine concentration in the synaptic cleft is $\sim 3\text{mM}$ and glycine is cleared by glycine transporters (GlyTs) in $\sim 0.7\text{ ms}$ (Beato, 2008). Furthermore, glycine receptors are insensitive to rapid desensitization, which may help contribute to their ability to

match high frequency of excitatory inputs (Awatramani, Turecek, & Trussell, 2004; Singer & Berger, 1999).

The different GlyRs are distinguishable from their spontaneous inhibitory post-synaptic currents (sIPSCs) (Figure 1.5). The sIPSCs that result from different GlyR α subunits have different kinetics, which include their rise time and decay time (τ_{decay}). Rise time is defined as the time it takes for the amplitude of the sIPSC to rise from 10% to 90% of its peak (Figure 1.5A). The τ_{decay} is defined as the time it takes for the current to fall from peak to 37% (D_{37}) of the peak (Figure 1.5B). A shared characteristic across the four heteromeric glycine alpha receptors is a rapid rise time between approximately 2 and 7 ms (Gill, Veruki, & Hartveit, 2006; Russell & Werblin, 2010). Similarly, the four heteromeric glycine alpha receptors exhibit similar binding affinities, although these estimates vary across systems (Lynch, 2004). The four heteromeric GlyR alpha subunit mediated sIPSCs have distinct τ_{decay} times. (Table 1.1) (Majumdar, Heinze, Haverkamp, Ivanova, & Wassle, 2007; Majumdar, Weiss, & Wassle, 2009). Although estimates of the decays of the various alpha subunits have been published, the currents were recorded at room temperature, which is known to slow down current kinetics (Majumdar, Heinze, Haverkamp, Ivanova, & Wassle, 2007; Majumdar, Weiss, & Wassle, 2009). My experiments were conducted at 36° C and I found the τ_{decay} is faster for each subunit compared to the previously published data (Table 1.1). Under these conditions, GlyR α 1 has the fastest τ_{decay} with an average of ~3ms; GlyR α 3 has a slightly slower τ_{decay} with an average of ~7ms, and GlyR α 2 and GlyR α 4 both have

much slower τ_{decay} each with an average of ~ 20 ms. These different decay kinetics suggest that the different types of GlyRs have specific independent functions as inhibitory receptors.

Throughout the CNS, glycine receptors are associated with mechanisms that shaping temporal excitatory responses. They tune rhythmic motor output in the spinal cord, sustained and transient OFF responses in RGCs, and they match temporal suppression of high frequency excitatory responses in the mammalian calyx of Held (Awatramani et al., 2004; Bracci, Ballerini, & Nistri, 1996; Caldwell, Daw, & Wyatt, 1978; Nobles et al., 2012). The need for a variety of glycine receptor alpha subunit specific kinetics is demonstrated in inhibitory circuits found in both bushy and T stellate cells of the ventral cochlear nucleus (VCN). In the bushy cells of the VCN, kinetically slow GlyRs tonically adjust voltage-gated ion channels to modulate EPSC driven spike timing that ultimately increases the spike threshold and improves spike precision (Xie & Manis, 2013). Conversely, kinetically fast GlyRs expressed on the T stellate cells of the VCN mediate inhibition that coincides with fast EPSC input that does not interfere with spike threshold but inhibits slow NMDA currents (Xie & Manis, 2013). These two examples illustrate the need for precise temporal inhibition of varying kinetics, which can modulate specific excitatory signal in consonance or in interpolation.

Table 1.1 (τ_{decay} of GlyR α subtypes)

GlyR α Subunit	τ_{decay} (ms) at 36°C
$\alpha 1$	2.96 \pm 0.3 ms
$\alpha 2$	26.59 \pm 0.5 ms
$\alpha 3$	9.23 \pm 0.2 ms
$\alpha 4$	21.85 \pm 0.4 ms

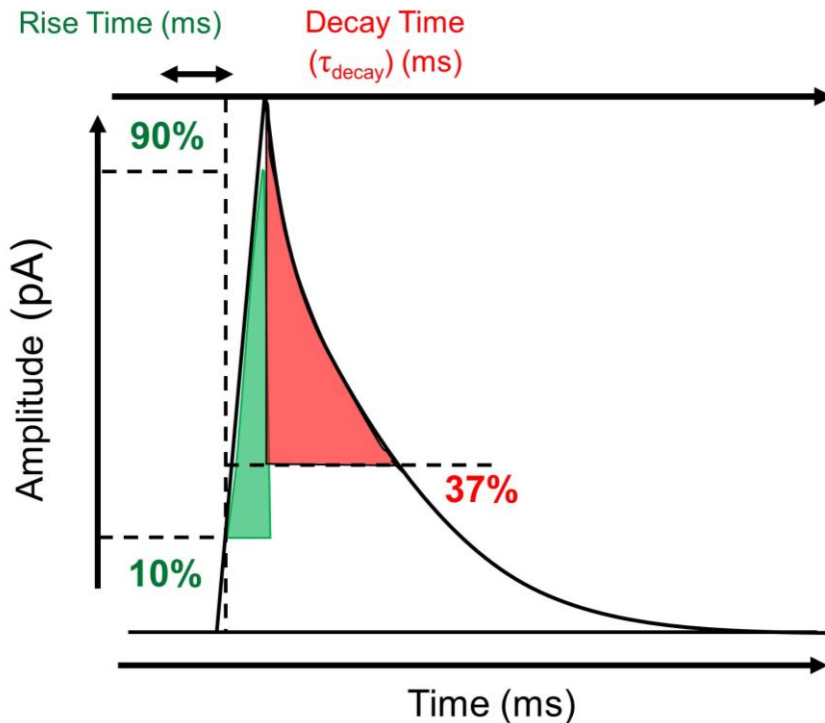
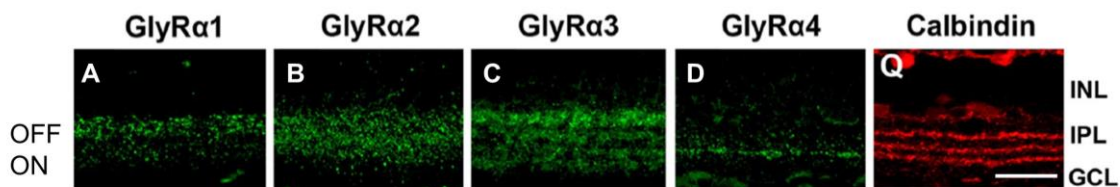


Figure 1.5 Representative examples of an IPSC waveform demonstrating both rise time and τ_{decay} . The example of an IPSC rise time measurement is the time it takes for the amplitude to rise from 10% to 90% of the peak (in green). An example of an IPSC τ_{decay} time measurement is the time it takes for amplitude to descend from the peak to 37% of the peak (in red).

1.15 Differential Expression of GlyR α Subunits in the IPL of the retina

In the retina, the GlyR β subunit is expressed ubiquitously, whereas each of the GlyR α subunits is expressed differentially across the IPL (Figure 1.6). GlyR α 1 expression is found in both the OFF and ON sublamina of the IPL, with higher expression in the OFF sublamina of the IPL (Figure 1.6A). The expression is likely higher in the OFF sublamina because the AII amacrine cell (the most abundantly expressed amacrine cell) makes inhibitory synapses with OFF cone bipolar cells and OFF ganglion cells, while it makes gap junctions with ON ganglion cells (Demb & Singer, 2012). The GlyR α 2 expression density throughout the IPL is the most

abundant of the GlyRs. (Figure 1.6B). The GlyR α 3 expression is in four distinct bands across the IPL, which appear to be separated by the three calbindin bands (Figure 1.6C). Finally, GlyR α 4 expression is concentrated in a distinct band in the upper ON sublamina and, with sparse expression throughout the rest of the IPL (Figure 1.6D). The combination of different decay kinetics and differential expression further implies functional differences among the four GlyR isoforms (Wassle et al., 2009).



Nobles et al. (2012), J Neuroscience

Figure 1.6 Representative confocal images of transverse wild type sections stained for glycine receptor subunit expression (green) across the IPL. **A)** GlyR α 1 puncta expression is distributed throughout the IPL, but more abundant in the OFF sublamina. **B)** GlyR α 2 puncta expression is substantial throughout the IPL. **C)** GlyR α 3 puncta expression is in a laminar pattern throughout the IPL. **D)** GlyR α 4 expression is limited to a distinct band in the upper ON sublamina, yet some sparse puncta are seen **E)** Calbindin (red) Representative confocal image of transverse INL, Inner nuclear layer; IPL, inner plexiform layer; GCL, ganglion cell layer. Scale bar, 20 μ m. (Image from Nobles et al. (2012), J Neuroscience).

In the inner retina, evaluation of the decay kinetics of glycinergic sIPSCs as well as immunohistochemistry show that OFF cone and rod BCs express GlyR α 1 and that ON cone BCs have no glycinergic inputs (Figure 1.1) (Eggers et al., 2007; Ivanova, Muller, & Wassle, 2006; Majumdar et al., 2007; Wassle et al., 2009). Assays of a small subset of morphologically identified ACs indicate differential expression of GlyRs. Narrow-field ACs express GlyR α 2, AII ACs express either

GlyR α 3 and/or GlyR α 1 (Gill et al., 2006), and starburst ACs (SACs) express GlyR α 4 and may also express GlyR α 2 (Haverkamp et al., 2004; Heinze et al., 2007; Majumdar et al., 2009; Weiss et al., 2008). In addition, the large soma OFF α RGC express only GlyR α 1 (C. Zhang et al., 2014).

Zhang et al. determined that GlyR α 1 input on OFF α RGCs helps modulate the spontaneous excitatory activity to improve the signal to noise ratio and slightly hyperpolarizes the cell reducing the spiking probability. Furthermore, GlyR α 1 input in OFF α RGCs helps diminish the rebound excitation caused by the transient suppression of spiking from ON cone bipolar cells during an OFFset stimulus. Finally, OFF α RGCs express GlyR α 1, which receives crossover inhibition mediated by glycinergic input from the AII amacrine cell during the onset of light. Does GlyR α 1 have a similar role in other GlyR α 1 only expressing RGCs or does its role differ based on the retinal ganglion cell response properties? Collectively the RGCs with the largest soma diameters only make up about 8% of all RGCs expressed in the retina (Sanes & Masland, 2015). Which GlyRs are expressed on the other ~92% of RGCs is unknown and a significant gap in our knowledge. Furthermore, these cells may express or co-express any of the four different GlyR α subunits, and these GlyRs may serve different functions. Using established techniques, we intend to further unveil the unique GlyR expression of specific types of retinal ganglion cells.

II. SPECIFIC AIMS

Ramón Y Cajal caricaturized elegant and accurate descriptions of retinal cells. These images and descriptions inspired many to investigate and decipher

retinal circuitry and the components that facilitate vision. As the previous review portrays, we know a great deal about the components and function of the retina. Retinal biologists continue to discover new cells types, genes, transcription factors, and circuit pathways at a rapid pace. These newly discovered components of the retina generate new questions and new gaps in our knowledge. For instance, we have limited understanding of the subunit-specific GlyR expression in the RGCs, even though we know there is differential expression of all four different GlyRs throughout the IPL. Furthermore, subunit-specific glycine receptor function is unknown and they could play different roles depending on the specific RGC visual response properties. I set out to identify subunit specific GlyR expression in RGCs using the following aims.

Aim 1 – Identify Glycinergic Expression on a Subset of Retinal Ganglion Cells

Aim 1 of my dissertation is to identify and characterize the glycinergic expression across nine different RGC types and one displaced amacrine cell. Ideally, these ten cell types will collectively include all four glycine receptor subunits. First I will examine three of the four RGCs with the largest somas, the ON α , ON τ , and OFF δ . Together with the previously examined OFF α RGC, these RGCs complete a homolog set for major visual response properties- ON/OFF and transient/sustained. The glycine alpha subunit receptor expression of OFF α RGCs was identified by Zhang et al., and I will verify this finding using a similar assay (C. Zhang et al., 2014). I will examine glycine receptor expression in the following other retinal cell types: ON starburst amacrine cells, bistratified ON/OFF direction selective (ooDS) RGCs, local edge detectors, high definition RGCs, ultra-high

definition RGCs, asymmetric F-mini RGCs, and JAMB RGCs. Together, these cells represent about 60% of all RGC types in the mouse retina and characterize a variety of distinctive morphology and visual response properties.

Aim 2 - Examine the GlyR α Expression of ooDS RGCs using an rAAV-Glra4shRNA

Aim 2 of my dissertation is to investigate the glycine receptor expression of the ooDS RGC. In the absence of GlyR α 2 or GlyR α 4, glycinergic sIPSC frequency does not change, although in the double knockout of GlyR α 2 and GlyR α 4 the glycinergic sIPSC frequency is almost completely reduced. Thus, a mechanism must exist that compensates for the loss of one of the glycine receptors in these RGCs. We will use an adeno-associated virus (rAAV) delivered short hair pin RNA (shRNA) to knockdown GlyR α 4 expression and determine if the glycinergic sIPSC frequency decreases. This experiment will indicate if a compensatory mechanism exists in the amacrine cells (which will not lose GlyR α 4) and if the compensation mechanism is present after full development of the synapse. Compensation mechanisms could include: an increase in glycine release from the presynaptic amacrine cells, due to an overall loss of glycinergic input in the upstream circuit or an increase in GlyR expression or trafficking to the postsynaptic site as a consequence of differential expression of these glycine alpha subunits during development.

CHAPTER II

EXPERIMENTAL MATERIALS AND METHODS

2.1 Animals

All experiments were carried out in accordance with the Association for Research in Vision and Ophthalmology “Statement for the Use of Animals in Ophthalmic and Visual Research” and with the approval of the Institutional Animal Care and Use Committee of the University of Louisville. The mice were housed in a facility at the University of Louisville Health Sciences Center and received daily care from the veterinary staff. The mice were kept on a 12-hour light 12-hour dark schedule and fed chow *ad libitum*.

I used three different single GlyR knockout (KO) mice (Table 2.1) as well as crosses between these knockout mice to form double GlyR knockout mice. I used reporter mouse lines that express fluorescent proteins in specific retinal ganglion cells (RGCs) for experiments to establish the baseline glycinergic responses and create hypotheses for which glycine receptors are expressed onto those specific ganglion cells (Table 2.1). These reporters were used alone for wild type (WT) controls and were also bred to single and double KOs as indicated in Table 2.1. To test for loss of glycine receptor function on specific ganglion cells, we used the single or double GlyR knockout lines crossed to the reporter lines (Table 2.1).

Table 2.1. List of Animal Lines Used for Experiments

Strain name	Source/Jackson lab stock#	Cells targeted	Chapter
<i>Gla2</i> ^{-/-}	Young-Pearse <i>et al.</i> , 2006; 007065		III,
<i>Gla3</i> ^{-/-}	Harvey <i>et al.</i> , 2004; 007065		III
<i>Gla4</i> ^{-/-}	Created in our lab	All RGCs	III, IV
<i>Gla2</i> ^{-/-} / <i>3</i> ^{-/-}	<i>Gla2</i> ^{-/-} X <i>Gla3</i> ^{-/-}		III
<i>Gla2</i> ^{-/-} / <i>4</i> ^{-/-}	<i>Gla2</i> ^{-/-} X <i>Gla4</i> ^{-/-}		III, IV
<i>Thy1</i> ^{Stp-EYFP}	Gift of J. Sanes;(Buffelli <i>et al.</i> , 2003); 005630	Cre expressing cells	III
<i>PV</i> ^{Cre}	<i>Pvalb</i> ^{Cre} X <i>Thy1</i> ^{Stp-EYFP} ; (Farrow <i>et al.</i> , 2013)		III
<i>Gla2</i> ^{-/-} / <i>PV</i> ^{Cre}	<i>Gla2</i> ^{-/-} X <i>PV</i> ^{Cre}	ooDS RGCs, ON α ,	III, IV
<i>Gla3</i> ^{-/-} / <i>PV</i> ^{Cre}	<i>Gla3</i> ^{-/-} X <i>PV</i> ^{Cre}	ON τ , OFF α , OFF δ ,	III
<i>Gla4</i> ^{-/-} / <i>PV</i> ^{Cre}	<i>Gla4</i> ^{-/-} X <i>PV</i> ^{Cre}	PV4, LED, OFF τ , F-mini	III, IV
<i>Gla2</i> ^{-/-} / <i>3</i> ^{-/-} / <i>PV</i> ^{Cre}	<i>Gla2</i> ^{-/-} / <i>3</i> ^{-/-} X <i>PV</i> ^{Cre}		III
<i>Gla2</i> ^{-/-} / <i>4</i> ^{-/-} / <i>PV</i> ^{Cre}	<i>Gla2</i> ^{-/-} / <i>4</i> ^{-/-} X <i>PV</i> ^{Cre}		III, IV
<i>TRHR-GFP</i>	Gift of A. Huberman		III, IV
<i>Gla4</i> ^{-/-} / <i>TRHR</i>	<i>Gla4</i> ^{-/-} X <i>TRHR</i>	ooDS RGCs	III, IV
<i>Gla2</i> ^{-/-} / <i>4</i> ^{-/-} / <i>TRHR</i>	<i>Gla2</i> ^{-/-} / <i>4</i> ^{-/-} X <i>TRHR</i>		III, IV
<i>ChAT-cre/Ai9</i>	Gift of W. Guido; <i>ChAT-cre</i> (006410) X <i>Ai9</i> (007905)		III
<i>Gla4</i> ^{-/-} / <i>ChAT-cre/Ai9</i>	<i>Gla4</i> ^{-/-} X <i>ChAT-cre/Ai9</i>	ON SACs	III
<i>Gla2</i> ^{-/-} / <i>4</i> ^{-/-} / <i>ChAT-cre/Ai9</i>	<i>Gla2</i> ^{-/-} / <i>4</i> ^{-/-} X <i>ChAT-cre/Ai9</i>		III
<i>TYWY3</i>	Gift of J. Sanes;	LED, HD1, HD2,	III
<i>Gla3</i> ^{-/-} / <i>W3</i>	<i>Gla3</i> ^{-/-} X <i>W3</i>	UHD	III
<i>TYWY7</i>	Gift of J. Sanes;	ON τ , OFF α , OFF δ	III
<i>HoxD10-GFP</i>	Gift of D. Berson; (MMRRC id 32065)		III
<i>Gla2</i> ^{-/-} / <i>HoxD10</i>	<i>Gla2</i> ^{-/-} X <i>HoxD10</i>	HoxD10	III
<i>JAMB</i> ^{CreER} / <i>STP</i>	Gift of J. Sanes;		III
<i>Gla4</i> ^{-/-} / <i>JAMB</i> ^{CreER} / <i>STP</i>	<i>Gla4</i> ^{-/-} X <i>JAMB</i> ^{CreER} / <i>STP</i>	JAMB	III
<i>Gla2</i> ^{-/-} / <i>4</i> ^{-/-} / <i>JAMB</i> ^{CreER} / <i>STP</i>	<i>Gla2</i> ^{-/-} / <i>4</i> ^{-/-} X <i>JAMB</i> ^{CreER} / <i>STP</i>		III

2.2 Viral Vector Construction and Packaging

To circumvent the problem of using a global knockout to eliminate all of one GlyR α subunit and affecting GlyR α subunit expression in bipolar cells and amacrine cells, we developed an rAAV delivered method to target just RGCs and eliminate their expression of specific GlyR α s using shRNA. Our lab successfully demonstrated this method in Zhang *et al.* 2014 where an rAAV virus was packaged with an shRNA that when expressed, knocked down the expression of GlyR α 1 only in RGCs; the methods used to create this virus were also published in Zhang *et al.* (Fig 2.2A) (Zhang et al., 2014). We used the same plasmid but switched out the shRNA target of *Gira1* for *Gira4*.

We tested a series of four different *Gira4* shRNA constructs using cell culture, transfection, and immunoblotting. Briefly, Human Embryonic Kidney (HEK293T) cells were cultured in high-glucose DMEM supplemented with 10% fetal bovine serum, 2 mM L-glutamine, 50 IU/ml penicillin, and 50 μ g/ml streptomycin. Cells were seeded on 6-well culture plates one day prior to transfection and transfected with a GlyR α 4 expression plasmid tagged with FLAG and Myc, with or without shRNA plasmids, using jetPrime reagent (Polyplus-transfection, New York, NY) according to the manufacturer's instructions. Thirty-six to sixty hours after transfection, cells were harvested in NP-40 lysis buffer (50mM Tris, 150mM NaCl, 2mM EDTA, and 1% Nonidet P40, pH 8.0, supplemented with protease inhibitor cocktail (Sigma-Aldrich, St. Louis, MO)) and disrupted by rotating for 45 min at 4°C followed by sonication. Cell debris was removed by centrifugation at 17,000 X g for 15 min at 4°C, the supernatant was

collected, and protein quantified using the Bradford reagent (Bio-Rad, Hercules, CA). Twenty-five μg of total protein lysates were loaded per lane and analyzed on 4–12% NuPAGE gels (Invitrogen, Thermo Fisher Scientific, Waltham, MA), transferred to PVDF membranes and blocked with Odyssey Blocking Buffer (LI-COR, Lincoln, NE). Membranes were incubated with primary antibodies (rabbit anti-Flag, 1:2000 and mouse anti- β -actin; 1:25000) diluted in Odyssey Blocking Buffer and washed four times with TBS containing 0.1% tween-20 (TBST). After incubating with IRDye800 CW and IRDye680 CW-conjugated secondary antibodies diluted in Odyssey Blocking Buffer, membranes were washed four times with TBST. Protein bands were visualized by scanning the membranes in an Odyssey Infrared Imaging System (LI-COR, Lincoln, NE) using both 700 and 800 nm channels. β -actin was used as a loading control (Figure. 2.1A-B).

We chose the 29mer shRNA-D to insert into the in the pGFP-V-RS vector, Origene, Rockville, MD) where the plasmid included: flanking Inverted terminal repeats, elongation factor-1 promoter, a tdTomato gene with a nuclear localization sequence, woodchuck hepatitis post-transcriptional regulatory element, a polyadenylation site to protect the mRNA from degradation, the H1 promoter and the *Gira4_{KD}*-shRNA cassette (Figure 2.1C). The plasmids were packaged into the recombinant 2/7 rAAV vector serotype using a standard triple-plasmid protocol by co-transfection of HEK293T cells to create the rAAV-*Gira4_{KD}*-shRNA (Grieger, Soltys, & Samulski, 2016; McClements & MacLaren, 2013; Reid & Lipinski, 2018) (Fig2.2B).

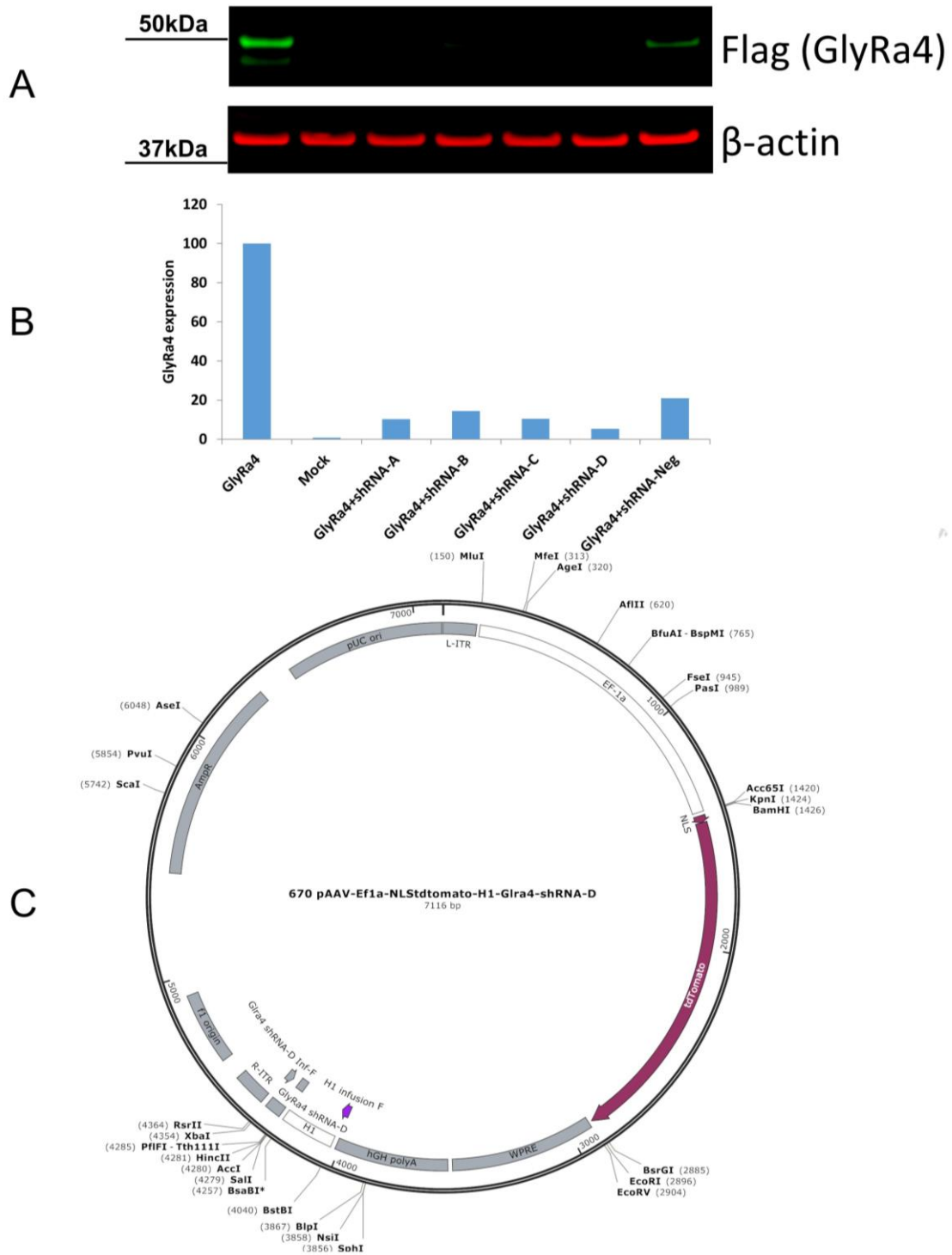


Figure 2.1. *Glra4*_{KD-D} chosen among four different shRNA candidates
 A) Immunoblots of HEK lysates transfected with Flag-tagged *Glra4* expression in each lane with: lane 1, *Glra4* expression alone, lane 2, mock, lanes 3-6 *Glra4*_{KD} shRNA candidates A-D, and lane 7, shRNA negative. B-actin expression was

used as a control. *B*) Quantified and normalized immunoblot data, note *Glra4* expression alone was normalized to 100%. All *Glra4_{KD}* candidates were successful, but shRNA-D was chosen due to the demonstration of the least *Glra4* expression. *C*) Plasmid map (image from SnapGene Viewer, GSL Biotech, Chicago, IL) for pAAV-Ef1a-NLSdtomato-H1-*Glra4*-shRNA-D, which was used to create the rAAV-*Glra4_{KD}*-shRNA

2.3 rAAV injection into Major Optic Nerve Targets of the Brain.

Anesthesia was induced by an intramuscular (IM), intraperitoneal (IP) injection of a mixture of ketamine (70mg/kg) (VetaKet, Akorn, Lake Forest, IL) and xylazine (12mg/kg) (AnaSed, LLOYD, Shenandoah, IA) and to maintain anesthesia, an additional booster (50% concentration of the original solution) was administered subcutaneously and the dosage and time administered was noted. The mouse vibrissae and scalp were shaved. The mouse was placed on a temperature feedback-controlled heating pad to maintain body temperature. The mouse head was secured in a stereotaxic frame with ear bars and a bite bar. Wetting eye drops (1.3% polyvinyl alcohol, OCuSOFT, Rosenberg, TX) were applied to both eyes and were covered with small plastic lenses to maintain lubrication. A ground wire was inserted subcutaneously above right shoulder. A midline incision was made to expose the skull, and a craniotomy was performed at 0.5 mm anterior and 0.5 mm temporally left of Lambda over the superior colliculus (SC), or at 2.5 mm posterior and 2.5 mm temporally to the left of Bregma over the dorsal lateral geniculate nucleus (dLGN). The craniotomies were 2mm by 2mm in size. To locate the SC or the dLGN a borosilicate glass pipette (inner diameter of 40-50 μm) was filled with $\sim 10 \mu\text{l}$ of Ringer's solution and positioned over the craniotomy. The pipette was lowered from the surface of the brain to between 1000 μm and 1200 μm for the SC and 2700 μm and 3000 μm for the

dLGN. The pipette contained an electrode, which was connected to an FHC Xcell-3+ microelectrode amplifier (FHC, Bowdoin, ME) and a Grass Instruments AM-10 audio monitor (Grass Instruments, Warwick, RI). The contralateral eye was stimulated with a full field light source, and audible spiking responses from the amplifier and monitor were used to verify the tip of the electrode had penetrated the SC or dLGN. The depth of the pipette tip was recorded and the exploratory pipette was carefully removed. A second pipette with an inner diameter $\sim 20 \mu\text{m}$ was filled with $3.0 \mu\text{l}$ of the virus solution and positioned over the same coordinates as the exploratory pipette. The virus filled pipette was lowered to the recorded depth and $2.5 \mu\text{l}$ of the virus was injected into the SC or dLGN. The pipette was slowly removed from the injection site after 10 minutes to ensure the virus solution did not flow out of the injection site.

The mouse was then removed from the stereotaxic and placed on a heating pad where its scalp was sutured using a tissue adhesive (VetBond, 3M, St. Paul, MN). The animal was given a $100 \mu\text{l}$ dose of Carprofen (1.25 mg/ml) (Putney, Portland, ME) subcutaneously above the shoulder blades. Four weeks post rAAV injection, RGCs with tdTomato positive nuclei were targeted in the retina for patch experiments.

2.4 Tissue Dissection and Preparation

Under dim red light and at room temperature, dark-adapted animals were euthanized, eyes enucleated, and the lens and cornea were removed leaving the eyecup. The retina was carefully removed from the eyecup and incubated in a solution of Ringers, collagenase (241 units/ml) and hyaluronidase (34.5 nM per ml)

(Worthington Biochemicals, Lakewood, NJ) for 10 minutes to break down the vitreous attached to the retina. Remaining vitreous was carefully removed and the enzyme solution was washed 3 times with fresh oxygenated Ringers. The retinas were quartered, each quarter was placed RGC side up onto a coverslip, and a harp was placed on top of the retina to hold it in place. The entire apparatus was placed into the microscope bath perfused with oxygenated Ringer's solution and kept at 36°C using a preheated Ringer's source and a feedback temperature controlled microscope bath.

2.5 Electrophysiology Recording of Retinal Ganglion Cells

RGCs were observed using a Nikon Eclipse E600FN microscope with a Nikon Fluor 60x water immersion objective with Hoffman Modulation Contrast (Nikon, Tokyo, Japan). When targeting RGC somas in the *PV^{Cre}* or TRHR reporter line retinas, fluorescent protein-expressing somas were observed using a Lumen Dynamics X-Cite Series 120Q lamp. In virus-infected retinas, RGC somas double labeled with GFP (green) and tdTomato positive (red) nuclei were targeted. Glass electrodes (5-7 M Ω of resistance) were made using Kwik-Fil borosilicate glass capillaries (1B150F-4, World Precision Instruments, Sarasota, FL), which were pulled using a P-97 Flaming/Brown micropipette puller (Sutter Instruments, Novato, CA). The electrodes were filled with an intracellular solution that consisted of: (in mM) 12.5 CsCl, 107 CsOH, 107 D-Gluconic Acid, 10 Na⁺ HEPES, 10 BAPTA, 5 QX-314(Br), 4 ATP, and 0.5 GTP, 5 lidocaine N-ethyl bromide (QX314-Br), 2 Lucifer Yellow CH Lithium Salt, 7.5 neurobiotin tracer (pH 7.2 adjusted with CsOH).

Cell recordings were obtained using an Axon MultiClamp 700B patch clamp amplifier (Molecular Devices, San Jose, CA) and the signals were digitized at 10 kHz using an Axon Digidata 1322A (Molecular Devices, San Jose, CA). Signal input and output were monitored and recorded using Axon MultiClamp 700B and Clampex 10.2 software (Molecular Devices, San Jose, CA). RGCs were held at the reverse cation potential (VHold) of +15 mV (0mV after accounting for the liquid junction potential) to determine the GlyR α subunit expression. At this holding potential, and under three different pharmacological conditions, I recorded spontaneous inhibitory postsynaptic currents (sIPSCs).

2.6 Pharmacological Manipulations of sIPSCs

To isolate specific RGC activity, the cell could be recorded in three different bath conditions: 1) A Control bath solution, which consists of Ringer's solution (in mM) 110 NaCl, 2.5 KCl, 1 CaCl₂, 1.6 MgCl₂, 10 D-glucose and 22 NaHCO₃, bubbled with 5% CO₂/95% O₂, pH 7.4) was used to perfuse the tissue. sIPSCs recorded in the control condition include both GABARs and GlyR activity. 2) Ringer's solution containing the GABAR blockers: picrotoxin [20 μ M] – GABA_AR antagonist (PTX) & TPMPA [50 μ M] – GABA_CR antagonist). The sIPSCs recorded in this condition are isolated spontaneous glycinergic sIPSCs. 3) Ringer's solution containing the two GABAR blockers and the GlyR blocker strychnine (STRYCH) [10 μ M] – GlyR antagonist. sIPSCs recorded in this condition would come from an inhibitory receptor excluding GABARs or GlyRs.

2.7 Light Stimulation

During patch clamp recordings, I measured light-evoked inhibitory and excitatory postsynaptic currents and inhibitory postsynaptic currents using a full-field light stimulus presented with a light emitted diode (LED) positioned above the patched cell. The LED emitted a photopic stimulating luminance of $3.7E^{03} R^*$ for all experiments. The light stimuli protocol consisted of a 30ms light presentation followed by a 2 second interstimulus interval followed by a 2 seconds light stimulus. A protocol consisted of 5 total presentations with a period of 15.25 seconds in between repeats. The responses to the five presentations were averaged and analyzed using Clampfit software (Molecular Devices, San Jose, CA). Statistical analyses were performed using GraphPad Prism (GraphPad, San Diego, CA).

2.8 Immunohistochemistry

After patch clamp recording, the pieces of retina with recorded and filled RGCs (Lucifer Yellow and neurobiotin) were fixed in 4% paraformaldehyde for 12 minutes, washed three times with 0.01 M phosphate buffer saline (PBS), and placed into a 24-well plate. Retina pieces were incubated in blocking solution consisting of PBX (0.5% Triton-X 100 in PBS) and 10% normal serum (donkey or goat) for 60 minutes. Each retina piece was then reacted with a combination of primary antibodies to stain for the either GlyR α 1, GlyR α 2, GlyR α 3, or GlyR α 4 or a combination of two GlyR α Xs, and Lucifer yellow overnight at 4°C (Table 2.2). In the case where the Lucifer yellow antibody was not compatible, streptavidin was used to stain for the filled cell, but was added with the secondary antibodies. The single GlyR antibody or combination of GlyR antibodies were selected based on our observed τ_{decay} estimates that we matched with the τ_{decay} estimates from the

literature (Table 3.2) (Gill et al., 2006; Majumdar et al., 2007; Majumdar et al., 2009; Veruki et al., 2007; Wassle et al., 2009) The primary antibodies were washed off by a series of washes with PBX. Afterwards, a combination of secondary antibodies and Hoechst stain (or also streptavidin) in normal serum was added to label the primary antibodies and it was left on the tissue overnight at 4°C (Table 3.2). The Hoechst stain was used to label the DNA in the somas and distinguish between the retina nuclear and plexiform layers. The tissue was then washed with PBS and mounted onto a slide and covered using VECTASHIELD (Vector Labs, Burlingame, CA) clear mounting medium and a coverslip.

Table 2.2. List of Antibodies Used for Immunohistochemistry Experiments

Ab host / type	Target	CONC.	Manufacturer	Catalog No.
mouse monoclonal 1°	GlyR α 1	1:500	Synaptic systems	Cat # 146 111
goat polyclonal 1°	GlyR α 2	1:50	Santa Cruz Biotech.	Cat #SC17279
rabbit polyclonal 1°	GlyR α 3	1:100	Chemicon	Cat# AB5472
rabbit polyclonal 1°	GlyR α 4	1:100	Chemicon	Cat# AB9696
Rabbit polyclonal 1°	Lucifer yellow	1:1000	ThermoFisher	Cat# A-5750
donkey / Alexa 555 2°	anti-mouse	1:200	Life Technologies	Cat# A31570
donkey / Cy3 2°	anti-goat	1:200	JAX ImmunoResearch	Cat# 115165003
goat / Cy3 2°	anti-mouse	1:200	JAX ImmunoResearch	Cat# 111165003
goat / Cy3 2°	anti-rabbit	1:200	JAX ImmunoResearch	Cat# 705165003
DAPI (Vectashield)	DNA cong.	1.5 μ g/ml	Vector Laboratories	Cat# H-1500
Hoescht	DNA cong.	1:1000	Life technologies	Cat# H3570

The recorded and filled RGCs in the mounted tissue were imaged using an Olympus FV1000 confocal microscope. Whole RGC images were acquired using a 40x water immersion (NA 1.15) objective, and dendrites and puncta expression were acquired using a 60x oil immersion objective (NA 1.4). Images were recorded

with Fluoview software (Olympus, Tokyo, Japan). The depths of the RGC's dendritic ramifications were measured relative to the top of the GCL and the bottom of the INL. Combining a RGC's dendritic ramification depth, dendrite arbor diameter, and light response help identify and verify specific RGC types.

2.9 Electrophysiology Recording Analysis

The Mini Analysis program (Synaptosoft, Decatur, GA) was used to identify sIPSCs and determine their decay time constant " τ ." In raw recordings, an sIPSC was defined as a waveform whose peak exceeded twice the root mean squared (RMS) of the noise in the system (the noise in our system was usually between 1.5 and 5.0 pA). Single sIPSCs were detected from a template that had a fast monotonic rise time to a single peak, and an exponential decay (Figure 1.5). The 10-90% rise time, and frequency of these sIPSCs were measured and their decay kinetics were estimated from a least-square fit of 10-90% of the decay phase, using a single exponential decay function. The goodness of fit was determined by comparing to a least-square fit of 10-90% of the decay phase a single to a double exponential function. All of the sIPSCs included in further analyses met these criterion and were used to calculate the average decay tau (τ_{decay}), again using a single exponential fitting to a least-square fit of 10-90% of the decay phase (Figure 1.5). Only sIPSCs that represented isolated events were used to calculate the τ_{decay} of glycinergic sIPSCs. The τ_{decay} of the average glycinergic sIPSC from each cell was also fit to both a single exponential and a double exponential. The R squared values for the single and double exponentials were always similar, indicating the single exponential was a sufficient fit to the average sIPSC. The

sIPSC τ_{decay} data was plotted in cumulative frequency distributions, frequency distributions, and average sIPSC τ_{decay} per cell. These τ_{decay} distributions were compared across cells classes in WT, KO, and injected animals using the Kolmogorov–Smirnov test. The number of sIPSCs measured in 100sec was used to determine the frequency of sIPSCs/sec for each cell. The mean frequencies for each cell type were compared across other cell classes in WT, KO, and injected animals using a one-way ANOVA with a Bonferroni *post-hoc* test.

CHAPTER III

EXPRESSION OF DISTINCT GLYCINE RECEPTOR SUBUNITS IS FOUND ACROSS IDENTIFIED RETINAL GANGLION CELL TYPES

INTRODUCTION

The retina is a laminar structure with each layer populated by specific classes of neurons. The vertical connections among these cells across layers form a variety of parallel circuits that encode the visual scene into electrical signals. The retinal ganglion cells (RGCs) represent the culmination of this signaling and their output forms the substrate for vision throughout the rest of the brain. There are about 40 different RGCs and they are defined by their genetic makeup, morphology, and visual responses (Baden et al., 2016; Bae et al., 2018; Masland, 2001; Sanes & Masland, 2015). The differences in the responses across the different types of RGCs arise from direct, feedforward inhibition as well as many forms of inhibition that modulate their excitatory input (Franke et al., 2017; Masland, 2012; Sanes & Masland, 2015; Werblin, 2011). Unlike most other areas of the CNS, the retina utilizes both GABA and glycine neurotransmitters and receptors in inhibitory processing (Franke & Baden, 2017; Werblin, 2011; C. Zhang et al., 2015).

Where GABA receptors are heteropentamers composed of a combination of five of 17 different subunits (α , β , γ , δ , and ρ subunits) glycine receptors

(GlyRs) have a simpler composition (Bormann, 2000; Yang, 2004). Retinal GlyRs are heteropentamers with three of the same β subunits and two of the same α subunits, in a stoichiometry of $3\beta:2\alpha$. (Betz & Laube, 2006; Grudzinska et al., 2005; Nobles et al., 2012). There are four different α subunits (α_1 , α_2 , α_3 , and α_4) that underlie four different GlyRs isoforms: GlyR α_1 , GlyR α_2 , GlyR α_3 , and GlyR α_4 (Dutertre et al., 2012; Wassle et al., 2009). The rise time of the glycinergic sIPSCs across the four GlyRs is similar; the 10% to 90% of peak rise time ranges between 1 and 3ms (Wassle et al., 2009; Weiss et al., 2008). In contrast, the decay kinetics (τ_{decay}) of GlyR sIPSCs mediated by the four isoforms differs. At room temperature their decays have been measured as: fast GlyR α_1 (2-4 ms), medium GlyR α_3 (~10ms) to slow GlyR α_2 and GlyR α_4 (20-40 ms) (Lynch, 2004; Majumdar et al., 2007; Majumdar et al., 2009).

In the mature spinal cord, brain stem, and sub-cortical regions, GlyR α_1 is the primary glycinergic isoform with GlyR α_3 expressed to a lesser extent (Lynch, 2004, 2009). In contrast, all four α subunit isoforms are expressed in the retina. The pattern of expression of each of the GlyRs differs across the inner plexiform layer (IPL) (Nobles et al., 2012; Wassle et al., 2009). Both the expression of these subunits and their pattern of expression is conserved across a broad range of species such as zebrafish to non-human primates (David-Watine et al., 1999; Harvey et al., 2000; Leacock et al., 2018; Matzenbach et al., 1994). GlyR α_1 expression is found throughout the IPL, with its densest expression in the OFF sublamina, where it is localized on the OFF cone bipolar cells (Haverkamp et al., 2004; Nobles et al., 2012). GlyR α_2 expression is dense and uniform throughout

the IPL (Haverkamp et al., 2004; Nobles et al., 2012). GlyR α 3 is expressed in three distinct lamina across the IPL and it has been suggested this pattern indicates GlyR α 3 is involved in different glycinergic circuits (Haverkamp et al., 2003; Haverkamp et al., 2004; Nobles et al., 2012). GlyR α 4 is expressed in a thin band along the top of the ON sublamina of the IPL and co-localizes with the ON Choline Acetyltransferase (ChAT) band associated with ON starburst amacrine cells (SACs) (Heinze et al., 2007; Nobles et al., 2012).

Subunit specific GlyR expression has been identified in several retinal cell classes. OFF cone and rod bipolar cells express GlyR α 1 (Eggers et al., 2007; Haverkamp, 1995; Sassoe-Pognetto, Wassle, & Grunert, 1994). Some subsets of the narrow-field cells, such as AC type 5/6 and type 7 express GlyR α 2 (Majumdar et al., 2009; Weiss et al., 2008). But this is not the rule, AII amacrine cells, which also are narrow-field, express GlyR α 3 and possibly GlyR α 1 (Demb & Singer, 2012; Gill et al., 2006; Majumdar et al., 2009; Weiss et al., 2008), and the GABAergic wide-field SACs express GlyR α 4 (Haverkamp et al., 2004; Majumdar et al., 2007; Weiss et al., 2008). Among the α RGCs, GlyR α 1 is expressed by OFF α RGCs (Majumdar et al., 2007; Sun, Li, & He, 2002; Veruki et al., 2007; C. Zhang et al., 2014). This then suggest that GlyR α subunit specific inhibition is diverse across retinal cell types and because of their different decay kinetics could represent additional diversity of inhibitory processing that is likely to influence visual processing.

To begin to expand our view of the role glycine subunit specific inhibition, we characterized the rise and decay kinetics of GlyR α mediated synaptic events,

e.g., glycinergic spontaneous inhibitory postsynaptic potentials (sIPSCs) in eight identified wild type (WT) RGC types. In addition, we examined GlyR α subunit specific expression, using immunohistochemistry. Based on these characteristics, we formulated hypotheses about the composition of GlyR α subunits in each of these eight RGCs types. We tested our ideas by altering GlyR α subunit specific expression, using global GlyR α 2, 3 or 4 knockout (KO) mice and retrogradely transported rAAV shRNA to knockdown expression of GlyR α subunits within mature RGCs.

We found significant GlyR α subunit diversity across identified RGCs. Like OFF α RGCs, the other three α RGCs (those with the largest somas/dendritic arbors) also expressed GlyR α 1 (Farrow et al., 2013; Krieger, Qiao, Rousso, Sanes, & Meister, 2017; Majumdar et al., 2007; Sanes & Masland, 2015). In contrast, the other six RGC types that we studied (e.g., local edge detectors, high definition, ultra-high definition, F-mini OFF transient, Junction adhesion molecule “B” (J-RGCs) (Jacoby & Schwartz, 2017; Liu & Sanes, 2017; Rivlin-Etzion et al., 2011; Rousso et al., 2016; Sanes & Masland, 2015) as well as the ON SACs expressed two different GlyR α s. In some, the decay kinetics were similar (both fast or both slow) and in other RGCs, the decay kinetics differed (one fast and one slow). Thus, GlyR diversity is likely to be the basis for enhanced subunit specific inhibition in the modulation of RGC visual responses.

MATERIALS AND METHODS

Animals

We used cell type specific mouse reporter lines to target RGCs for these analyses (Table 1). All experiments followed the ARVO Statement for the Use of Animals in Ophthalmic and Visual Research and were approved by the Institutional Animal Care and Use Committee (IACUC) of the University of Louisville. We induced GFP expression in *JAM-B-CreER* mice by daily intraperitoneal injections of 100 μ l of 20 mg/ml tamoxifen solution (100mg of tamoxifen (Sigma-Aldrich, St. Louis, MO) in 5 ml corn oil) for three days.

Table 3.1. List of Animal Lines and their Labeled Cells Used for Experiments

Mouse line	KO crosses	cell types labeled	References
<i>B6-Pvalb^{tm1(cre)Arbr/J/Thy1^{STP}-EYFP (Pv^{Cre}/Thy1^{STP})}</i>	<i>Gla2^{-/-}, Gla3^{-/-}, Gla4^{-/-}, Gla2^{-/-}/Gla3^{-/-}, Gla2^{-/-}/Gla4^{-/-}</i>	ON α , ON ^{Trans} , OFF α , OFF δ , ooDS RGC,	Hippenmeyer et al. 2005, Zhang et al. 2014 Farrow et al., 2013
TYW7		OFF α , OFF δ	(I. J. Kim, Zhang, Meister, & Sanes, 2010)
TYW3 (W3)	<i>Gla3^{-/-}</i>	LED, HD1, HD2, UHD	(Jacoby & Schwartz, 2017; I. J. Kim, Zhang, Meister, & Sanes, 2010; Y. Zhang, Kim, Sanes, & Meister, 2012)
ChAT-cre/Ai9	<i>Gla2^{-/-}, Gla4^{-/-}, Gla2^{-/-}/Gla4^{-/-}</i>	Displaced ON starburst amacrine cell	ChAT-cre (Jackson Laboratory) (Rossi et al., 2011) Ai9 (Allen Institute)
JAM-B-CreER	<i>Gla2^{-/-}, Gla2^{-/-}/Gla4^{-/-}</i>	Intrinsically asymmetric orientation selective RGCs	(Liu & Sanes, 2017)

Viral Vector Construction and Production

Methods to create the rAAV-*Gla1*-shRNA have been published (Zhang et al 2014), and are briefly described here. Serotype 2/7 recombinant rAAVs were made using a standard triple-plasmid protocol by a transient co-transfection of an vector plasmid, rAAV helper plasmid (harboring Rep/Cap), and Ad-helper plasmid (pGHTI-aden01) into HEK293T cells. The rAAV vector plasmid was a pGFP-V-RS vector, Origene, Rockville, MD), which included: flanking Inverted terminal repeats,

elongation factor-1 promoter, a tdTomato gene with a nuclear localization sequence, woodchuck hepatitis post-transcriptional regulatory element, a polyadenylation site to protect the mRNA from degradation, the H1 promoter and the 21mer *Gira1*-shRNA cassette (Figure 1). The transfected cells were cultured in high-glucose DMEM supplemented with 10% fetal bovine serum, 2 mM L-glutamine, 50 IU/ml penicillin, and 50 µg/ml streptomycin. The packaged rAAVs were concentrated and purified from the total cell lysate using iodixanol gradient centrifugation and collected in the 40% iodixanol band. Genome copy number titration was evaluated using RT-PCR (Applied Biosystems, TaqMan reagents). The titer of the rAAV-*Gira1*-shRNA was 3.5×10^{12} vg/ml.

Viral Injections in the Dorsal Lateral Geniculate Nucleus or Superior Colliculus

Methods to inject virus into the dLGN have been published (C. Zhang et al., 2014) and also are described briefly. In addition, we also injected virus into the superior colliculus (SC), using a similar approach. Mice were anesthetized, placed on a feedback controlled heating pad to maintain body temperature at ~ 36°C and their heads were secured in a stereotaxic with ear cups and a bite bar. Eyes were lubricated with 1.3% polyvinyl alcohol and the corneas protected from dehydration with plastic contact lenses. All injections used stereotaxic coordinates (Paxinos & Franklin, 2004) to locate the craniotomy over either the dLGN or the SC. For SC injections, a midline incision was made in the skin over the skull, and a craniotomy was performed at 0.5 mm anterior and 0.5 mm temporal to Lambda. A borosilicate glass pipette (interior diameter of 40-50µm), filled with ~10 µL of Ringer's solution, was positioned over the craniotomy and lowered between 800µm and 1200µm

from the surface. The dLGN or SC was located by recording visually evoked spiking activity as the pipette was lowered. The depth was recorded where clear visually evoked responses were obtained and the Ringer's pipette was removed. A second pipette (interior diameter of 18-22 μm), filled with 3.0 μL of virus was positioned at the same stereotaxic coordinates as the Ringer's filled pipette and at the same depth. Light-evoked responses also were used to refine pipette placement. Using light pressure, 2-2.5 μL of virus was injected into the SC. Mice were recovered from anesthesia, the incision was closed with skin glue (VetBond, 3M, St. Paul, MN) and the animal was given a subcutaneous 100 μl dose of Carprofen (1.25 mg/ml) (Putney, Portland, ME). Four weeks post injection, retinas were dissected, quartered, and mounted for whole cell patch clamp.

Immunohistochemistry

After patch clamp recording, the pieces of retina with recorded and filled RGCs (Lucifer Yellow and neurobiotin) were fixed in 4% paraformaldehyde for 12 minutes, washed three times with 0.01 M phosphate buffer saline (PBS), and placed into a 24-well plate. Retina pieces were incubated in blocking solution consisting of PBX (0.5% Triton-X 100 in PBS) and 10% normal serum (donkey or goat) for 60 minutes. Each retina piece was then reacted with a combination of primary antibodies to stain for the either GlyR α 1, GlyR α 2, GlyR α 3, or GlyR α 4 or a combination of two GlyR α s, and Lucifer yellow overnight at 4°C (Table 1). In the case where the Lucifer yellow antibody was not compatible, streptavidin was used to stain for the filled cell, but was added with the secondary antibodies. The single GlyR antibody or combination of GlyR antibodies were selected based on our

observed τ_{decay} estimates that we matched with the τ_{decay} estimates from the literature (Table 3.2) (Gill et al., 2006; Majumdar et al., 2007; Majumdar et al., 2009; Veruki et al., 2007; Wassle et al., 2009) The primary antibodies were washed off by a series of washes with PBX. Afterwards, a combination of secondary antibodies and Hoechst stain (or also streptavidin) in normal serum was added to label the primary antibodies and left on the tissue overnight at 4°C (Table 3.2). The Hoechst stain was used to label the DNA in the somas and distinguish between the retina nuclear and plexiform layers. The tissue was then washed with PBS and mounted onto a slide and covered using Vectashield (Vector Labs, Burlingame, CA) clear mounting medium and a coverslip.

Table 3.2. Primary and Secondary Antibodies used for Immunohistochemistry

Ab host / type	Target	CONC.	Manufacturer	Catalog No.
mouse monoclonal 1°	GlyR α 1	1:500	Synaptic systems	Cat # 146 111
goat polyclonal 1°	GlyR α 2	1:50	Santa Cruz Biotech.	Cat #SC17279
rabbit polyclonal 1°	GlyR α 3	1:100	Chemicon	Cat# AB5472
rabbit polyclonal 1°	GlyR α 4	1:100	Chemicon	Cat# AB9696
Rabbit polyclonal 1°	Lucifer yellow	1:1000	ThermoFisher	Cat# A-5750
donkey / Alexa 555 2°	anti-mouse	1:200	Life Technologies	Cat# A31570
donkey / Cy3 2°	anti-goat	1:200	JAX ImmunoResearch	Cat# 115165003
goat / Cy3 2°	anti-mouse	1:200	JAX ImmunoResearch	Cat# 111165003
goat / Cy3 2°	anti-rabbit	1:200	JAX ImmunoResearch	Cat# 705165003
Hoescht	DNA cong.	1:1000	Life technologies	Cat# H3570
Streptavidin-Cy2	Neurobiotin	1:1000	JAX ImmunoResearch	Cat# 016220084

Confocal Image Acquisition and Colocalization Analysis

We imaged the filled RGCs, using an Olympus Fluoview FV1000 confocal microscope with Fluoview software (Olympus, Tokyo, Japan) and characterized

their soma and dendritic morphology. The depths of the RGC's dendritic ramifications were measured relative to the top of the RGC layer and the bottom of the INL. The dendritic arbor diameter was measured using the polygon measurements tool in the Fluoview software. Each RGC's dendritic ramification depth, dendritic arbor diameter, and light response were used to identify the specific RGC type. Individual dendrites and puncta expression were imaged with a 60x oil immersion objective (NA 1.4).

Expression of individual GlyR α subunits was evaluated using Imaris software (Bitplane, Zurich, CH) on filled RGCs after immunohistochemical reactions. To improve the sensitivity of our image analysis, images of cell dendrites and GlyR puncta were deconvolved using constrained iterative deconvolution in cellSens (Olympus, Tokyo, Japan). GlyR puncta (color channel 1) coincident on or within dendritic processes (color channel 2) were counted and the length of the dendritic process was measured using the Filaments tool. The counting process was performed using one of two methods. The Imaris puncta co-localization tool was used to count the puncta for the: ON α RGCs, ON^{Transient} RGCs, OFF δ RGCs, the GlyR α 3 expression on the F-mini RGCs, and the ON SACs. The Imaris surfaces (to identify puncta) and surface to filament co-localization tools were used to count puncta on the: LED, UHD, HD, and for the expression measurement of GlyR α 2 on the F-mini RGCs. To determine specificity of the coincident puncta, the puncta channel (channel 1) was rotated along its x/y axis and coincident GlyR puncta were recounted. The “rotated” puncta represent an estimate of coincident expression, i.e. puncta not expressed on the dendrite of the filled cell. The original

puncta count was compared to the random puncta count using a one-tailed paired t-test to verify positive puncta expression on the dendrite. Finally, the rotated coincident puncta was subtracted from the “original” puncta density to provide an estimate of “corrected” puncta density.

Whole Mount Retinal Preparation for Electrophysiological Recordings

Animals were dark adapted for 30 minutes, given an IP injection of a cocktail of ketamine and xylazine, and sacrificed using cervical dislocation. The eyes were enucleated, the front of the eye removed and the retinas dissected under dim red light at room temperature. The retina was incubated in a solution of Ringer’s with collagenase (241 units/mL) and hyaluronidase (34.5nM per mL) (Worthington Biochemicals, Lakewood, NJ) for 10 minutes to break down and remove the vitreous attached to the retina. Remaining vitreous was carefully removed and retinas were washed 3 times with fresh oxygenated Ringers to eliminate the enzymes. Retinal whole mounts were quartered and each piece was placed RGC side up onto a cover slip and placed into an oxygenated chamber until used. To record from RGCs, a harp was placed on top of the retina to stabilize it and the coverslip was placed into a chamber (Cell MicroControls, Norfolk, VA) on the stage of the microscope. Wholemounds were continuously bathed in an oxygenated Ringer’s solution at 36°C. The Ringer’s solution was preheated to 36° and the exact temperature in the chamber controlled by a feedback controller (Cell MicroControls, Norfolk, VA) in the chamber.

Electrophysiology and Pharmacology

Recordings were performed under light-adapted conditions. Either GFP fluorescent RGCs, or GFP fluorescent RGCs with rAAV infected nuclei, positive for tdTomato expression, were targeted for whole cell patch recordings to record spontaneous inhibitory postsynaptic currents (sIPSCs). Oxygenated Ringer's bath solution (in mM: 125 NaCl, 2.5 KCl, 2.0 CaCl₂, 1.0 MgCl₂, 20 D-glucose, and 1.25 NaH₂PO₄, and 26 NaHCO₃) (Sigma-Aldrich, St. Louis, MO) was held at 36°C using an NBD TC2 BIP (Bipolar) temperature controller (Cell MicroControls, Norfolk, VA). The intracellular pipette solution consisted of (in mM: 12.5 CsCl, 107 CsOH, 107 D-Gluconic Acid, 10 Na⁺ HEPES, 10 BAPTA, 5 QX-314(Br), 4 ATP, and 0.5 GTP). The solution also contained either (in mM: 2.2 Lucifer yellow or 12.4 neurobiotin), which labelled the RGC's complete dendritic arbor morphology. After obtaining a gigaohm seal, the membrane was broken with swift negative pressure and the membrane potential (V_{Hold}) was held at -60 mV. All recordings were sampled at 10 kHz and were filtered using a 4-pole Bessel filter.

Holding the RGC membrane potential at +15 mV (0mV after correcting for the liquid junction potential), the reversal potential for cations, we isolated and recorded inhibitory sIPSCs for 100 seconds in control Ringer's solution. The RGC membrane potential was stepped to -60 mV and GABA_A and GABA_CR antagonists (picrotoxin (PTX) [20 μM], and (1,2,5,6-Tetrahydropyridin-4-yl)methylphosphonic acid (TPMPA) [50 μM], respectively) were added to the bath solution (Ringer's) for ten minutes. The RGC membrane potential was stepped back to +15 mV and isolated glycinergic sIPSCs were recorded for 100 seconds. At the end of this recording, we added the GlyR antagonist (strychnine (STRYCH) [10 μM]) to the

bath with the GABA antagonists for 5 minutes, recorded residual sIPSCs for 100 seconds to verify if all sIPSCs were eliminated.

Visual Stimulation

Immediately after a whole cell configuration was achieved, we determined the visually evoked responses of the RGC using a full field light stimulus. From this response we classified RGCs as ON, OFF or ON/OFF where the cell responded to the ONset of the light stimulus, the OFFset of the light stimulus, or both.

Electrophysiological Analysis

We used Mini Analysis software (Synaptosoft, Decatur, GA) to identify sIPSCs and quantify their frequency, rise time, amplitude, and τ_{decay} from 100 second long voltage clamp recordings of ooDS RGCs held at the reverse cation potential. We first selected candidate sIPSC peaks whose amplitude exceeded a minimum threshold of twice the root mean squared (RMS) of the noise in each recording. The noise was usually between 1.5 and 5 pA. Each sIPSC that met this criterion was then evaluated using a model that has a fast rise time (10-90% peak, 1-6 ms), a single peak, and a single exponential decay time (peak to 37% of peak (D37), 2-120 ms). Each sIPSC that fit this model was counted as a sIPSC. From this analysis, the frequency of glycinergic sIPSCs is calculated by the software over the duration of the 100 second recording. Subsequently, isolated individual glycinergic sIPSCs, with single peaks only, were examined and the τ_{decay} and rise time of each sIPSC were measured using a single exponential. Double or multi-peaked sIPSCs were only included in the frequency data since they cannot be reliably measured for τ_{decay} or rise time. The data of the sIPSCs from each cell was

grouped with like cells and pharmacological conditions. The τ_{decay} times of the sIPSCs of these groups were compared using the Kolmogorov–Smirnov test. The mean τ_{decay} , rise time, frequency, and amplitude data of the sIPSCs of these groups were compared using a one-way Analysis of Variance, with a Bonferroni Post-Hoc test to compare the data for each cell type or the pharmacological condition or genotype in which it was recorded.

RESULTS

All α RGCs ($ON\alpha$, $OFF\alpha$, $OFF\delta$, and ON_T) Express $GlyR\alpha1$

Previously, we and others observed $GlyR\alpha1$ mediated sIPSCs and expression in $OFF\alpha$ RGCs (Zhang et al., Majumdar et al., 2007). We targeted GFP+ cells (in $PV^{Cre}/Thy1^{STP}$ or $W7$ retinas) (Farrow et al., 2013; Sanes & Masland, 2015) whose soma diameters were $> 15\mu\text{m}$ and characterized their $GlyR\alpha$ isoform-specific currents. Both reporter retinas contain GFP+ $OFF\alpha$, $ON\alpha$ and $ON\delta$ RGCs and the $PV^{Cre}/Thy1^{STP}$ reporter retina, also contains GFP+ ON_{Trans} (ON_T) RGCs (Krieger et al., 2017). We confirmed our previous observation that WT $OFF\alpha$ glycinergic sIPSCs have a mean decay time (τ_{decay}) of $2.6\pm 0.1\text{ms}$ ($OFF\alpha$, $N= 15$) (C. Zhang et al., 2014) (Figure 3.1A-E).

All of the characteristics of the glycinergic sIPSCs in the four α RGCs were similar (Figure 3.1; One-way Analysis of Variance, Bonferroni Post-Hoc tests). The mean τ_{decay} of glycinergic sIPSCs (Figure 1.1 B-E) were: $3.0\pm 0.2\text{ms}$ ($ON\alpha$, $N = 8$), $2.9\pm 0.2\text{ms}$ (ON_T , $N = 10$), and $2.7\pm 0.2\text{ms}$ ($OFF\delta$, $n = 8$) (Figure 3.1D; $p > 0.05$). The mean frequency of glycinergic sIPSCs were: 24.2 ± 2.5 ($ON\alpha$), 27.5 ± 3.6 (ON_T), 28.1 ± 2.4 ($OFF\alpha$), and 26.4 ± 5.3 events/sec ($OFF\delta$) (Figure 3.1F; $p > 0.05$). The

mean glycinergic sIPSC amplitudes were similar: 42.7 ± 6.0 (ON_{α}), 52.1 ± 10.0 (ON_T), 69.6 ± 14.3 (OFF_{α}), and 87.4 ± 18.0 pA (OFF_{δ}) (Figure 3.1G; $p > 0.05$). The mean glycinergic sIPSC rise times were similar: 1.7 ± 0.2 (ON_{α}), 1.3 ± 0.2 (ON_T), 1.7 ± 0.3 (OFF_{α}), and 1.9 ± 0.3 ms (OFF_{δ}) (Figure 3.1H; $p > 0.05$). Thus, we hypothesized that ON_{α} , ON_T , OFF_{α} , and OFF_{δ} RGCs express only GlyR α 1.

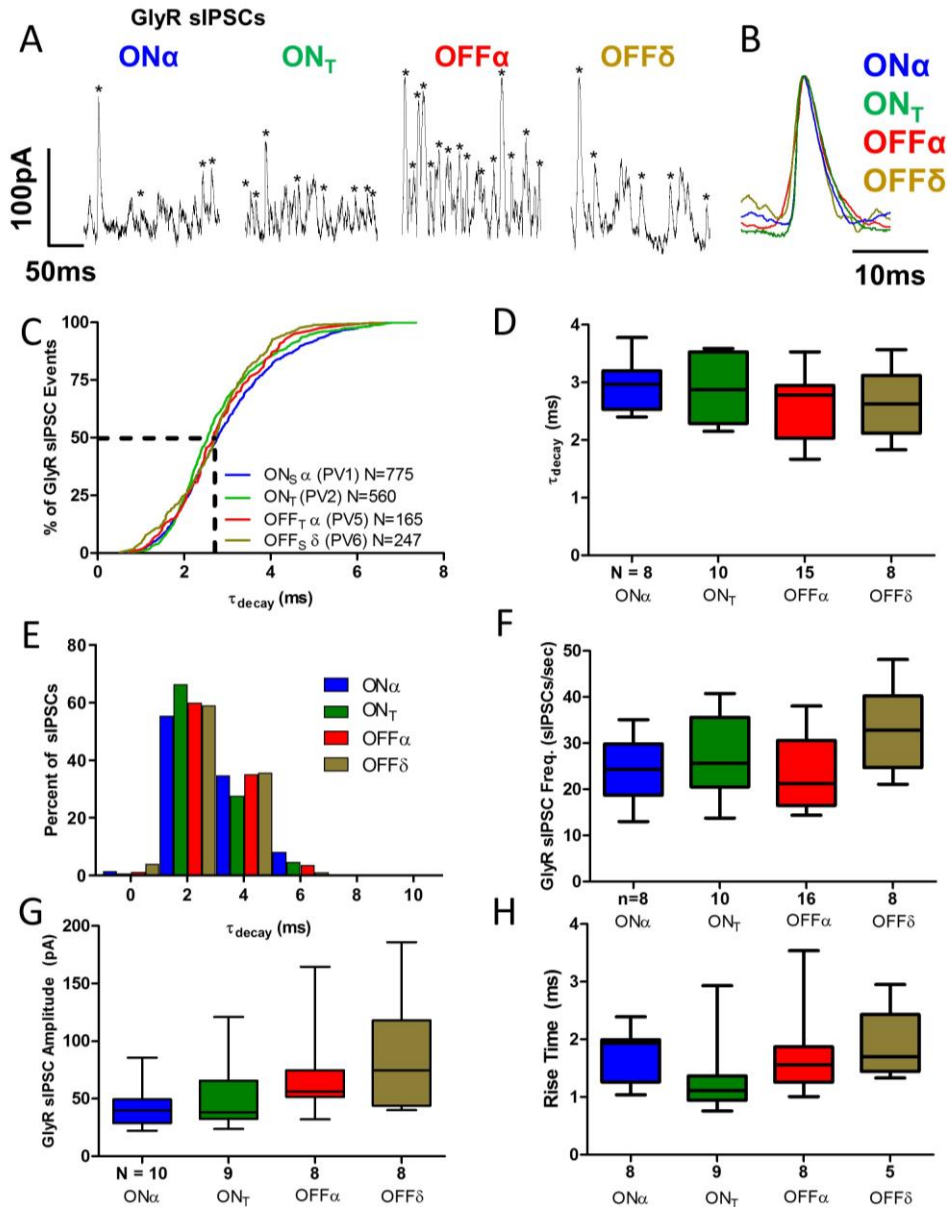


Figure 3.1. In WT RGCs with the largest soma diameters Glycinergic sIPSCs are fast and mediated by GlyR α 1 A) Raw traces of glycinergic sIPSCs of ON_{α} , ON_T , OFF_{α} , and OFF_{δ} RGCs in the presence of PTX and TPMPA to isolate GlyR-

mediated sIPSCs. The “ * ” indicates a glycinergic sIPSC. B) Average traces of glycinergic sIPSCs of ON α , ON τ , OFF α , and OFF δ RGCs. C) Cumulative distribution of glycinergic sIPSC τ_{decay} times (ms) for ON α , ON τ , OFF α , and OFF δ RGCs. The cumulative distributions among the different cell types were similar (Kolmogorov–Smirnov test $p < 0.05$). D) The Mean glycinergic sIPSC τ_{decay} for ON α , ON τ , OFF α , and OFF δ RGCs were all similar ($p > 0.05$, One-Way Analysis of Variance, Bonferroni Post-Hoc test) E) Frequency distribution of glycinergic sIPSC τ_{decay} times indicating a similar distribution among the ON α , ON τ , OFF α , and OFF δ RGCs. F) Mean glycinergic sIPSC frequency (events/sec) for was similar among the ON α , ON τ , OFF α , and OFF δ RGCs, ($p > 0.05$, One-Way Analysis of Variance, Bonferroni Post-Hoc test). G) The Mean glycinergic sIPSC amplitude among the ON α , ON τ , OFF α , and OFF δ RGCs was similar ($p > 0.05$, One-Way Analysis of Variance, Bonferroni Post-Hoc test). H) Mean glycinergic sIPSC rise time was similar among the ON α , ON τ , OFF α , and OFF δ RGCs ($p > 0.05$, One-Way Analysis of Variance, Bonferroni Post-Hoc test).

To validate our recording results, we assessed GlyR α 1 immunoreactivity on the dendrites of ON α , ON τ , OFF α , and OFF δ RGCs. We measured the GlyR α 1 puncta that colocalized with the dendrites of OFF α RGCs and confirmed our results 0.27 ± 0.03 puncta $\cdot \mu\text{m}^{-1}$ (OFF δ , N= 4 cells n=8 areas, data not shown) previously published results (C. Zhang et al., 2014). The average GlyR α 1-positive puncta density on OFF α RGCs was similar to 0.3 ± 0.03 (ON α , N=8, n=15), 0.14 ± 0.02 (ON τ , N=8, n=12), and 0.2 ± 0.02 puncta $\cdot \mu\text{m}^{-1}$ (OFF δ , N=9 n=16) (Figure 3.2C). We estimated randomly associated GlyR α 1-positive puncta and compared that density to the original co-localized puncta and found that the randomly associated puncta were significantly lower for each α RGC type (Figure 3.2C; $p < 0.001$). Finally, we estimated the puncta density by subtracting random from co-localized puncta and these also were similar across α RGCs: 0.15 ± 0.02 (ON α , N=2, n=4), 0.09 ± 0.02 (ON τ , N=2, n=3), and 0.13 ± 0.01 puncta $\cdot \mu\text{m}^{-1}$ (OFF δ , N=2, n=4) including the previously reported 0.21 ± 0.2 puncta $\cdot \mu\text{m}^{-1}$ (OFF α ; (C. Zhang et al., 2014). These

results are consistent with our electrophysiological recording and verify that only GlyR α 1 mediated glycinergic input is at α RGC synapses.

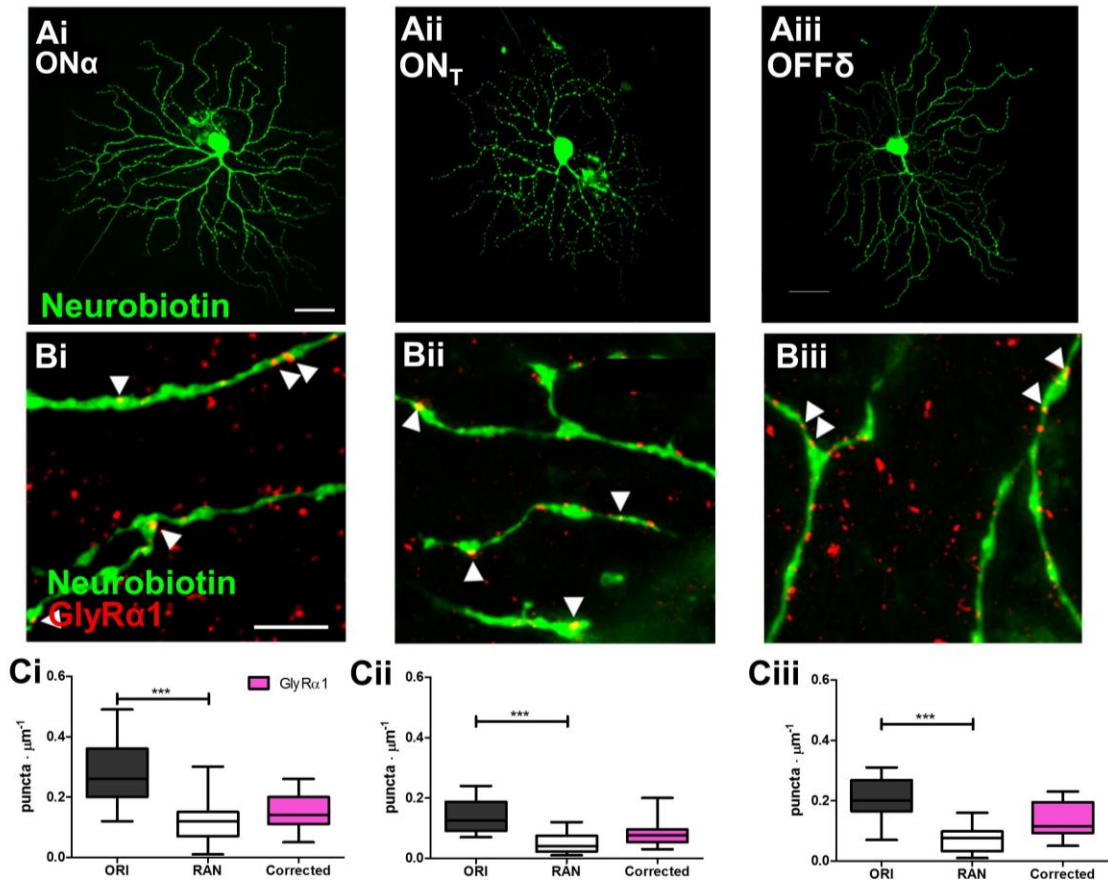


Figure 3.2. RGCs with the largest soma diameters Express GlyR α 1. Ai-Aiii) Wholemount images of ON α , ON τ , and OFF δ RGCs filled with neurobiotin (scale bar: 40 μm). Bi-Biii) Wholemount images of ON α , ON τ , and OFF δ RGC dendrites stained for GlyR α 1 expression (red) (Images and data sourced from (C. Zhang, 2015) (scale bar: 5 μm). White arrows indicate representative co-localization of GlyR α 1. Ci-Ciii) Dendrites in WT ON α , ON τ , and OFF δ RGCs have significantly more GlyR α 1 puncta density co-localization (μm^{-1}) in the original (ORI) orientation than coincidence co-localization in the flipped (RAN) orientation (Wilcoxon Matched-pairs T-test). The corrected puncta density for these cells: ON α is $0.15 \pm 0.02 \mu\text{m}^{-1}$, ON τ is $0.09 \pm 0.02 \mu\text{m}^{-1}$, and OFF δ is $0.13 \pm 0.01 \mu\text{m}^{-1}$.

rAAV-Mediated RNAi Eliminates GlyR α 1-Mediated sIPSCs in rAAV-Gla1-shRNA

Infected A RGCs

We used our successful knockdown approach (Zhang et al., 2014) to verify our observations that all four α RGCs expressed only GlyR α 1. We recorded glycinergic sIPSCs in α RGCs infected with rAAV-*Glr1*-shRNA (Zhang et al., 2014) to knockdown (KD) GlyR α 1 expression and compared frequency in WT to KD α RGCs. Representative recordings of GABAergic and glycinergic sIPSCs in control solution are illustrated in Figure 3.3A*i* and their absence is shown when the GABAergic antagonists PTX and TPMPA were added to the bath (3.3A*ii*). Virtually no glycinergic sIPSCs remained in rAAV-*Glr1*-shRNA infected α RGCs was: 0.7 ± 0.2 events/sec (ON α , N = 6), 0.9 ± 0.2 events/sec (ON τ , N = 9), $2.3.1 \pm 0.4$ events/sec (OFF α , N = 6), and 1.2 ± 0.4 events/sec (OFF δ , N = 4) (Figure 3.3B). On average the reduction in sIPSCs was (97.2% reduction (ON α), 96.8% (ON τ), 90.4% (OFF α), and 96.3% (OFF δ) (Figure 3.3A,B). These results show that ON α , ON τ , OFF α , and OFF δ RGCs express only GlyR α 1. Furthermore, the OFF α results are similar to those found in (C. Zhang et al., 2014) where a ~95% reduction in glycinergic sIPSC activity was found in the rAAV-*Glr1*-shRNA infected OFF α RGCs.

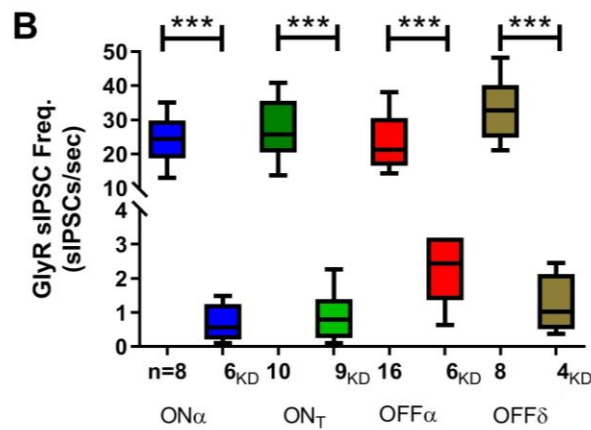
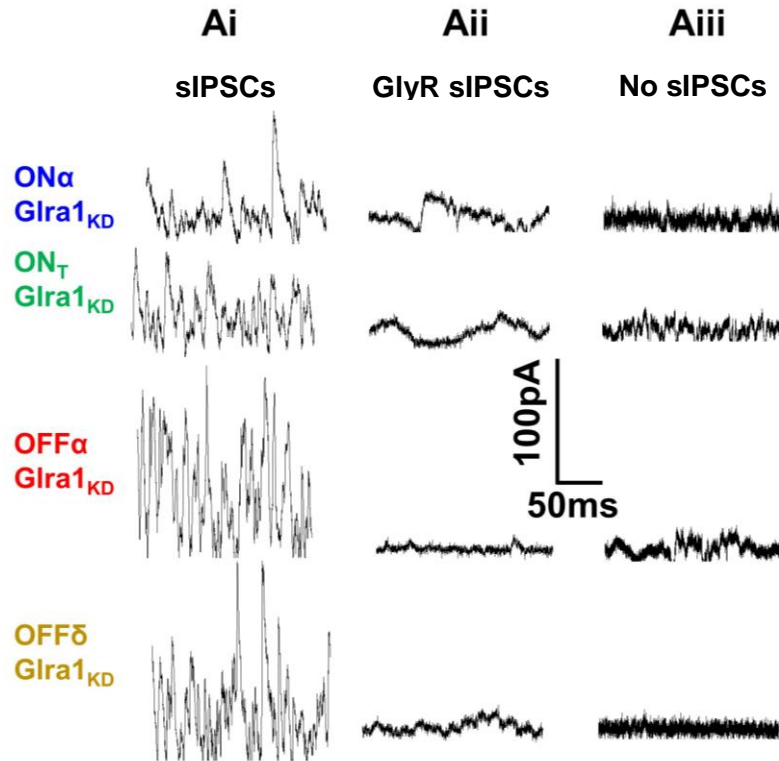


Figure 3.3. rAAV-*Glra1*-shRNA knocks down GlyR α 1 expression in alpha and delta RGCs. Ai) Raw traces of total sIPSCs of rAAV-*Glra1*-shRNA infected ON α , ON_T, OFF α , and OFF δ RGCs. Aii) Raw traces of glycinergic sIPSCs in rAAV-*Glra1*-shRNA infected ON α , ON_T, OFF α , and OFF δ RGCs recorded in the presence of TPMPA and PTX. The vast majority of glycinergic activity is depleted in these infected RGCs. Aiii) Raw traces recorded in rAAV-*Glra1*-shRNA infected ON α , ON_T, OFF α , and OFF δ RGCs in the presence of PTX/TPMPA/STYCH – no sIPSCs were observed. The vast majority of glycinergic activity is depleted in these infected RGCs. B) The mean glycinergic sIPSC frequency of both uninfected and infected ON α , ON_T, OFF α , and OFF δ RGCs. The mean infected

RGC glycinergic sIPSC frequency was significantly less than the mean uninfected RGC counterpart (** $p < 0.0001$, One-Way Analysis of Variance, Bonferroni Post-Hoc test)

rAAV-Mediated RNAi Eliminates GlyR α 1 Puncta Expression in Infected α RGCs

To validate the knockdown of *Glr1* expression, we quantified coincident GlyR α 1 puncta on the dendrites of rAAV-*Glr1*-shRNA infected α RGCs (Figure 3.3A,B). When compared to uninfected *PV^{Cre}/Thy1^{STP}* α RGCs, the rAAV-*Glr1*-shRNA infected RGCs showed significantly lower puncta density (Figure 3.4B, $p < 0.02$, Unpaired Mann-Whitney Test). When corrected for chance coincidence, there were very few GlyR α 1-immunoreactive coincident puncta on the dendrites. The average corrected GlyR α 1 puncta coincidence was -0.004 ± 0.002 (ON α), -0.006 ± 0.007 (ON τ), and 0.001 ± 0.005 puncta $\cdot \mu\text{m}^{-1}$ (OFF δ RGCs) (Figure 3.4B). Remaining GlyR α 1 puncta found throughout the IPL but not on RGC dendrites could be expression on amacrine or bipolar cells. Or, some GlyR α 1-positive puncta could also represent expression that was not fully eliminated by the *Glr1*-shRNA (C. Zhang et al., 2014).

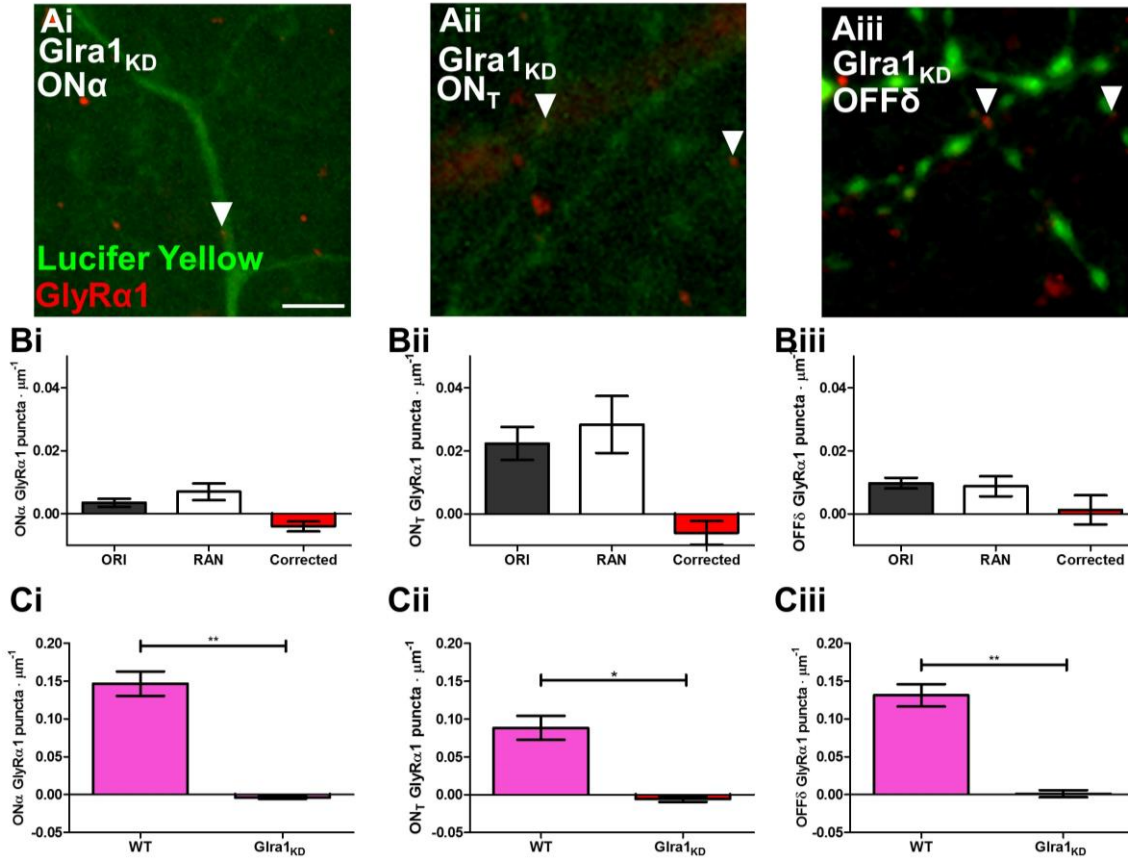


Figure 3.4. GlyR α 1 puncta expression is knocked down in rAAV-*Glra1*-shRNA infected ON α , ON T , and OFF δ RGCs. Ai-Aiii) Wholemount images of ON α , ON T , and OFF δ RGC dendrites (green) with GlyR α 1 expression (red) (scale bar: 5 μ m). White arrows indicate representative co-localization of GlyR α 1. Bi-Biii) Dendrites in ON α , ON T , and OFF δ RGCs with rAAV-*Glra1*-shRNA are similar between GlyR α 1 puncta density co-localization in the original (ORI) orientation and coincidence co-localization in the rotated (RAN) orientation (Wilcoxon Matched-pairs T-test). The corrected puncta density for these cells: ON α is $-0.004 \pm 0.002 \mu\text{m}^{-1}$, ON T is $-0.006 \pm 0.004 \mu\text{m}^{-1}$, and OFF δ is $0.001 \pm 0.005 \mu\text{m}^{-1}$. Ci-Ciii) The corrected puncta density for the *Glra1* KD rAAV ON α , ON T , and OFF δ RGCs is significantly lower than for WT RGCs (* $p < 0.05$, ** $p < 0.01$, Two-Tailed Mann Whitney U-test).

All Local Edge Detector, High Definition, and Ultra High Definition RGCs Express GlyR α 1 and GlyR α 3

We examined the glycinergic isoform-specific expression and sIPSCs in fluorescently labeled WT RGCs in W3 reporter mice (Jacoby & Schwartz, 2017; T.

Kim, Soto, & Kerschensteiner, 2015). The GFP+ RGCs include three functional types, local edge detector (LED), high definition (HD), and ultra-high definition (UHD) RGCs. We compared the WT data across individual RGC types to determine if they differed in their measured GlyR kinetics. We found no difference in the glycinergic sIPSCs among these cells and we combined their results for the remainder of the analysis (Supplemental Figure 1). The mean τ_{decay} of the glycinergic sIPSCs in all of the GFP+ RGCs was $7.5 \pm 0.2 \text{ms}$ (Figure 3.5C), which is similar to previously published values for GlyR $\alpha 3$ (Gill et al., 2006; Majumdar et al., 2007) and significantly longer than the mean τ_{decay} for α RGCs that express GlyR $\alpha 1$ (Figure 3.5B,C; $p < 0.003$, Two-tailed Mann Whitey U-test (C) Kolmogorov–Smirnov test $p < 1.3e^{-121}$ (D)). The frequency distribution of glycinergic sIPSC τ_{decay} times in W3 RGC appeared to display a skewed distribution (Figure 3.5D), indicating that not only the fast GlyR $\alpha 3$ mediates glycinergic synaptic events, but a GlyR α isoform with different kinetics may also play a role.

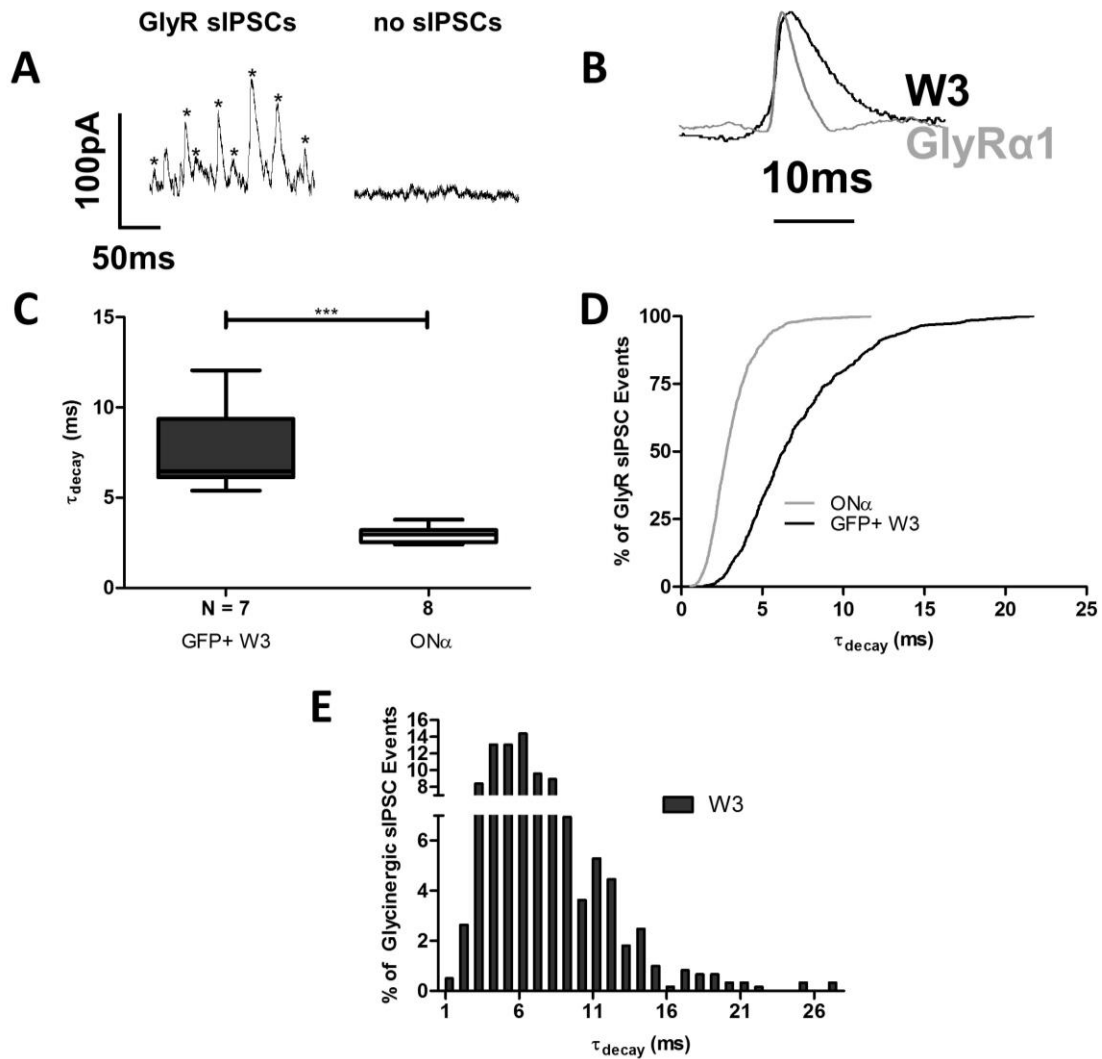


Figure 3.5. W3 RGCs appear to have GlyR α 3-mediated sIPSCs. A) Raw traces of W3 RGC glycinergic sIPSCs in PTX/TPMPA, and PTX/TPMPA/STRYCH. B) Average traces of W3 (black) and ON α (grey) RGC glycinergic sIPSCs. C) The mean glycinergic sIPSC τ_{decay} of W3 RGCs is significantly slower than the ON α RGCs (** p <0.003, Mann-Whitney U-test). D) Cumulative distributions of glycinergic sIPSC τ_{decay} times (ms) for W3 and ON α RGCs. The cumulative distribution of glycinergic sIPSC τ_{decay} in W3 RGCs is slower than the representative GlyR α 1 expressing ON α RGC (Kolmogorov–Smirnov test). E) Frequency distribution of glycinergic sIPSC τ_{decay} times for W3 RGCs (bin width is 1 ms).

WT W3 Glycinergic Synaptic Input is Mediated by GlyR α 3, Glycinergic sIPSC frequency is reduced in Glra3^{-/-} W3 RGCs

Our electrophysiological data is consistent with the expression of GlyR α 3 in WT GPF+ W3 RGCs. To test this hypothesis, we recorded glycinergic sIPSCs in *Gla3^{-/-}*/W3 retinas (Jacoby & Schwartz, 2017; I. J. Kim et al., 2010). The frequency of the glycinergic sIPSCs in *Gla3^{-/-}*/W3 RGCs (regardless of RGC type) was 9.6 ± 1.2 events/sec, which is significantly lower (~ 35%) than W3 WT RGCs, which was 13.1 ± 0.8 events/sec (Figure 3.6C; $p < 0.01$, One-way Analysis of Variance, Bonferroni Post-Hoc test). This result supports the idea that GlyR α 3 is expressed by W3 RGCs, and the substantial frequency of the remaining glycinergic sIPSCs indicates that a second glycine receptor also mediates synaptic events. None of the sIPSC kinetics in the *Gla3^{-/-}*/W3 differed significantly from WT. Further, the frequency distributions of the τ_{decay} of the WT and *Gla3^{-/-}* did not differ. Because neither decay frequency distribution had sIPSCs longer than 9ms, we hypothesized that GlyR α 1 also contributed to glycinergic synaptic input. We tested this hypothesis and examined the rise time, amplitude, and decay characteristics of the remaining glycinergic sIPSCs. The remaining sIPSCs in the *Gla3^{-/-}* were eliminated in the presence of strychnine (Figure 3.6A) In the *Gla3^{-/-}*/W3 RGCs the average glycinergic sIPSC rise time remained 3.3 ± 0.3 , which was the same as WT RGCs, 3.1 ± 0.3 (Figure 3.6D, $p > 0.05$, One-way Analysis of Variance, Bonferroni Post-Hoc test). The mean glycinergic sIPSC amplitude was 21.3 ± 2.7 pA, which was also similar to WT at 23.3 ± 1.4 pA (Figure 3.6E, $p > 0.05$, One-way Analysis of Variance, Bonferroni Post-Hoc test). The mean glycinergic sIPSC τ_{decay} in *Gla3^{-/-}*/W3 RGCs was 7.4 ± 0.9 ms, and was similar to 7.5 ± 0.9 ms in the WT (Figure 3.6F, $p > 0.05$, One-way Analysis of Variance, Bonferroni Post-Hoc test). The cumulative

glycinergic sIPSC τ_{decay} distribution of the remaining glycinergic sIPSCs of the *Gla3^{-/-}* W3 RGCs was also similar to the WT W3 RGCs (Figure 3.6F; Kolmogorov–Smirnov test, $p > 0.4$). However, since the *Gla3^{-/-}* W3 glycinergic sIPSC τ_{decay} distribution made no shift, it suggested the remaining glycinergic sIPSCs are mediated by GlyR α 1, whose mean τ_{decay} is ~ 3 msec (Figure 3.6F). If the distribution had shifted to the right it would indicate the remaining glycinergic sIPSCs were slow such as GlyR α 2 or GlyR α 4. We tested this idea and infected WT W3 retinas with rAAV-*Gla1*-shRNA.

Glycinergic sIPSC frequency is reduced in rAAV-Gla1-shRNA W3 RGCs

In rAAV-*Gla1*_{KD}-shRNA infected WT GFP+ W3 RGCs, the glycinergic sIPSC frequency was significantly lower than both WT and *Gla3^{-/-}* (2.5 ± 0.5 events/sec) (Figure 3.6C; $p < 0.0001$, One-way Analysis of Variance, Bonferroni Post-Hoc test) and the cumulative glycinergic sIPSC τ_{decay} in rAAV-*Gla1*-shRNA infected W3 RGCs was significantly slower than WT, (Figure 3.6F; Kolmogorov–Smirnov test, $p < 4.95e^{-13}$). The mean τ_{decay} was 10.1 ± 1.0 ms, and was similar to WT (Figure 3.6F, $p > 0.05$). Together these results indicate that GlyR α 1 mediated glycinergic synaptic inputs in W3 WT RGCs. In the absence of GlyR α 1 expression, did not alter either the rise time or the amplitude of the remaining glycinergic sIPSCs compared to WT. Average rise time was 2.5 ± 0.4 ms and amplitude was 26.9 ± 3.1 pA (Figure 3.6D, F; $p > 0.05$ for both, One-way Analysis of Variance, Bonferroni Post-Hoc test). To test the idea that both GlyR α 3 and GlyR α 1 are expressed and mediate sIPSCs, we infected *Gla3^{-/-}* W3 retinas with the rAAV-*Gla1*-shRNA, and characterized the remaining glycinergic sIPSCs.

Glycinergic sIPSCs are eliminated in rAAV-Glra1-shRNA/Glra3 KO W3 RGCs

Glycinergic sIPSCs were eliminated in *Glra3^{-/-}/Glra1_{KD}* W3 RGCs (0.4 ± 0.1 events/sec), which is statistically lower than WT and represents a 97% reduction of sIPSCs from WT (Figure 3.6C; $p < 0.0001$, One-way Analysis of Variance, Bonferroni Post-Hoc test). Together, these results indicate that W3 RGCs express both GlyR α 3 and GlyR α 1. The few glycinergic sIPSCs that remained in *Glra3^{-/-}/Glra1_{KD}* W3 RGCs, could result from an incomplete knockdown of GlyR α 1 receptors, consistent with our previous findings (Zhang et al., 2014).

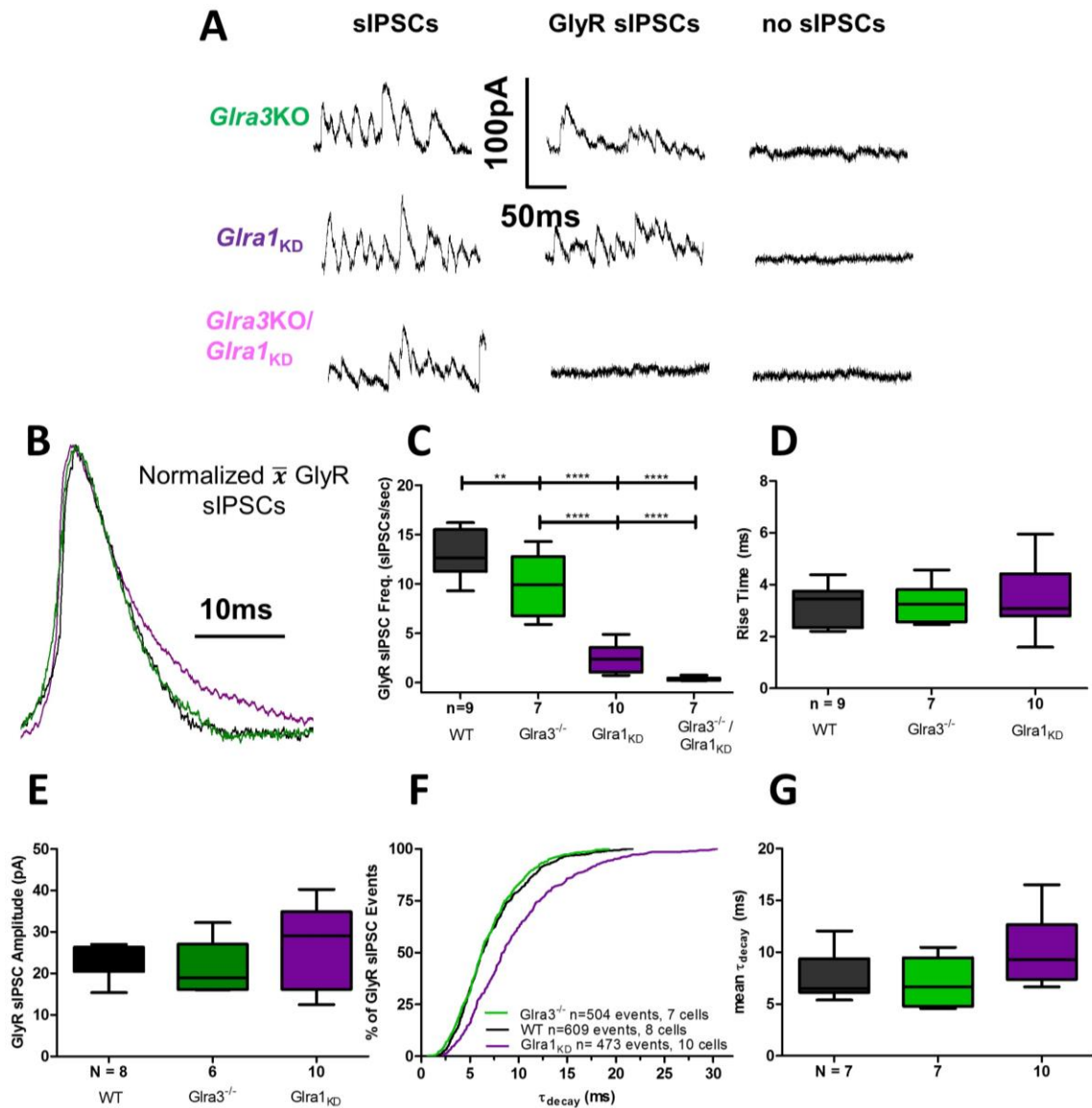


Figure 3.6. rAAV-mediated RNAi to *Glra1* eliminates GlyR α 1 sIPSC activity; *Glra3^{-/-}* eliminates GlyR α 3 sIPSC activity, in W3 RGCs. A) Raw traces of total, glycinergic (recorded in the presence of PTX/TPMPA), and strychnine sensitive (recorded in the presence of PTX/TPMPA/STRYCH) sIPSCs of *Glra3^{-/-}*, *Glra1_{KD}*, and *Glra3^{-/-}/*Glra1_{KD}** W3 RGC. B) Average traces of WT (black), *Glra3^{-/-}* (green), and *Glra1_{KD}* (purple) W3 RGC glycinergic sIPSCs. C) Mean glycinergic sIPSC frequency (events/sec) for WT, *Glra3^{-/-}*, *Glra1_{KD}* rAAV, and *Glra3^{-/-}/*Glra1_{KD}** rAAV W3 RGCs. The average glycinergic sIPSC frequencies of *Glra3^{-/-}* and *Glra1_{KD}* rAAV are significantly lower than WT, and the frequency in *Glra3^{-/-}/*Glra1_{KD}** rAAV is almost zero (One-Way Analysis of Variance with Bonferroni Post-Hoc test). D) Mean glycinergic sIPSC rise time (ms) for WT, *Glra3^{-/-}*, *Glra1_{KD}* rAAV W3 RGCs is similar (One-Way Analysis of Variance with Bonferroni Post-Hoc test). E) Average glycinergic sIPSC amplitude (pA) for WT, *Glra3^{-/-}*, *Glra1_{KD}* rAAV W3 RGCs is similar (One-Way Analysis of Variance with Bonferroni Post-Hoc test). F) Cumulative distribution of GlyR sIPSC decay times for WT (black), *Glra3^{-/-}* (green), and *Glra1_{KD}* (purple) W3 RGCs. G) Mean GlyR sIPSC decay time (ms) for WT, *Glra3^{-/-}*, and *Glra1_{KD}* rAAV W3 RGCs is similar (One-Way Analysis of Variance with Bonferroni Post-Hoc test).

Post-Hoc test). F) Cumulative distributions of glycinergic sIPSC τ_{decay} times (ms) for WT, *Gla1_{KD}*, and *Gla3^{-/-}* W3 RGCs. The cumulative distribution of glycinergic sIPSC τ_{decay} is significantly faster than WT in the *Gla3^{-/-}* and significantly slower than WT in the *Gla1_{KD}*AAV (Kolmogorov–Smirnov test). G) Mean τ_{decay} is similar among WT, *Gla1_{KD}*, and *Gla3^{-/-}* W3 RGCs (One-Way Analysis of Variance with Bonferroni Post-Hoc test).

GlyRa1 but not GlyRa3 expression on WT W3 dendrites

Immunohistochemical analysis were used to assess GlyRa3 and GlyRa1 expression in WT W3 RGCs. The density of GlyRa3 puncta that co-localized with W3 dendrites did not differ from randomly associated puncta (Figure 3.7B,Di). GlyRa3 expression is dense throughout the IPL, although in a laminar pattern, and our assay, microscope, and deconvolution analysis are sensitive enough to adequately image these puncta. The W3 RGCs have dense bushy dendrites, which confound this analysis, especially if the overall expression of GlyRa3 on these cells is low, as indicated in the fact that *Gla1_{KD}* reduces the glycinergic sIPSC frequency more than the *Gla3^{-/-}*. Similarly, immunohistochemical analysis showed GlyRa1 expression co-localizes with W3 dendrites in both the original and random configurations (Figure 3.7B,Dii). From our immunohistochemical analysis of GlyRa1 expression on α RGCs, GlyRa1 puncta expression is dense throughout the IPL and we successfully measured corrected puncta density. However, the W3 RGC bushy dense dendrites, and the possibility of low GlyRa1 expression on these cells, may prevent our immunohistochemical analysis from being sensitive enough to detect GlyRa1 puncta expression on W3 RGCs.

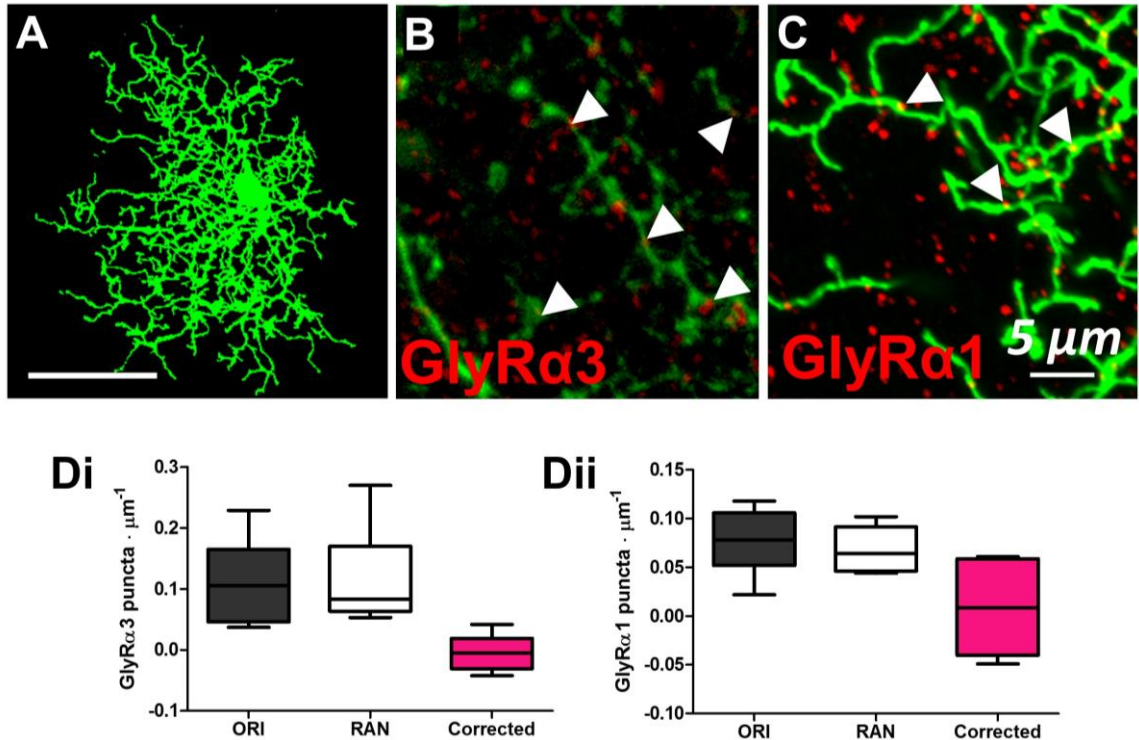


Figure 3.7. GlyRa1 and GlyRa3 puncta are not detectable on W3 RGCs (Ai-Aiii) Wholemount image of W3 RGC (UHD RGC) (scale bar: 40 μ m). B) Wholemount image of W3 RGC dendrites stained for GlyRa1 expression (red). White arrows indicate representative co-localization of GlyRa1. C) Wholemount image of Dendrites of W3 RGC dendrites stained for GlyRa3 expression (red) (scale bar: 5 μ m). Di) W3 RGCs have similar GlyRa3 puncta density co-localization (μm^{-1}) to coincidence co-localization in the flipped (RAN) orientation (Wilcoxon Matched-pairs U-test). The corrected puncta density of GlyRa3 for W3 RGCs is $-0.004 \pm 0.012 \mu\text{m}^{-1}$. Dii) W3 RGCs have similar GlyRa1 puncta density co-localization (μm^{-1}) with coincidence co-localization in the flipped (RAN) orientation (Wilcoxon Matched-pairs U-test). The corrected puncta density of GlyRa3 for W3 RGCs is $0.008 \pm 0.021 \mu\text{m}^{-1}$.

Asymmetric OFF τ (F-mini) WT RGCs Glycinergic Synaptic Input is Mediated by GlyRa2 and GlyRa3

We examined the glycinergic isoform-specific expression and synaptic currents in F-mini RGCs that are GFP+ in *PV^{Cre}/Thy1^{STP}* reporter mice. We identified F-mini RGCs among other GFP+ RGCs because of their small somas

(~10 μ m dia.), asymmetric dendritic arbor that ramified in the OFF sublamina of the IPL and their OFF_{Transient} visually-evoked responses. These cells also have been referred to as PV7 RGCs (Farrow et al., 2013; Rousso et al., 2016). In the presence of PTX [20 μ M] and TPMPA [50 μ M], the glycinergic sIPSCs in WT F-mini RGCs had an average τ_{decay} of 6.5 \pm 0.5 ms, similar to the average in W3 WT RGCs and to published τ_{decay} values for GlyR α 3 mediated sIPSCs (Figure 3.8A-C) (Gill et al., 2006; Majumdar et al., 2007). The frequency distribution of their τ_{decay} appears to be skewed and includes sIPSCs with decays slower than GlyR α 1 or > 3 msec. We considered that this could indicate expression of either GlyR α 2 or GlyR α 4 (Figure 3.8D).

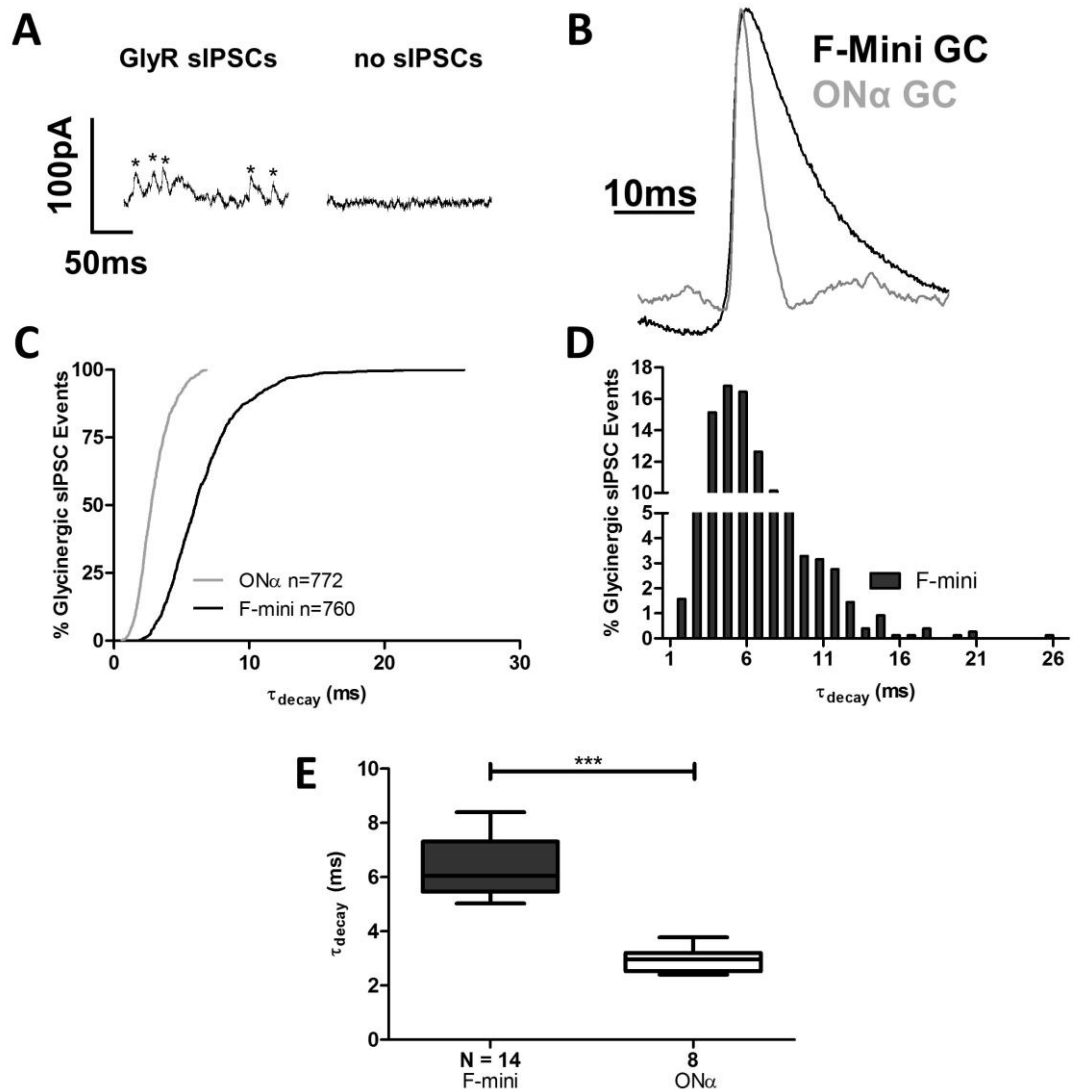


Figure 3.8. F-mini RGCs appear to have GlyR α 3-mediated sIPSCs. A) Raw traces of F-mini RGC glycinergic sIPSCs and strychnine sensitive sIPSCs. The “*” indicates a glycinergic sIPSC. B) Average traces of F-mini (black) and ON α (grey) RGC glycinergic sIPSCs. C) Cumulative distributions of glycinergic sIPSC τ_{decay} times (ms) for F-mini and ON α RGCs. The cumulative distribution of glycinergic sIPSC τ_{decay} in F-mini RGCs is slower than the representative GlyR α 1 expressing ON α RGC (Kolmogorov–Smirnov test). D) Frequency distribution of glycinergic sIPSC τ_{decay} times for F-mini RGCs (bin width is 1 ms). E) The mean glycinergic sIPSC τ_{decay} of F-mini RGCs is significantly slower than the ON α RGCs (Mann-Whitney U-test).

Glycinergic sIPSC frequency is reduced in Glra3^{-/-} F-mini RGCs

To test the hypothesis that WT F-mini RGCs express GlyR α 3, we recorded glycinergic sIPSCs in *Glr3*^{-/-} F-mini RGCs and found that their frequency was significantly lower compared to WT (4.4 \pm 1.1 vs. 14.1 \pm 1.3 events/sec; respectively; Figure 3.9C; $p < 0.0001$, One-way Analysis of Variance, Bonferroni Post-Hoc test). The average τ_{decay} of the remaining glycinergic sIPSCs (10.2 \pm 0.4 ms) was significantly slower than WT (Figure 3.9F, $p < 0.04$, One-way Analysis of Variance, Bonferroni Post-Hoc test) and the cumulative sIPSC τ_{decay} curve was shifted to larger values (Figure 3.9G, Kolmogorov–Smirnov test, $p < 2.3e^{-74}$). We characterized the remaining glycinergic sIPSCs and found their mean amplitude was significantly lower than WT (21.8 \pm 2.8 vs 31.8 \pm 2.6 pA; respectively; Figure 3.9E, $p < 0.002$, One-way Analysis of Variance, Bonferroni Post-Hoc test). Their rise time was similar to WT (2.5 \pm 0.4 vs 1.8 \pm 0.1 ms; respectively; Figure 3.9D, $p > 0.05$, One-way Analysis of Variance, Bonferroni Post-Hoc test). Together the data suggest that WT F-mini's express GlyR α 3 and one of the glycine α subunits with slow decay kinetics, GlyR α 2 or GlyR α 4.

Glycinergic sIPSC frequency is reduced in Glr2^{-/-} F-mini RGCs

To test the hypothesis that GlyR α 2 receptors mediate synaptic currents in F-mini OFF_{Transient} RGCs, we recorded sIPSCs in *Glr2*^{-/-} F-mini RGCs. The frequency of glycinergic sIPSCs was significantly less in *Glr2*^{-/-} F-mini RGCs (8.5 \pm 1.3 events/sec) compared to WT (14.1 \pm 1.3 events/sec); Figure 3.9C; $p < 0.0001$, One-way Analysis of Variance, Bonferroni Post-Hoc test). The average *Glr2*^{-/-} F-mini glycinergic sIPSC τ_{decay} (7.8 \pm 0.4 ms) was similar to WT (Figure 3.9G, $p > 0.05$, One-way Analysis of Variance, Bonferroni Post-Hoc test) and

surprisingly, their cumulative sIPSC τ_{decay} curve shifted significantly to slower values compared to WT (Figure 3.9F, Kolmogorov–Smirnov test, $p < 2.46e^{-10}$). This was surprising since GlyR α 3-mediated sIPSCs are slower than WT and we expected this curve to shift to slower values. The average rise time of the glycinergic sIPSCs in the *Gla2*^{-/-} F-mini RGCs was similar to WT and to *Gla3*^{-/-} (2.0 ± 0.1 ms; Figure 3.9D, $p > 0.05$, One-way Analysis of Variance, Bonferroni Post-Hoc test). The mean amplitude of *Gla2*^{-/-} F-mini RGCs glycinergic sIPSCs also was similar to WT (22.4 ± 3.0 pA; Figure 3.9E, $p > 0.05$, One-way Analysis of Variance, Bonferroni Post-Hoc test). These results suggest that both GlyR α 2 and GlyR α 3 mediate synaptic inputs in F-mini RGCs.

Glycinergic sIPSC frequency is eliminated in Gla2^{-/-}/Gla3^{-/-} F-mini RGCs

When we recorded glycinergic synaptic inputs in *Gla2*^{-/-}/*Gla3*^{-/-} double KO F-mini RGCs there were almost no sIPSCs (0.6 ± 0.3 events/sec a decrease of ~96%), which was significantly lower than WT and *Gla2*^{-/-} F-mini RGCs (Figure 3.9C; $p < 0.0001$, One-way Analysis of Variance, Bonferroni Post-Hoc test). These results combined with the puncta expression results demonstrate that F-mini RGCs express both GlyR α 2 and GlyR α 3.

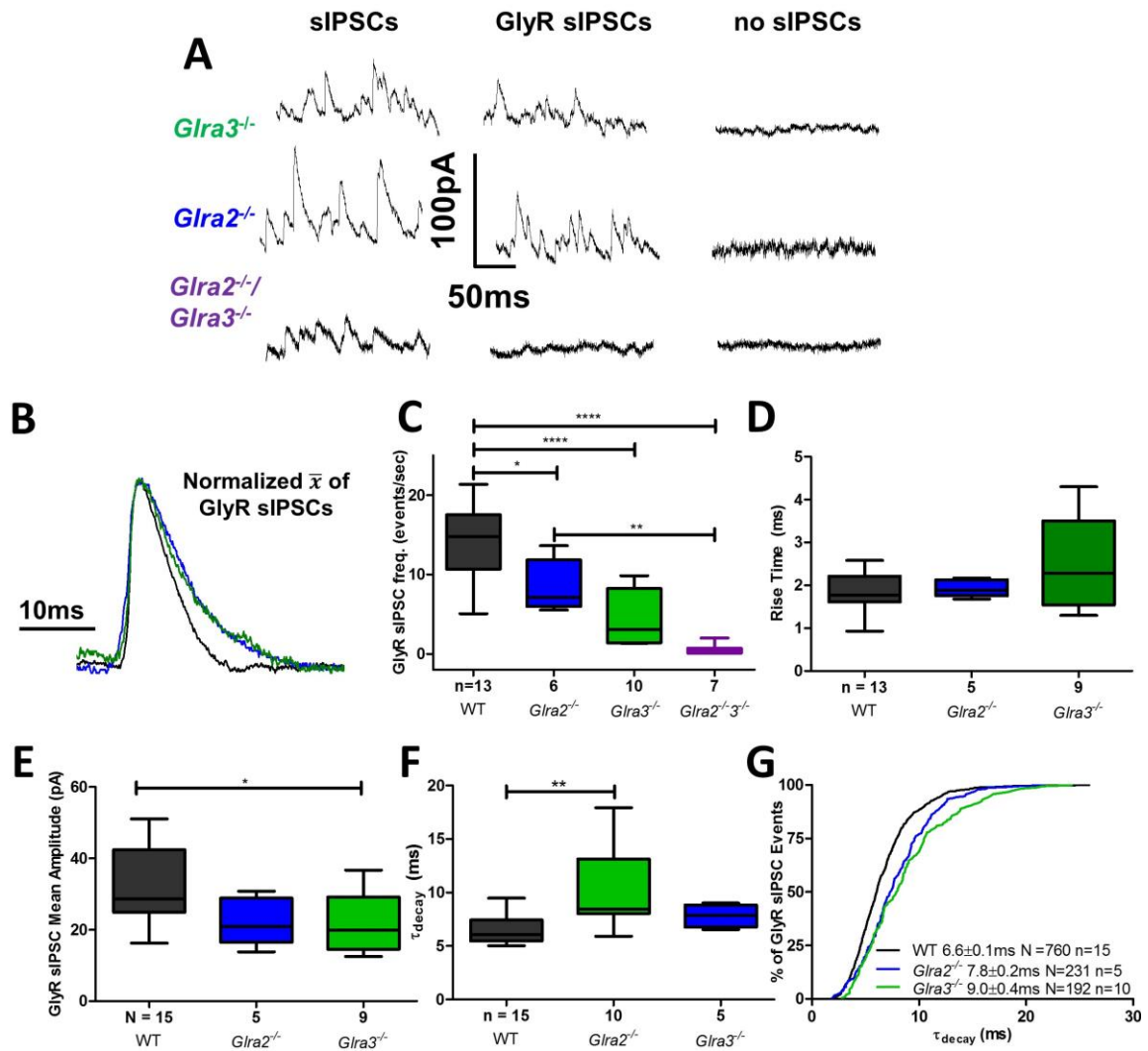


Figure 3.9. F-mini RGC glycinergic sIPSC activity is eliminated in *Glra2^{-/-}/
*Glra3^{-/-}**. A) Raw traces of total and glycinergic sIPSCs of *Glra3^{-/-}*, *Glra2^{-/-}*, and *Glra2^{-/-}/
*Glra3^{-/-}** F-mini RGCs. B) Average traces of WT (black), *Glra3^{-/-}* (green), and *Glra2^{-/-}* (blue), F-mini RGC glycinergic sIPSCs. C) Mean glycinergic sIPSC frequency (events/sec) for WT, *Glra3^{-/-}*, *Glra2^{-/-}*, and *Glra2^{-/-}/
*Glra3^{-/-}** F-mini RGCs. The average glycinergic sIPSC frequencies of *Glra3^{-/-}* and *Glra2^{-/-}* are significantly lower than WT, and the frequency in *Glra2^{-/-}/
*Glra3^{-/-}** is almost zero (One-Way Analysis of Variance with Bonferroni Post-Hoc test). D) Mean glycinergic sIPSC rise times (ms) for WT, *Glra3^{-/-}*, *Glra2^{-/-}*, and *Glra2^{-/-}/
*Glra3^{-/-}** F-mini RGCs are similar (One-Way Analysis of Variance with Bonferroni Post-Hoc test). E) The Average glycinergic sIPSC amplitude (pA) for *Glra2^{-/-}* is similar to both WT, and *Glra3^{-/-}* (One-Way Analysis of Variance with Bonferroni Post-Hoc test). The average glycinergic sIPSC amplitude for *Glra3^{-/-}* is significantly lower than WT (One-Way Analysis of Variance with Bonferroni Post-Hoc test). F) The mean glycinergic sIPSC τ_{decay} time of the *Glra3^{-/-}* F-mini RGC is significantly

slower than WT, however no different from the *Gla2*^{-/-} F-mini RGC. The *Gla2*^{-/-} F-mini RGC mean glycinergic sIPSCs τ_{decay} time is similar to WT. G) Cumulative distribution of glycinergic sIPSC τ_{decay} times (ms) for WT, *Gla2*^{-/-}, *Gla3*^{-/-} F-mini RGCs. The cumulative distribution of glycinergic sIPSC τ_{decay} is significantly slower in the *Gla2*^{-/-}, *Gla3*^{-/-}, and *Gla2*^{-/-}/*Gla3*^{-/-} (Kolmogorov–Smirnov test).

GlyRa2 and GlyRa3 expression on WT F-mini dendrites

To validate our electrophysiological recordings, we assessed the immunoreactivity of F-mini WT RGCs dendrites for GlyRa3 and GlyRa2 positive puncta. We measured the density of each of these puncta and compared them to an estimate of random puncta coincidence. Both GlyRa3 and GlyRa2 puncta density was significantly higher than random coincidence (GlyRa3 0.16 ± 0.01 puncta· μm^{-1} ; GlyRa2 0.28 ± 0.03 puncta· μm^{-1} ; respectively (Figure 3.10*Di, Dii*, $p < 0.0003$; 0.0001 (paired one-tailed T-test). Their average corrected puncta density was (GlyRa3 0.05 ± 0.01 puncta· μm^{-1} ; GlyRa2 0.22 ± 0.02 puncta· μm^{-1}). These results support our hypothesis that synaptic input to WT F-mini RGCs is mediated by both GlyRa3 and GlyRa2.

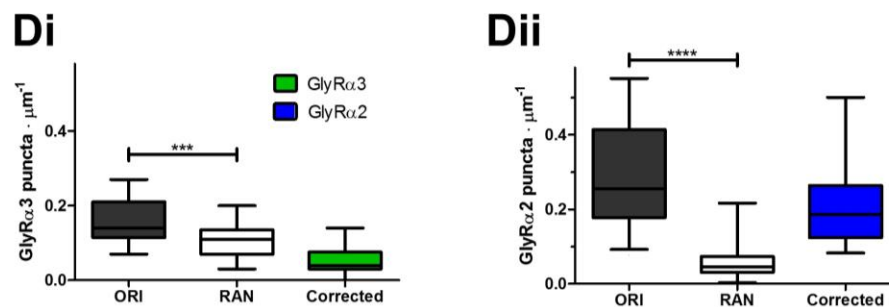
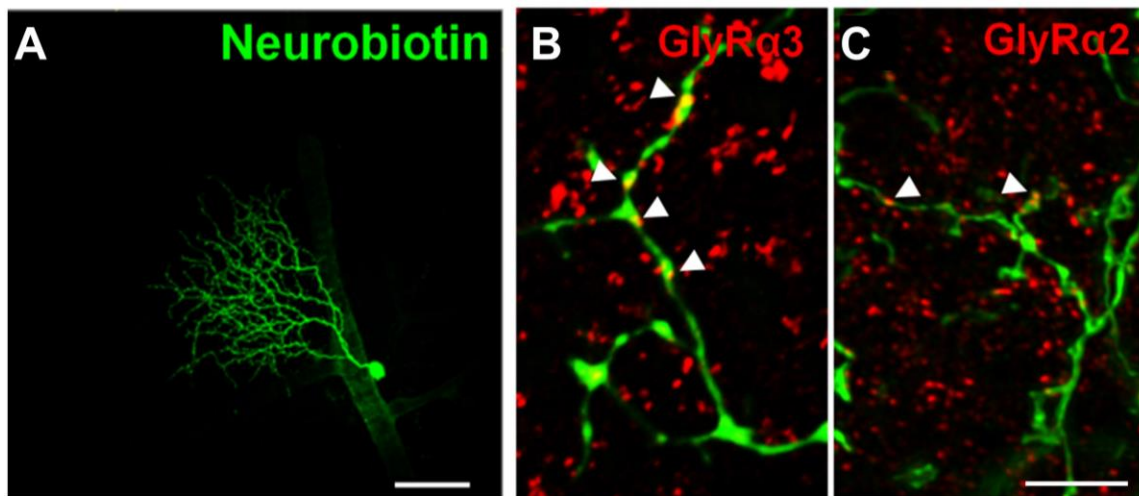


Figure 3.10. F-mini RGCs Express GlyRα2 and GlyRα3. (Images and GlyRα3 puncta count data sourced from (C. Zhang, 2015). A) Wholemount image of F-mini RGC filled with neurobiotin (scale bar: 40μm). B) Wholemount image of F-mini RGC dendrites stained for GlyRα3 expression (red) (scale bar: 5μm). White arrows indicate representative co-localization of GlyRα3. C) Wholemount image of F-mini RGC dendrites stained for GlyRα2 expression (red) (scale bar: 5μm). White arrows indicate representative co-localization of GlyRα2. Di) Dendrites in WT F-mini RGCs have significantly more GlyRα3 puncta density co-localization (μm^{-1}) than coincidence co-localization in the flipped (RAN) orientation (Wilcoxon matched-pairs U-test). The corrected puncta density for GlyRα3 puncta on F-mini RGCs is $0.05 \pm 0.01 \mu\text{m}^{-1}$. Dii) Dendrites in WT F-mini RGCs have significantly more GlyRα2 puncta density co-localization (μm^{-1}) than coincidence co-localization in the flipped (RAN) orientation (Wilcoxon matched-pairs U-test). The corrected puncta density for GlyRα2 puncta on F-mini RGCs is $0.22 \pm 0.02 \mu\text{m}^{-1}$.

Glycinergic Synaptic Input to J-RGCs is Mediated by GlyRα2

We examined the glycinergic isoform-specific expression and sIPSCs in asymmetric, intrinsically orientation selective J-RGCs. These were included in

color encoding YFP+ J-RGCs in tamoxifen injected JAM-B^{Cre}ER reporter mice (Figure 3.11) (I. J. Kim, Zhang, Yamagata, Meister, & Sanes, 2008; Liu & Sanes, 2017; Sanes & Masland, 2015). In the presence of GABA_AR and GABA_CR antagonists, the average τ_{decay} of glycinergic sIPSCs in WT J-RGCs was 23.3 ± 0.5 ms (Figure 3.11B-D). The in presence of strychnine, all glycinergic sIPSCs were eliminated (Figure 3.11A). The slow τ_{decay} indicates that synaptic glycinergic currents in J-RGCs are mediated by either GlyR α 2 or GlyR α 4 whose mean sIPSC τ_{decays} are slower than τ_{decays} mediated by either GlyR α 1 or GlyR α 3 (Figure 3.11B,C). Furthermore, the frequency distribution of J-RGC glycinergic sIPSC τ_{decay} is skewed and may represent the expression of more than one slow GlyR α subunit (Figure 3.11D).

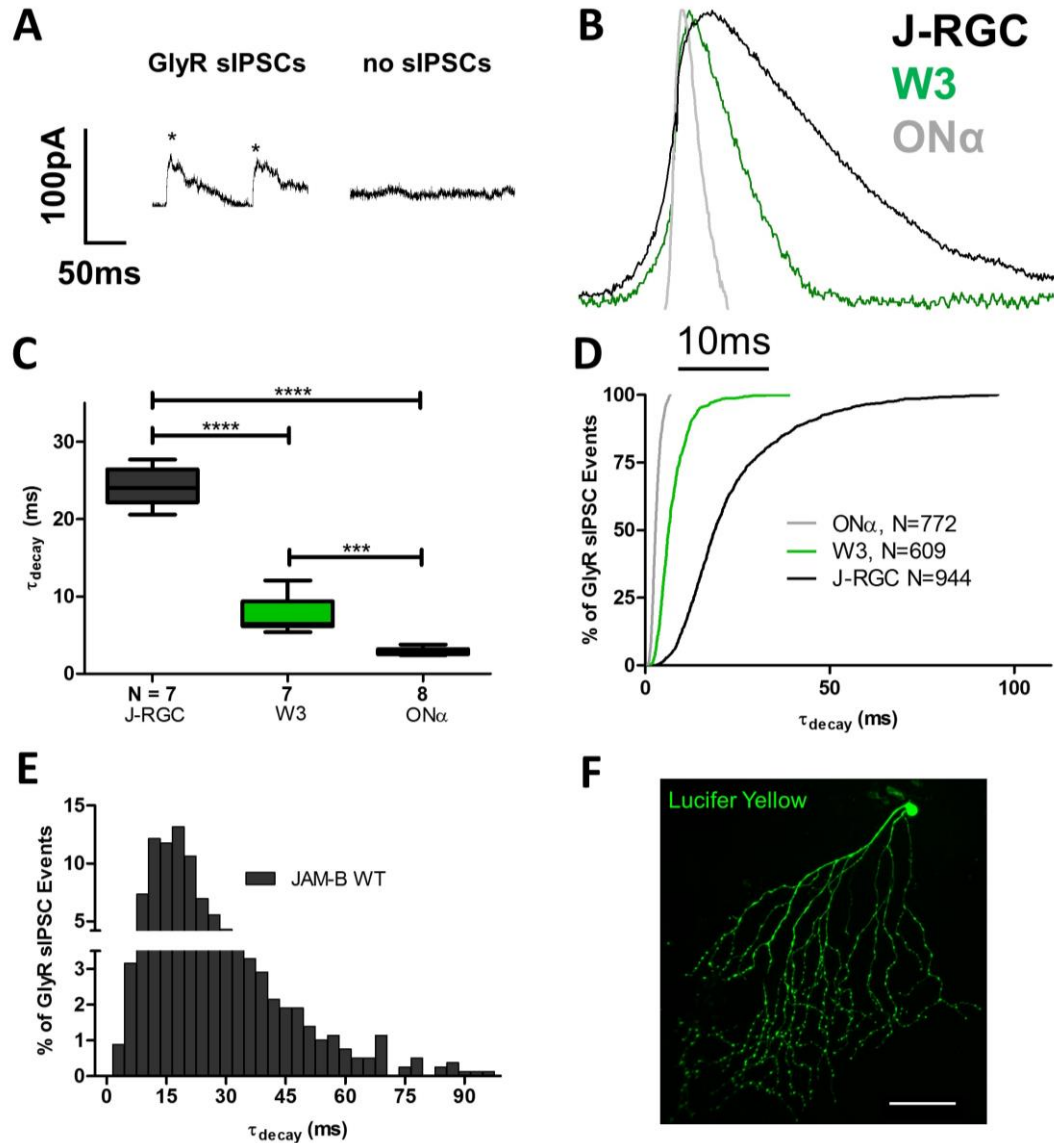


Figure 3.11. J-RGCs appear to have GlyR α 2 or GlyR α 4-mediated sIPSCs. **A)** Raw traces of J-RGC glycinergic sIPSCs. The “ * ” indicates a glycinergic sIPSC. Glycinergic sIPSCs are isolated in the presence of PTX/TPMPA and eliminated in the presence of PTX/TPMPA/STRYCH. **B)** Average traces of J-RGC (black), W3 (green), and ON α RGC (grey) glycinergic sIPSCs. **C)** The mean τ_{decay} of J-RGC glycinergic sIPSCs is significantly more than the mean τ_{decay} of both WT and ON α RGCs (One-Way Analysis of Variance with Bonferroni Post-Hoc test). **D)** Cumulative distributions of glycinergic sIPSC τ_{decay} times (ms) for J-RGCs (black), W3 RGCs (green) and ON α RGCs (grey). The cumulative distribution of glycinergic sIPSC τ_{decay} in J-RGCs is slower than both the representative GlyR α 1 expressing ON α RGCs and the representative GlyR α 3 expressing W3 RGCs (Kolmogorov–Smirnov test). **E)** Frequency distribution of glycinergic sIPSC τ_{decay}

times for J-RGCs is skewed (bin width is 3 ms). F) Wholemount image of J-RGC filled with Lucifer Yellow (scale bar: 50 μ m).

J-RGCs express GlyRa2

We tested the hypothesis that J-RGCs express GlyR α 2 and recorded glycinergic sIPSCs in *Gla2*^{-/-}/J-RGCs and found the average frequency was significantly less than WT (1.2 \pm 0.2 vs. 2.6 \pm 0.4 events/sec, respectively; Figure 3.12C; $p < 0.001$, One-way Analysis of Variance, Bonferroni Post-Hoc test). The average *Gla2*^{-/-}/J-RGC glycinergic sIPSC τ_{decay} was significantly faster than WT (16.3 \pm 0.6 ms; Figure 3.12D; $p < 0.01$, One-way Analysis of Variance, Bonferroni Post-Hoc test). Similarly, the cumulative distribution curve of glycinergic sIPSC τ_{decay} in *Gla2*^{-/-}/J-RGCs was shifted to faster decays compared to WT (Figure 3.12E; $p < 8.14e^{-16}$, Kolmogorov–Smirnov test). The rise time of *Gla2*^{-/-} J-RGCs was significantly slower than WT J-RGCs (4.9 \pm 0.4 vs 3.5 \pm 0.2, respectively; (Figure 3.12F, $p < 0.05$, One-way Analysis of Variance, Bonferroni Post-Hoc test) although their amplitude was similar to WT (21.3 \pm 2.2 pA; Figure 3.12G, $p > 0.05$, One-way Analysis of Variance, Bonferroni Post-Hoc test). These data suggest that the remaining sIPSCs in *Gla2*^{-/-} J-RGCs are mediated by GlyR α 4 and we tested this idea, by recording sIPSCs in *Gla2*^{-/-}/*Gla4*^{-/-} J-RGCs. These remaining glycinergic sIPSCs were eliminated in the presence of strychnine (Figure 3.12A).

Gla2^{-/-}/*Gla4*^{-/-} J-RGCs Have Similar Synaptic Input to *Gla2*^{-/-}

In *Gla2*^{-/-}/*Gla4*^{-/-} J-RGCs, the frequency of glycinergic sIPSC was significantly lower compared to WT (0.7 \pm 0.1, a 72% reduction; Figure 3.12C; $p < 0.01$, One-way Analysis of Variance, Bonferroni Post-Hoc test). Although the

frequency of glycinergic sIPSCs in *Gla2^{-/-}/Gla4^{-/-}* compared to *Gla2^{-/-}* J-RGCs it did not differ significantly (Figure 3.12C, $p > 0.05$, One-Way Analysis of Variance with Bonferroni Post-Hoc test). The characteristics of the remaining glycinergic sIPSCs were similar to WT, the average rise time of *Gla2^{-/-}/Gla4^{-/-}* J-RGCs glycinergic sIPSCs was still slow, and the amplitude also did not vary (19.0 ± 1.0 ; Figure 3.12F,G, $p > 0.05$, One-way Analysis of Variance, Bonferroni Post-Hoc test). While the average τ_{decay} was similar to WT (Figure 3.12D; $p < 0.05$, One-way Analysis of Variance, Bonferroni Post-Hoc test); the cumulative τ_{decay} was significantly slower compared to WT (Figure 3.12E, Kolmogorov–Smirnov test, $p < 5e^{-10}$). It is clear from these results that WT J-RGCs synaptic inputs are mediated by GlyR α 2. What remains to be tested is whether GlyR α 4 also mediates J-RGC glycinergic sIPSCs and if the puncta of *GlyR α 2* and *GlyR α 4* are colocalized on the J-RGC dendrites.

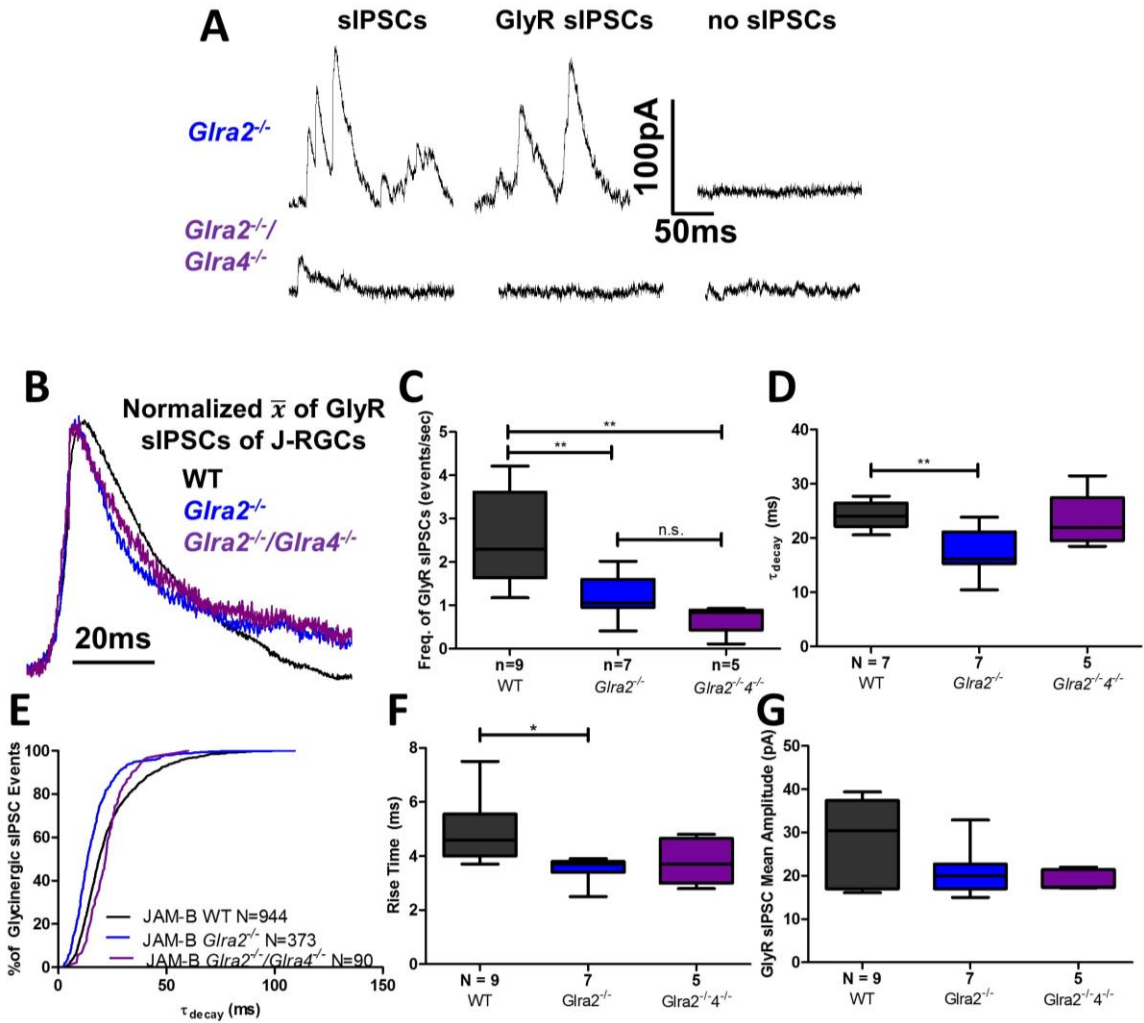


Figure 3.12. *Glra2^{-/-}/Glra4^{-/-}* eliminates glycinergic sIPSC activity in J-RGCs. A) Raw traces of total and glycinergic sIPSCs of *Glra2^{-/-}* and *Glra2^{-/-}/Glra4^{-/-}* J-RGCs. GlyR sIPSCs are isolated in the presence of PTX/TPMPA and the all sIPSCs are eliminated in the presence of PTX/TPMPA/STRYCH. B) Average traces of WT (black), *Glra2^{-/-}* (blue), and *Glra2^{-/-}/Glra4^{-/-}* (purple) J-RGC glycinergic sIPSCs. C) The Mean glycinergic sIPSC frequency (events/sec) for WT, *Glra2^{-/-}*, *Glra2^{-/-}/Glra4^{-/-}* J-RGCs. The average glycinergic sIPSC frequencies of *Glra2^{-/-}* and *Glra2^{-/-}/Glra4^{-/-}* are significantly lower than WT, however the glycinergic sIPSC frequency was similar between the *Glra2^{-/-}* and *Glra2^{-/-}/Glra4^{-/-}* (One-Way Analysis of Variance with Bonferroni Post-Hoc test). D) The mean glycinergic sIPSC τ_{decay} time of the *Glra3^{-/-}* F-mini RGC is significantly slower than WT, however no different from the *Glra2^{-/-}* F-mini RGC. The *Glra2^{-/-}* F-mini RGC mean glycinergic sIPSCs τ_{decay} time is similar to WT. E) Cumulative distribution of glycinergic sIPSC τ_{decay} times (ms) for WT, *Glra2^{-/-}*, and *Glra2^{-/-}/Glra4^{-/-}* J-RGCs. The cumulative distribution of glycinergic sIPSC τ_{decay} is significantly faster the

Gla2^{-/-}, then *Gla2*^{-/-}/*Gla3*^{-/-} (Kolmogorov–Smirnov test). F) The mean rise times (ms) of J-RGC glycinergic sIPSCs for WT, *Gla2*^{-/-}, and *Gla2*^{-/-}/*Gla4*^{-/-}. The mean *Gla2*^{-/-} J-RGC glycinergic sIPSC rise time was significantly faster than WT (one-way analysis of variance with Bonferroni post-hoc test). G) The Average glycinergic sIPSC amplitude (pA) for WT, *Gla2*^{-/-}, and *Gla2*^{-/-}/*Gla4*^{-/-} was similar among these three genotypes (One-Way Analysis of Variance with Bonferroni Post-Hoc test).

WT ON SAC Glycinergic Synaptic Input is Mediated by GlyR α 2

We targeted ON SACs using tdTomato+ ChAT-cre/ai9 mouse (Rossi et al., 2011). In the presence of PTX [20 μ M] and TPMPA [50 μ M], ON SAC glycinergic sIPSCs were slow and had an average τ_{decay} of 28.4 \pm 0.7 ms, suggesting GlyR α 2 and/or GlyR α 4 mediate these synaptic events, and these events were eliminated in the presence of strychnine (Figure 3.13A-D) It was previously reported that the ON SACs express slow glycinergic sIPSCs (Majumdar et al., 2009). The frequency distribution of the ON SAC glycinergic sIPSC τ_{decay} shows a skewed distribution, indicative of the expression of more than one kinetically disparate GlyR (Figure 3.13E).

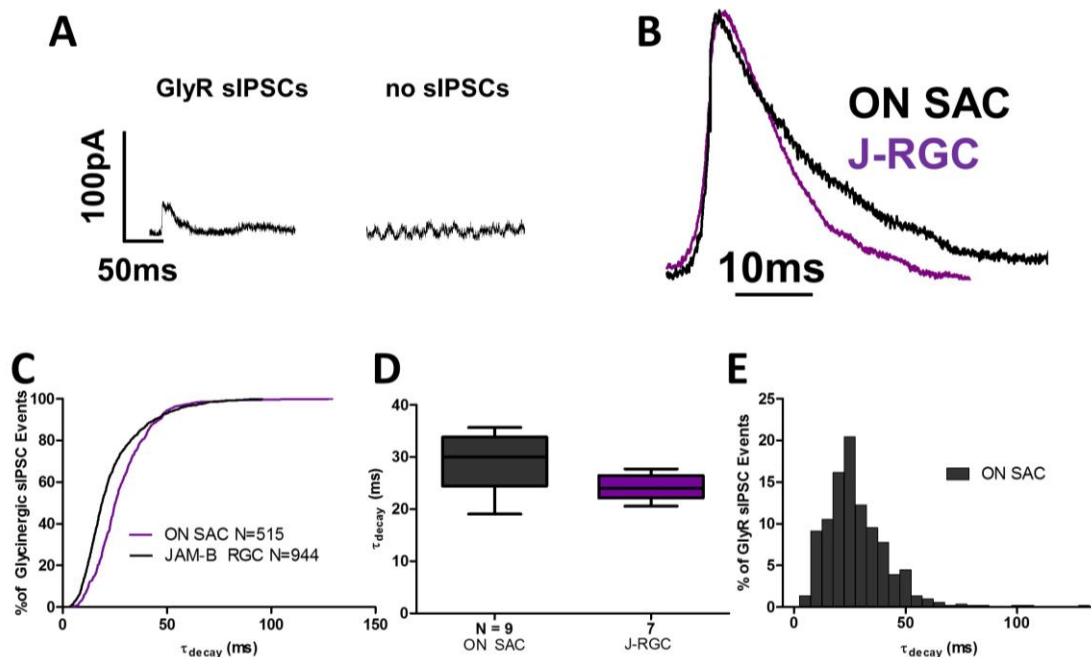


Figure 3.13. ON SAC glycinergic sIPSCs are slow and mediated by either GlyR α 2 or GlyR α 4. A) Raw trace of glycinergic sIPSC of ON SACs. GlyR sIPSCs are isolated in the presence of PTX/TPMPA and all sIPSCs are eliminated in the presence of PTX/TPMPA/STRYCH. B) Average trace of ON SAC glycinergic sIPSCs with similar GlyR α 2 mediated J-RGC trace for reference. C) Cumulative distribution of glycinergic sIPSC τ_{decay} times (ms) for ON SAC and J-RGCs. There is a significant difference between the different genotypes (Kolmogorov–Smirnov test). D) Mean glycinergic sIPSC τ_{decay} for ON SACs and J-RGCs were similar ($p > 0.05$, Mann-Whitney t-test). E) Frequency distribution of glycinergic sIPSC τ_{decay} of ON SACs.

Glycinergic sIPSC frequency is reduced in $Glr2^{-/-}$ ON SACs

We characterized the remaining glycinergic sIPSCs in $Glr2^{-/-}$ ON SACs and found that the average frequency was significantly lower compared to WT (0.4 ± 0.1 vs. 1.13 ± 0.2 events/sec, respectively; Figure 3.14C, $p < 0.002$, One-way Analysis of Variance, Bonferroni Post-Hoc test). The remaining glycinergic sIPSCs were eliminated in the presence of strychnine (Figure 3.14A). As noted in the J-RGCs, comparisons of the average of glycinergic sIPSC τ_{decays} between $Glr2^{-/-}$ and WT ON SAC were similar (25.72 ± 0.92 ms vs. 25.5 ± 2.4 ms, respectively), but the cumulative distribution curves of $Glr2^{-/-}$ and WT ON SACs differed significantly and $Glr2^{-/-}$ ON SAC decays were faster (Figure 3.14F; Kolmogorov–Smirnov test, $p < 6.5e^{-5}$). Neither glycinergic sIPSC rise time (3.6 ± 0.5 ms) nor amplitude (18.9 ± 1.5 vs 27.5 ± 2.7 pA; Figure 3.14D,E, $p > 0.05$, One-way Analysis of Variance, Bonferroni Post-Hoc test) of $Glr2^{-/-}$ ON SACs differed from WT. The significant decrease in glycinergic sIPSC frequency suggests that WT ON SACs express GlyR α 2. The characteristics of the remaining $Glr2^{-/-}$ ON SAC glycinergic sIPSCs indicates that their glycinergic synaptic inputs also might be mediated by GlyR α 4.

Glycinergic sIPSC frequency is Not Reduced in $Glr4^{-/-}$ ON SACs

We also recorded glycinergic sIPSCs in *Gira4^{-/-}* ON SAC and found that while the frequency was about half of WT, it was not statistically different (0.6 ± 0.2 events/sec; Figure 3.14D; $p > 0.05$, One-way Analysis of Variance, Bonferroni Post-Hoc test). The characteristics of the glycinergic sIPSCs in the *Gira4^{-/-}* ON SACs were all similar to WT and were eliminated in the presence of strychnine (Figure 3.14A-F, $p > 0.05$ for all, One-way Analysis of Variance, Bonferroni Post-Hoc test).

*Glycinergic sIPSCs are not reduced further in *Gira2^{-/-}/Gira4^{-/-}* ON SACs*

We recorded glycinergic sIPSCs in the *Gira2^{-/-}/Gira4^{-/-}* ON SACs and while their mean frequency was lower (0.3 ± 0.1 events/sec) it did not differ significantly from *Gira2^{-/-}* or *Gira4^{-/-}* single KO cells (Figure 3.14C; $p < 0.0002$, One-way Analysis of Variance, Bonferroni Post-Hoc test). These remaining sIPSCs were eliminated by strychnine (Figure 3.14A). The mean amplitude of the glycinergic sIPSCs in *Gira2^{-/-}/Gira4^{-/-}* ON SACs was significantly lower than WT (16.8 ± 1.1 pA; Figure 3.14E, $p < 0.02$, One-way Analysis of Variance, Bonferroni Post-Hoc test), which indicates a reduction in presynaptic glycine release and potential upstream modifications. The rise time and the τ_{decay} of the remaining glycinergic sIPSCs were similar to WT (Figure 3.14D,F, $p > 0.5$ for both, One-way Analysis of Variance, Bonferroni Post-Hoc test). The cumulative distribution of ON SAC glycinergic sIPSC τ_{decay} also was similar to *Gira2^{-/-}* ON SACs (Figure 3.14F, Kolmogorov–

Smirnov test, $p > 0.1$). From these data, we conclude the ON SACs express GlyR α 2.

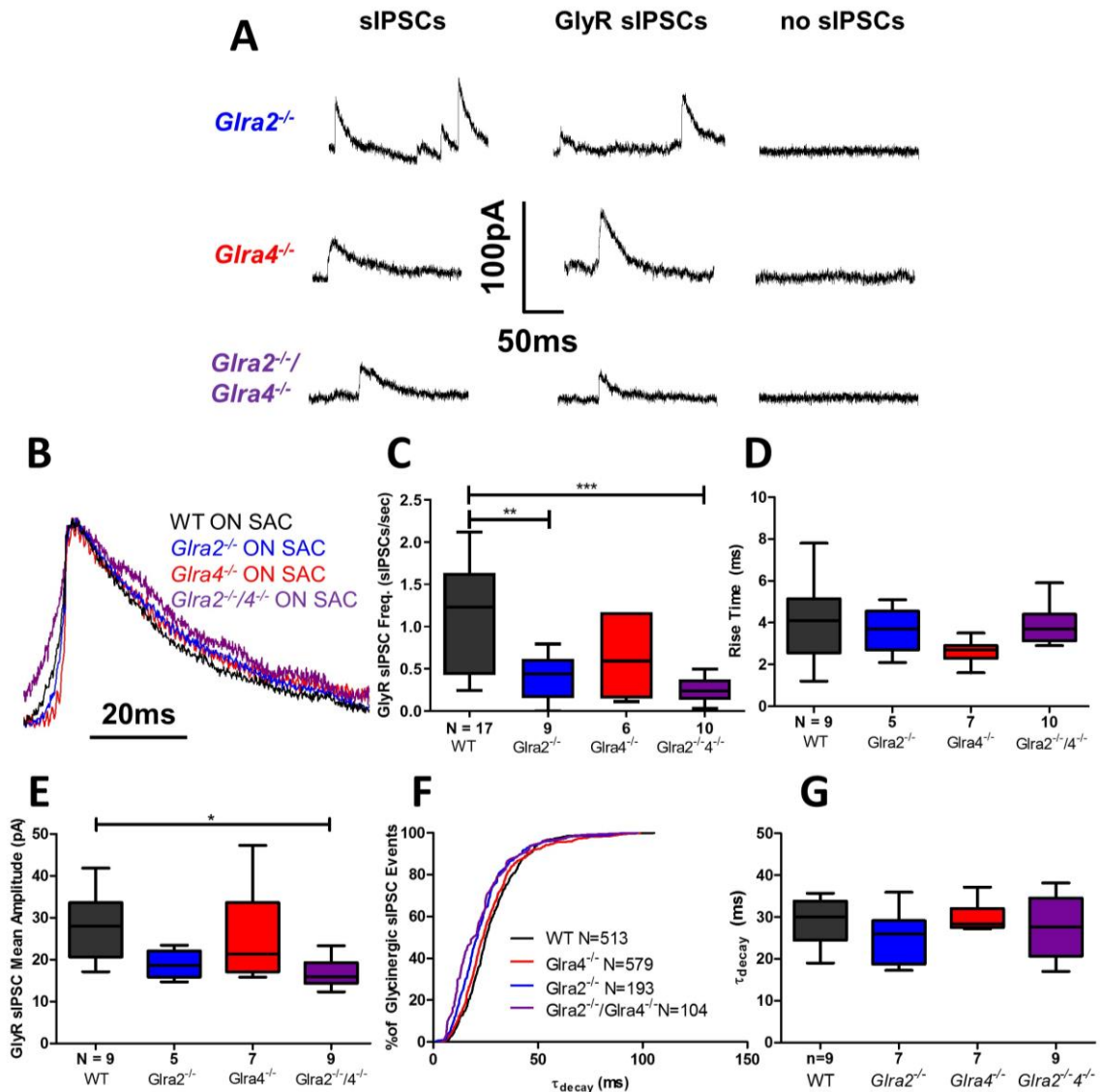


Figure 3.14. ON SAC glycinergic sIPSCs are slow and mediated by GlyR α 2. A) Raw traces of glycinergic sIPSCs of ON SACs in *Glra2*^{-/-}, *Glra4*^{-/-} and *Glra2*^{-/-}/*Glra4*^{-/-}. GlyR sIPSCs were isolated in the presence of PTX/TPMPA and all sIPSCs were eliminated in the presence of PTX/TPMPA/STRYCH. B) Average traces of ON SAC glycinergic sIPSCs in WT, *Glra2*^{-/-}, *Glra4*^{-/-} and *Glra2*^{-/-}/*Glra4*^{-/-}. C) Mean glycinergic sIPSC frequency (events/sec) for WT, *Glra2*^{-/-}, *Glra4*^{-/-}, and *Glra2*^{-/-}/*Glra4*^{-/-} ON SACs. The average glycinergic sIPSC frequencies (events/sec) of *Glra2*^{-/-} and *Glra2*^{-/-}/*Glra4*^{-/-} are significantly less than WT, the latter being almost zero (one-way analysis of variance with Bonferroni post-hoc test). D) Mean glycinergic sIPSC rise time (ms) for WT, *Glra2*^{-/-}, *Glra4*^{-/-}, and

Glr2^{-/-}/Glr4^{-/-} ON SACs. All rise times observed were similar ($p > 0.05$, One-Way Analysis of Variance with Bonferroni Post-Hoc test). E) Mean amplitude observed for the ON SACs in WT, *Glr2^{-/-}*, *Glr4^{-/-}* and *Glr2^{-/-}/Glr4^{-/-}*. Only the mean amplitude (pA) in the *Glr2^{-/-}/Glr4^{-/-}* was significantly lower than WT ($p < 0.02$, One-Way Analysis of Variance with Bonferroni Post-Hoc test). F) Cumulative distribution of glycinergic sIPSC τ_{decay} times (ms) for WT, *Glr2^{-/-}*, *Glr4^{-/-}*, and *Glr2^{-/-}/Glr4^{-/-}* ON SACs. The *Glr2^{-/-}* and the *Glr2^{-/-}/Glr4^{-/-}* curves were both significantly different from WT, but were similar to each other (Kolmogorov–Smirnov test). G) The mean glycinergic sIPSC τ_{decay} was similar among the WT, *Glr2^{-/-}*, *Glr4^{-/-}*, and *Glr2^{-/-}/Glr4^{-/-}* ON SACs ($p > 0.05$, One-Way Analysis of Variance with Bonferroni Post-Hoc test).

GlyR α 2 and GlyR α 4 Expression on WT ON SACs processes

Previously published data reported that ON SACs express GlyR α 4 (Heinze et al., 2007; Majumdar et al., 2009; Weiss et al., 2008). Our electrophysiology data suggest the ON SACs express GlyR α 2, GlyR α 4, or both. We examined puncta expression on ON SACs express and found that the average GlyR α 2-positive puncta density coincident with ON SAC dendrites was $0.15 \pm 0.02 \mu\text{m}^{-1}$ and the average random GlyR α 2-positive puncta density was significantly less ($0.08 \pm 0.01 \mu\text{m}^{-1}$; Figure 3.15C, *Dii*; $p < 0.005$, one tailed paired T-test). The average corrected GlyR α 2-positive puncta density was $0.07 \pm 0.01 \mu\text{m}^{-1}$ (Figure 3.15D*ii*). We also found the average GlyR α 4-positive puncta density coincident with ON SAC dendrites was similar to that of GlyR α 2 and was $0.17 \pm 0.02 \mu\text{m}^{-1}$. The average random GlyR α 4-positive puncta density was ($0.12 \pm 0.03 \mu\text{m}^{-1}$) and significantly lower than the original puncta density (Figure 3.15B, *Di*; $p < 0.05$, one-tailed paired T-test). The average corrected GlyR α 4-positive puncta density was 0.05 ± 0.01

(Figure 3.15Di). While the GlyR α 2 expression supports our electrophysiological data, more work is needed to reconcile the GlyR α 4 expression on these ACs.

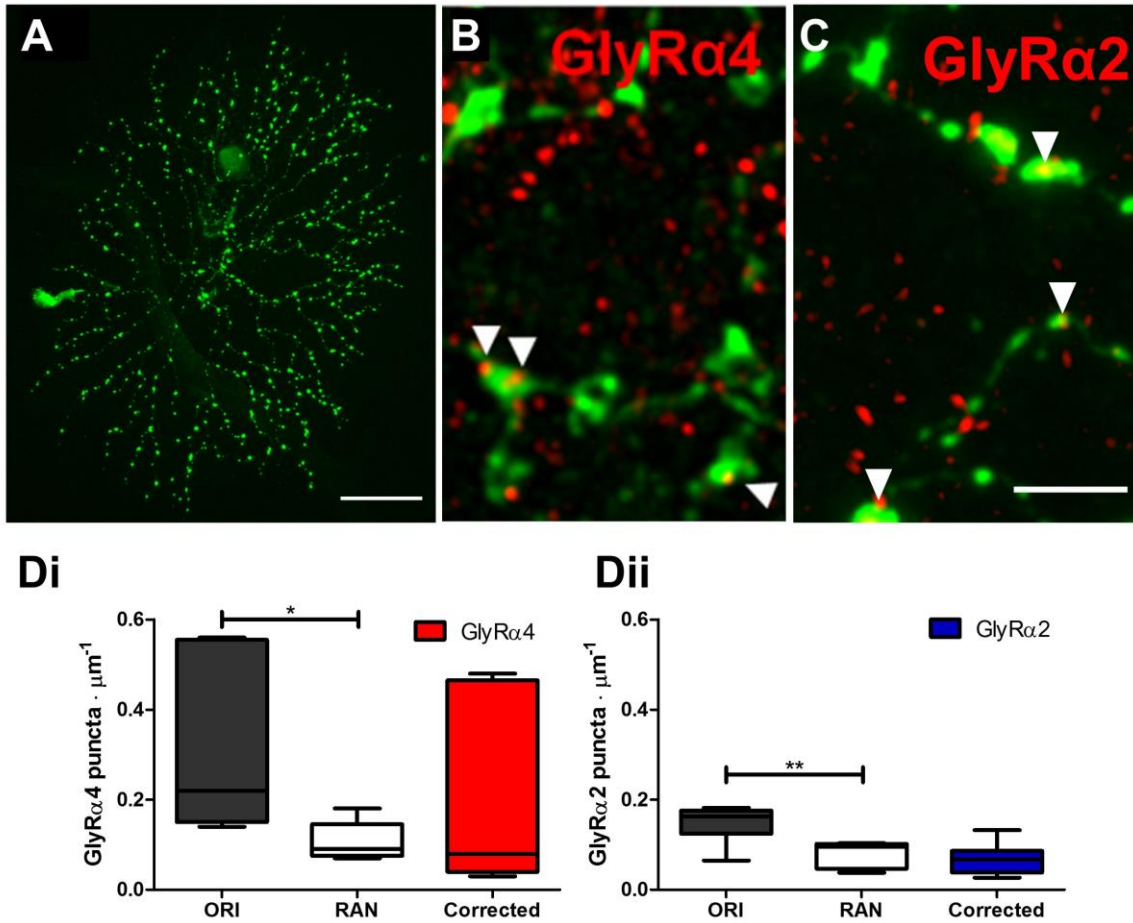


Figure 3.15. ON SACs Express GlyR α 2 and GlyR α 4 puncta. (Images sourced from (C. Zhang, 2015). A) Wholemount image of ON SAC filled with neurobiotin (scale bar: 40 μm). B) Wholemount image of ON SAC dendrites stained for GlyR α 4 expression (red) (scale bar: 5 μm). White arrows indicate representative co-localization of GlyR α 4. C) Wholemount image of ON SAC dendrites stained for GlyR α 2 expression (red) (scale bar: 5 μm). White arrows indicate representative co-localization of GlyR α 2. Di) Dendrites in ON SACs have significantly more GlyR α 4 puncta density co-localization than coincidence co-localization in the flipped (RAN) orientation (Wilcoxon matched-pairs U-test). The corrected puncta density for GlyR α 4 puncta on SACs is $0.05 \pm 0.01 \mu\text{m}^{-1}$. Dii) Dendrites in SACs have significantly more GlyR α 2 puncta density co-localization (μm^{-1}) than coincidence co-localization in the flipped (RAN) orientation (Wilcoxon matched-pairs U-test). The corrected puncta density for GlyR α 2 puncta on SACs is $0.07 \pm 0.01 \mu\text{m}^{-1}$.

DISCUSSION

The four heteromeric GlyRs found in the retina have different decay kinetics, and their expression is differential. One can speculate on GlyR inhibitory function, but given the diversity of GlyR expression on the RGCs we assessed, their function should be measured based on individual RGC specific GlyR expression and the specific RGC type and visual response properties. Until recently, GlyR expression on specific RGCs was only predicted and has been verified for one RGC, the OFF α RGC (C. Zhang et al., 2014). Using a similar approach with rAAV-*Gira1*-shRNA to knock down the expression of GlyR α 1 and a variety of GlyR KO models, we resolved the GlyR expression for a nine different RGCs and one AC that encompass roughly 50% of all RGCs found in the mouse retina (Sanes & Masland, 2015), as well as the ON SAC. Our survey of GlyR expression in RGCs presents an opportunity to elucidate the function of GlyRs in specific inhibitory circuits, involving specific RGCs.

ON α , ON τ , OFF α , and OFF δ RGC Glycinergic Synaptic Inputs

Our lab previously determined OFF α RGCs express GlyR α 1, the GlyR with the fastest kinetics (C. Zhang et al., 2014). Using the same approach, we ascertained that all RGCs with the largest soma diameters (ON α , ON τ , OFF α , and OFF δ) express only GlyR α 1. The τ_{decay} of GlyR α 1 mediated sIPSCs elsewhere in the CNS is about 2-4 ms, thus our identification of GlyR α 1 expression on the RGC types with the largest somas is comparable to the kinetics of other confirmed GlyR α 1 mediated currents (Figure 3.1) (Legendre, 1999; Majumdar et al., 2007). Furthermore, we assessed the GlyR α 1-positive puncta on the α RGC dendrites,

and positively identified its expression in WT α RGCs and its absence in rAAV-*Gla1*-shRNA infected α RGCs. Zhang et al. previously determined that GlyR α 1 input on OFF α RGCs helps modulate the spontaneous excitatory activity to improve the signal to noise ratio, and slightly hyperpolarizes the cell reducing the spiking probability. Furthermore, GlyR α 1 input in OFF α RGCs helps diminish the rebound excitation caused by the transient suppression of spiking from ON cone bipolar cells during an OFFset stimulus. Finally, OFF α RGCs receive crossover inhibition mediated by glycinergic input from the AII amacrine cell during the ONset of light. It is very likely the role of GlyR α 1 is similar in the other RGCs with the largest somas where it modulates spontaneous activity, and the fidelity of spiking responses is enhanced. However, further studies are necessary to elucidate the function of GlyR α 1 on the ON α , ON τ , and OFF δ RGCs since their dendrites ramify in different locations of the IPL, they likely receive input from glycinergic amacrine cells other than the AII, and they are part of different parallel pathways.

W3 RGC Glycinergic Synaptic Input

Using our electrophysiological analysis we established that all fluorescent RGCs found in the W3 reporter line express both GlyR α 1 and GlyR α 3; of the four GlyRs these two have the fastest kinetics (Gill et al., 2006; Majumdar et al., 2007; Majumdar et al., 2009). The established immunohistochemical approach we used to identify GlyR puncta expression was not sensitive enough to positively identify GlyR α 1 and GlyR α 3 on W3 RGCs. It is possible the GlyR expression on these cells is lower than GlyR expression on other cells where we successfully identified GlyR puncta expression. Additionally, each W3 RGC type has bushy and dense

dendrites, which complicate our analysis where randomly associated puncta expression could easily merge with a dendrite. Nevertheless, the drastic reduction in glycinergic sIPSC activity in the *Glr3^{-/-}* + rAAV-*Glr1*-shRNA indicate GlyR α 1 and GlyR α 3 are expressed on W3 RGCs.

All W3 RGCs (LED, HD, and UHD RGCs) have small somas, bushy dendritic fields, and stratify in the middle of the IPL. Additionally, these cells respond to both the ONset and OFFset of a receptive field center-sized spot stimulus (Jacoby & Schwartz, 2017). However, each W3 RGC type differs in its visual response kinetics, either sustained, transient, or a combination for the ON and OFF responses. Since these RGCs express two GlyRs, it is possible each one subserves a separate function, or a single function results from the complementary interaction of both GlyRs. Since the W3 RGCs receive input from both the ON and OFF pathway, it is likely that more sophisticated inhibitory synapses are required to help modulate both of these inputs. It is feasible these two GlyRs have a role in maintaining the spontaneous activity and improving the fidelity of the signal. Moreover, though we concluded all W3 RGCs express both GlyR α 1 and GlyR α 3, further study is needed evaluate the specific inhibitory function of these GlyRs on the individual LED, UHD, and HD RGCs.

F-mini RGC Glycinergic Synaptic Input

The F-mini OFF \uparrow RGCs express both GlyR α 2 and GlyR α 3; a slow GlyR and a fast GlyR, respectively (Haverkamp et al., 2004; Heinze et al., 2007; Majumdar et al., 2009; Weiss et al., 2008; C. Zhang et al., 2015). We demonstrated the puncta expression of both GlyR α 2 and GlyR α 3 on the dendrites of the F-mini

RGCs. However, in the *Glr3^{-/-}*, F-mini GlyR activity (which is presumed to be mediated by GlyR α 2) is much faster than isolated GlyR α 2 activity observed in other cells such as the ON SACs (Haverkamp et al., 2004; Weiss et al., 2008; C. Zhang & McCall, 2012; C. Zhang et al., 2015). Perhaps the GlyR α 2 expressed on F-mini RGCs is a second splice variant with much faster kinetics than the previously reported ~20-40 ms (Majumdar et al., 2009; Miller, Harvey, & Smart, 2004). Surprisingly, the F-mini glycinergic sIPSCs recorded in the *Glr2^{-/-}*, originating from GlyR α 3 receptors, have a similar average τ_{decay} to WT. Furthermore, the cumulative distribution curve of the *Glr2^{-/-}* glycinergic sIPSC τ_{decay} is shifted to the right from WT as opposed to the left. Thus, in the single KOs of F-mini RGCs, the independent GlyR α 2 and independent GlyR α 3 decay kinetics are slower than the complementary interaction of the two GlyRs in the WT F-mini RGCs. Though this result is confusing, it is possible it is derived from a change auxiliary protein modification of the remaining glycine receptor in the single KO, or from an alteration from connatural receptor expression density on the F-mini RGC. Further investigation using an rAAV-*Glr2_{KD}*-shRNA or rAAV-*Glr3_{KD}*-shRNA, which only infects RGCs, may better demonstrate the function of GlyRs on F-mini RGCs and also unveil how a global GlyR KO may disrupt spontaneous glycine release onto the RGCs.

J-RGC Glycinergic Synaptic Input

Our evidence indicates J-RGCs express GlyR α 2 since the glycinergic sIPSC activity in *Glr2^{-/-}* J-RGCs decreased significantly and the mean τ_{decay} was faster than WT. Glycinergic sIPSCs remained in the *Glr2^{-/-}* so we measured

synaptic glycinergic currents in the *Glr2^{-/-}/Glr4^{-/-}* but found little difference in these measurements from the *Glr2^{-/-}*. Our overall conclusion is J-RGCs express GlyR α 2. Despite the low glycinergic sIPSC frequency in the *Glr2^{-/-}* and *Glr2^{-/-}/Glr4^{-/-}*, it is apparent that kinetically slow glycinergic sIPSCs remain. It is also curious that the remaining J-RGC glycinergic sIPSCs in the *Glr2^{-/-}/Glr4^{-/-}* have a mean τ_{decay} similar to WT. Further investigation is needed to identify the remaining GlyR expression on J-RGCs, including an immunohistochemical analysis of GlyR puncta expression.

ON SAC Glycinergic Synaptic Input

We demonstrated using immunohistochemistry that ON SACs express both GlyR α 2 and GlyR α 4; the two kinetically slow GlyRs. Curiously, our glycinergic sIPSC analysis determined the ON SACs only express GlyR α 2. All authors investigating the glycinergic inhibition of ON SACs established these cells express GlyR α 4 (Majumdar et al., 2009; Weiss et al., 2008). Furthermore, immunohistochemical experiments indicate that there is dense GlyR α 4 expression in the ON ChAT band, which increases the likelihood of GlyR α 4 expression on any dendrites of cells that ramify in this location, such as the ON SACs (Haverkamp, 1995; Heinze et al., 2007; Majumdar et al., 2009; Nobles et al., 2012; Weiss et al., 2008). This discrepancy we observed may result from our electrophysiological assay being less sensitive for cells types that exhibit a low glycinergic sIPSC frequency. It is also important to take into consideration the global loss of GlyRs in these KO models. Some glycinergic ACs express GlyR α 2 and others may also express GlyR α 4 rendering contrasting electrophysiological results of our ON SAC

analysis while using global KOs. Considering the established expression of GlyR α 4 on ON SACs, our demonstration of GlyR α 2 and GlyR α 4 puncta expression on ON SACs, and our electrophysiological evidence of GlyR α 2-mediated sIPSCs from ON SACs, we conclude they express GlyR α 2 and likely express GlyR α 4.

The displaced ON SACs synaptically connect to the dendrites of the ON sublamina of the ON/OFF direction selective RGCs, and release GABA to facilitate direction selectivity (Rivlin-Etzion, Wei, & Feller, 2012; Wei & Feller, 2011; Wei, Hamby, Zhou, & Feller, 2011). Experiments blocking GlyR activity indicate GlyRs do not affect direction selectivity (Caldwell & Daw, 1978; Caldwell et al., 1978). Nevertheless, GlyR expression of two different GlyRs in ON SACs suggest the implicit need for inhibitory regulation to maintain the timing of GABA release. Further investigation is required to determine the explicit roles GlyR α 2 and GlyR α 4 perform in modulating the output of ON SACs. Experiments assessing the spatiotemporal visual response properties of these cells in WT, *Glr2*^{-/-}, *Glr4*^{-/-}, and *Glr2*^{-/-}/*Glr4*^{-/-} will help indicate, through a loss of function approach, the individual roles of these GlyRs in ON SACs.

CHAPTER IV

GLYCINE RECEPTOR SUBUNIT EXPRESSION IN MOUSE RETINAL ON-OFF DIRECTION SELECTIVE GANGLION CELLS

INTRODUCTION

In the retina, inhibition is mediated by both γ -aminobutyric acid (GABA)ergic and glycinergic neurotransmission. Like the GABA receptor, glycine receptors (GlyRs) are heteropentameric chloride ion channels comprised of β and α subunits in a stoichiometry of $3\beta:2\alpha$. There is only one β subunit, but there are four different α subunits (α_1 , α_2 , α_3 , α_4) making four different GlyRs (Cascio, 2006; Lynch, 2004). It is clear from the published literature that the four glycine receptor subunits (GlyR α_1 -4) are differentially expressed across the sublaminae of the retina's IPL (Haverkamp, 1995; Nobles et al., 2012; Veruki et al., 2007; Wassle et al., 2009). It is also established that retinal cells such as OFF cone BCs and rod BCs express GlyR α_1 , some narrow-field ACs express GlyR α_2 , while another narrow-field AC, the AII amacrine cell, likely expresses GlyR α_3 and or GlyR α_1 , and the wide-field starburst ACs express GlyR α_4 (Gill et al., 2006; Haverkamp et al., 2004; Majumdar et al., 2009; Weiss et al., 2008). However, cell type-specific GlyR expression on retinal ganglion cells (RGCs) is less sufficiently characterized.

The RGCs represent the culmination of retinal signal processing. They process, filter, interpolate, and relay an ever-changing visual scene to the rest of the brain. Using spiking signals that arise through the interplay of direct excitatory and inhibitory inputs, from bipolar cells (BCs) and amacrine cells (ACs), respectively. The RGCs form parallel circuits of information flow that arise in the retina and lay the foundation for visual perception. Of the roughly forty different RGC types, one of the most prominent types in the mouse retina is the ON/OFF direction selective (ooDS) RGC (Baden et al., 2016; Bae et al., 2018; Jacoby & Schwartz, 2017; Rivlin-Etzion et al., 2011; Sanes & Masland, 2015), which represents about 20% of all RGCs in the mouse retina (Sanes & Masland, 2015). The four types of ooDS RGCs each encode motion in one of the four cardinal directions. It is clear from the published literature that GABAergic mediated inhibition is crucial for both direction selectivity and response sensitivity in all ooDS RGCs, and GABA_A receptor (GABA_AR) activity promotes transient ON and OFF responses (Caldwell et al., 1978). However, much less is known about the role of glycinergic inhibition on the visual response properties of ooDS RGCs, although in the rabbit, intravitreal injections of strychnine, a glycine receptor antagonist, reduced ooDS RGC response sensitivity and decreased the timing of the OFF responses (Caldwell et al., 1978). In these studies, glycinergic inhibition was eliminated throughout the retina and consequently we cannot pinpoint the effects. They could result from direct glycinergic inhibition onto the ooDS RGCs or through glycinergic inhibition in the circuit(s) that modulate the direct excitatory and/or inhibitory inputs to these cells.

To determine if ooDS RGCs receive direct glycinergic synaptic input, we recorded spontaneous inhibitory postsynaptic currents (sIPSCs) and isolated glycinergic sIPSCs using GABA_A and GABA_C receptor antagonists. All ooDS RGCs receive glycinergic synaptic inputs, whose average τ_{decay} is slow, about 20ms. These slow decay kinetics indicates that synaptic inputs are mediated by GlyR α 4 or GlyR α 2. We tested this idea by eliminating the expression of both alpha receptors, using *Glr4*^{-/-}, *Glr2*^{-/-} and *Glr4*^{-/-}/*Glr2*^{-/-} mouse models. We also eliminated GlyR α 4 expression using retrogradely transported rAAV-*Glr4*_{KD}-shRNA or rAAV-*Glr2*_{KD}-shRNA, respectively. We confirmed the expression by using immunohistochemistry and confocal microscopy. GlyR expression in ooDS RGCs is consistent with our electrophysiological assessments.

MATERIALS AND METHODS

Animals

We used two reporter lines to target ooDS RGCs. Thyrotropin-releasing hormone receptor (TRHR-GFP) retinas express GFP in identified ooDS RGCs with a direction preference to posterior motion (Rivlin-Etzion et al., 2011). *B6-Pvalb^{tm1(cre)Arbr/J/Thy1^{STP}-EYFP(PV^{Cre}/Thy1^{STP})}* reporter mice express YFP in eight different RGCs, including ooDS RGCs representing all four cardinal directions (Farrow et al., 2013; Hippenmeyer et al., 2005). Both TRHR and *PV^{Cre}/Thy1^{STP}* mice were crossed and backcrossed to *Glr2*^{-/-}, *Glr4*^{-/-}, and *Glr2*^{-/-}/*4*^{-/-} to obtain GlyR global knockout models with labeled RGCs. All experiments were carried out in accordance with the Association for Research in Vision and Ophthalmology (ARVO) Statement for the Use of Animals in Ophthalmic and Visual Research and

with the approval of the Institutional Animal Care and Use Committee (IACUC) of the University of Louisville.

Viral Vector Construction and rAAV Production

To eliminate glycine receptor expression in the ooDS RGCs only, we used a retrogradely transported rAAV virus containing shRNAs to *Gira4*. This approach was used previously to knockdown expression of *Gira1* (Zhang et al. 2014). Briefly, we used our rAAV-*Gira1*-shRNA, an rAAV virus containing the shRNA *Gira1*, and switched out the shRNA target of *Gira1* for *Gira4* (29mer in the pGFP-V-RS vector, Origene, Rockville, MD). The new plasmid included: flanking Inverted terminal repeats, elongation factor-1 promoter, a tdTomato gene with a nuclear localization sequence, woodchuck hepatitis post-transcriptional regulatory element, a polyadenylation site to protect the mRNA from degradation, the H1 promoter and the *Gira4*-shRNA cassette (Figure 4.1). The plasmids were packaged into the recombinant 2/7 rAAV vector serotype using a standard triple-plasmid protocol by co-transfection of HEK293T cells to create the rAAV-*Gira4*_{KD}-shRNA (Grieger, Soltys, & Samulski, 2016; McClements & MacLaren, 2013; Reid & Lipinski, 2018). The creation of these plasmids was performed by the Gregg Lab (University of Louisville, Louisville, KY), and the virus was packaged by the Lipinski (Medical College of Wisconsin, Milwaukee, WI), or Roska Labs (Friedrich Miescher Institute, Basel Switzerland) labs.

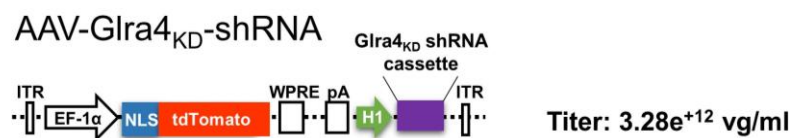


Figure 4.1. Schematic diagram of plasmid delivered via rAAV, used to change the expression of GlyR α 4 in ooDS RGCs. pAAV-Ef1a-NLStdTomato-H1 with *Gira*_{4KD} shRNA (rAAV-*Gira*_{4KD}-shRNA; 3.28×10^{12} vg/mL).

Viral Injections in SC or dLGN

The methods to inject rAAV into the dorsal lateral geniculate nucleus (dLGN) are published (Zhang et al., 2014). In many mice (aged between P30 and P45), we performed rAAV injections into the superior colliculus (SC) instead. Mice, were anesthetized using the administration of an intramuscular (IM), intraperitoneal (IP) injection of a mixture of ketamine (70mg/kg) (VetaKet, Akorn, Lake Forest, IL) and xylazine (12mg/kg) (AnaSed, LLOYD, Shenandoah, IA). Their scalps were shaved, heads secured in a stereotaxic with ear cups and a bite bar, and their body temperature (37°C) was maintained with a feedback controlled heating pad. Eyes were lubricated with 1.3% polyvinyl alcohol and corneas were protected with plastic contact lenses. Stereotaxic coordinates (Paxinos & Franklin, 2004) were used to locate a craniotomy over the SC. A midline incision was made in the skin over the skull, and a craniotomy was performed at 0.5 mm anterior and 0.5 mm temporal to Lambda. A borosilicate glass pipette (interior diameter of 40-50 μ m), filled with ~10 μ L of Ringer's solution, was positioned over the craniotomy and lowered between 800 μ m and 1200 μ m from the surface. Ringer's solution consisted of (in mM: 125 NaCl, 2.5 KCl, 2.0 CaCl₂, 1.0 MgCl₂, 20 D-glucose, and 1.25 NaH₂PO₄, and 26 NaHCO₃) (Sigma-Aldrich, Burlingame, CA). The SC was located when a clear visually evoked response was recorded through the pipette. The depth of the SC was recorded, the Ringer's pipette removed and a second pipette (interior diameter of 18-22 μ m), filled with 3.0 μ L of rAAV diluted in HBSS

(titer for each virus used listed in Figure 4.1) and positioned at the same stereotaxic coordinates of the Ringer's pipette. Light responses also were recorded again to confirm placement of the rAAV pipette. Using light pressure, 2-2.5 μ L of rAAV solution was injected into the SC and the pipette removed. The incision was closed with skin glue (VetBond, 3M, St. Paul, MN), the animal was given a subcutaneous 100 μ l dose of Carprofen (1.25 mg/ml) (Putney, Portland, ME) and were recovered from anesthesia.

Wholemout Retinal Preparation for Electrophysiological Recordings

Four weeks post injection, animals were dark adapted for 30 minutes, given an IP injection of a cocktail of ketamine/xylazine (409mg/kg and 54mg/kg, respectively) and sacrificed using cervical dislocation. The eyes were enucleated, the front of the eye removed and the retinas were incubated in a solution of Ringer's with collagenase (241 units/mL) and hyaluronidase (34.5nM per mL) (Worthington Biochemicals, Lakewood, NJ) for 10 minutes to break down and remove the vitreous attached to the retina. Remaining vitreous was carefully removed and retinas were washed 3 times with fresh oxygenated Ringer's to eliminate the enzymes. Then, the retinas were quartered and each piece was placed RGC side up onto a cover slip, a harp was placed on top of the retina to stabilize it, and the apparatus was placed into a chamber (Cell MicroControls, Norfolk, VA) on the stage of the microscope. Wholemounts were continuously bathed in oxygenated Ringer's solution at 36°C. The Ringer's solution was preheated to 36° and the exact temperature in the chamber controlled by an NBD

TC2 BIP (Bipolar) feedback controller (Cell MicroControls, Norfolk, VA) in the chamber.

Electrophysiological Recordings of RGCs and Pharmacology

RGCs were visualized on a Nikon Eclipse E600FN microscope with a Nikon Fluor 60x water immersion objective with Hoffman Modulation Contrast (Nikon, Tokyo, Japan). We targeted fluorescent GFP+ ooDS RGCs in *PV^{Cre}/Thy1^{STP}* or TRHR reporter mice and in rAAV infected retinas, we targeted double labeled ooDS RGCs; GFP+ (green) from the reporter gene and tdTomato+ (red) nuclei from rAAV infection. Glass electrodes were pulled from Kwik-Fil borosilicate glass capillaries (1B150F-4, World Precision Instruments, Sarasota, FL) on a P-97 Flaming/Brown micropipette puller (Sutter Instruments, Novato, CA). The resistance of these glass electrodes was 5-7 M Ω . Electrodes were filled with an intracellular solution that consisted of: (in mM) 12.5 CsCl, 107 CsOH, 107 D-Gluconic Acid, 10 Na⁺ HEPES, 10 BAPTA, 5 QX-314(Br), 4 ATP, and 0.5 GTP 5 lidocaine N-ethyl bromide (QX314-Br) (Sigma-Aldrich, St. Louis MO), 2.2 Lucifer yellow (Fisher Scientific, Hampton, NH) or 12.4 neurobiotin (Vector Labs, Burlingame, CA) (pH 7.2 adjusted with CsOH).

After obtaining a gigaohm seal, the membrane was broken with swift negative pressure, and the membrane potential (V_{Hold}) was held at -60 mV. All recordings were sampled at 10 kHz. First, a light emitted diode (LED) was positioned 2 cm above the tissue and presented a full field stimulus ($3.7E^{03}$ R*). The stimulation protocol consisted of: a single 30ms light pulse, followed by a 2 second interstimulus interval (ISI), which was then followed by a five presentations

of a 2 second light pulse with a 20 second ISI. The responses to the five, 2 second light stimuli were averaged, analyzed using Clampfit software (Molecular Devices, San Jose, CA) and used to determine if the RGC had an ON/OFF response.

We then characterized the sIPSCs in each ooDS RGC. The cell membrane potential was held at +15 mV, the cation reversal potential, and total sIPSCs (GABAergic and glycinergic) were recorded for 100 seconds and the membrane potential lowered back to -60 mV. GABA_A and GABA_CR antagonists (picrotoxin (PTX) [20 μM], and (1,2,5,6-Tetrahydropyridin-4-yl)methylphosphonic acid (TPMPA) [50 μM], respectively) were added to the bath solution (Ringer's) for ten minutes to isolate glycinergic sIPSCs. The RGC membrane potential was raised to +15 mV and isolated glycinergic sIPSCs recorded for 100 seconds. To verify that we had isolated glycinergic sIPSCs, the GlyR antagonist (strychnine (STRYCH) [10 μM]) was added to the bath containing the GABA antagonists and 5 minutes later the cell was held at +15 mV for 100 seconds. Residual sIPSCs were never recorded in the presence of GABA and GlyR antagonists.

Signal was monitored and recorded using an Axon Multiclamp 700B patch clamp amplifier (Molecular Devices, San Jose, CA). The signals were digitized at 10 kHz using an Axon Digidata 1322A and visualized using Clampex 10.2 software (Molecular Devices, San Jose, CA). To isolate sIPSCs, RGCs were held at the cation reverse potential (V_{Hold}) of +15 mV (0mV after correcting for the liquid junction potential).

Electrophysiological Data Analysis

We used Mini Analysis software (Synaptosoft, Decatur, GA) to identify sIPSCs in ooDS RGCs. First, we selected candidate sIPSC peaks whose amplitude exceeded a minimum threshold of twice the root mean squared (RMS) of the noise in each recording (between 1.5 and 5 pA). All the sIPSCs selected were used to evaluate the frequency (events/sec) for the 100 second recording. Next, these sIPSCs were further evaluated using a model sIPSC with a fast rise time (10-90% peak, 1-6 ms), a single peak, and a single exponential decay time (peak to 37% of peak (D37), 2-120 ms). Double or multi-peaked sIPSCs were only included in the frequency measurement; they were subsequently eliminated because their kinetics and amplitude measurements are unreliable. The remaining single peak sIPSCs were used in the analyses of the rise time, τ_{decay} , and amplitude of the sIPSCs. sIPSCs were never found in our +15 mV recordings with both GABA and GlyR antagonists in the bath.

Immunohistochemistry and Confocal Imaging

After patch clamp recording, the pieces of retina with recorded and filled RGCs (Lucifer Yellow and neurobiotin) were fixed in 4% paraformaldehyde for 12 minutes, washed three times with 0.01 M phosphate buffer saline (PBS), and placed into a 24-well plate. Retina pieces were incubated in blocking solution consisting of PBX (0.5% Triton-X 100 in PBS) and 10% normal serum (donkey or goat) for 60 minutes. Each retina piece was then reacted with a combination of primary antibodies to stain for the either GlyR α 2 or GlyR α 4 or a combination of both, and Lucifer yellow overnight at 4°C (Table 4.1). In the case where the Lucifer yellow antibody was not compatible, streptavidin was used to stain for the filled

cell, but was added with the secondary antibodies. The single GlyR antibody or combination of GlyR antibodies were selected based on our observed τ_{decay} estimates that we matched with the τ_{decay} estimates from the literature (Table 4.1) (Haverkamp et al., 2004; Heinze et al., 2007; Majumdar et al., 2009; Wassle et al., 2009). The primary antibodies were washed off by a series of washes with PBX. Afterwards, a combination of secondary antibodies and Hoechst stain (or also streptavidin) in normal serum was added to label the primary antibodies and left on the tissue overnight at 4°C (Table 4.1). The Hoechst stain was used to label the DNA in the somas and distinguish between the retina nuclear and plexiform layers. The tissue was then washed with PBS and mounted onto a slide and covered using Vectashield (Vector Labs, Burlingame, CA) clear mounting medium and a coverslip.

Table 4.1. Primary and Secondary Antibodies used for Immunohistochemistry

Primary Antibodies	Concentration	Host	Manufacturer
anti-Lucifer Yellow	1:1000	rabbit polyclonal	Life Technologies
anti-GlyR α 2	1:50	goat polyclonal	Santa Cruz Biotech
anti-GlyR α 4	1:100	rabbit polyclonal	Chemicon
Secondary Antibodies	Concentration	Host	Manufacturer
anti-goat IgG Cy3	1:200	donkey polyclonal	Jackson ImmunoResearch
anti-rabbit IgG 488	1:200	donkey polyclonal	Jackson ImmunoResearch
streptavidin Cy2 or 633	1:200	<i>conjugate</i>	Life Technologies
Hoechst nuclear stain	1:1000	<i>conjugate</i>	Life Technologies

The recorded and filled ooDS RGCs were imaged using an Olympus FV1000 confocal microscope. Whole RGC images were acquired using a 40x water immersion (NA 1.15) objective and dendrites and GlyR puncta expression were acquired using a 60x oil immersion (NA 1.4) objective. Images of ooDS RGC dendrites were recorded with Fluoview software (Olympus, Tokyo, Japan). The

depths of the RGC's dendritic ramifications were measured relative to the top of the RGC layer and the bottom of the INL. The combination of each RGC's dendritic ramification depth, dendrite arbor diameter, and light response were used to identify and verify that the RGC was an ooDS RGC.

Colocalization Analysis of GlyRs on ooDS RGCs

Expression of GlyRs were characterized in recorded/filled ooDS RGCs. Images of ooDS RGC dendrites and GlyR puncta were deconvolved, using constrained iterative deconvolution in cellSens (Olympus, Tokyo, Japan). Using the Imaris (Bitplane, Zurich, Switzerland) co-localization tool, coincident GlyR puncta (color channel 1) on or within dendritic processes (color channel 2) were counted and the length of the dendritic processes within the image was measured using the filaments tool. The coincident puncta divided by the dendritic length estimated puncta density. To determine which puncta were colocalized onto the dendrite, the puncta channel (channel 1) was flipped along the xy axis and coincident GlyR puncta were recounted. Then, the “flipped” or chance (RAN) puncta density was subtracted from the “original” (ORI) puncta density and the result estimated the “corrected” puncta density.

Statistical Analysis

The data of the sIPSCs from each cell was grouped with like cells and pharmacological conditions. The cumulative distribution of the τ_{decay} of the sIPSCs of these groups were compared using the Kolmogorov–Smirnov test. The mean τ_{decay} , rise time, frequency, and amplitude data of the sIPSCs of these groups were compared using a one-way Analysis of Variance, with a Bonferroni Post-Hoc test

to compare the data for each cell type or the pharmacological condition or genotype in which it was recorded. The *Gira2^{-/-}/Gira4_{KD}* data was compared to the *Gira4^{-/-}/Gira2^{-/-}* using a Two-tailed Mann-Whitney test. The ORI and RAN puncta density counts were compared using a paired Wilcoxon matched-pairs t-test. Finally, the corrected puncta density among three groups was compared using a Kruskal-Wallis One Way ANOVA test.

RESULTS

sIPSCs Indicate ooDS RGCs Express GlyRa2 and/or GlyRa4

We examined the glycinergic isoform specific expression and sIPSCs in ooDS RGCs, which were identified by their GFP expression in either TRHR or *PV^{Cre}/Thy1^{STP}* mouse lines. We identified ooDS RGCs as GFP+ medium-sized soma (~15µm in dia.) RGCs with ON/OFF light evoked responses and bistratified dendritic sublamina. In WT ooDS RGCs, the total sIPSCs (Figure 4.2Ai, sIPSCs) were a mixture of very slowly decaying, large amplitude sIPSCs and smaller amplitude rapidly decaying sIPSCs. In the presence of strychnine, the GABAergic sIPSCs consisted of large rapid rise, slow decaying currents (Figure 4.2Aii, GABA sIPSCs). In the presence of GABAR antagonists (picrotoxin and TPMPA) the large, slow currents were eliminated (Figure 4.2Aiii, GlyR sIPSCs) and the isolated glycinergic sIPSCs had a mean frequency of 5.7 ± 0.4 events/sec, an average rise time of 3.2 ± 0.2 ms, a mean amplitude of 61.4 ± 3.8 pA, and their average τ_{decay} was 21.7 ± 0.4 ms (Figure 4.2C). In the presence of both GABAR antagonists and strychnine, all sIPSCs were eliminated (Figure 4.2Aiv, no sIPSCs), confirming that the sIPSCs recorded in the presence of only GABA antagonists were isolated

glycinergic sIPSCs. The average τ_{decay} is significantly slower than either GlyR α 1 or GlyR α 3 (Figure 4.2B,D,E), which we determined in other studies (see Chapter 3) and were \sim 3.0 ms and \sim 9.0 ms, respectively. The slow τ_{decay} of the GlyR sIPSCs in WT ooDS RGCs suggests that they are mediated by GlyR α 2 and/or GlyR α 4 isoforms.

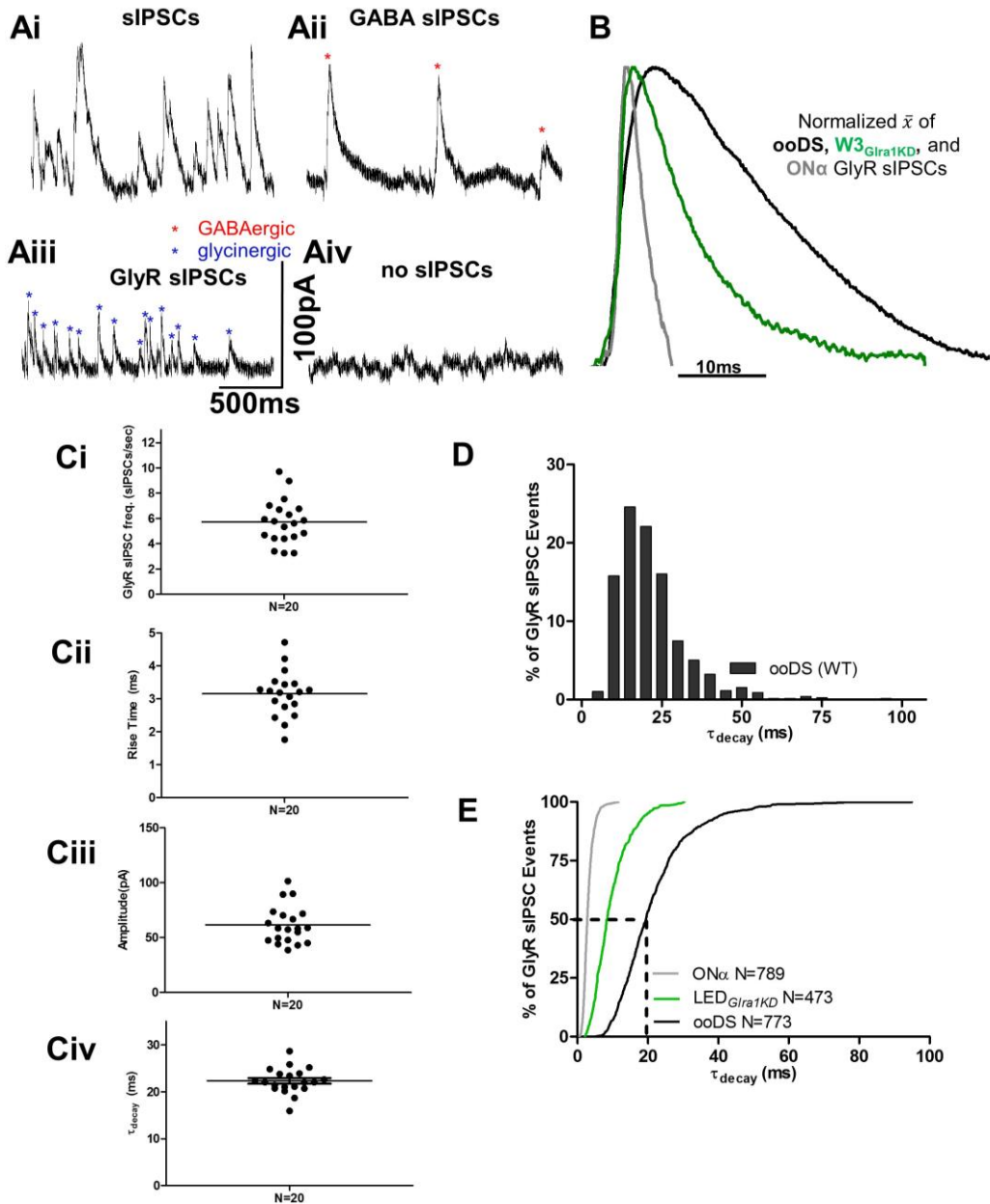


Figure 4.2. WT ooDS RGC Glycinergic sIPSCs are Slow and are Likely Mediated by GlyR α 4. A) Raw traces of sIPSCs (red asterisks = GABAergic sIPSC, blue asterisks = glycinergic sIPSC)(Ai), isolated GABAergic sIPSCs in the presence of STRYCH (Aii), isolated glycinergic sIPSCs in the presence of PTX/TPMPA (Aiii), and total block of sIPSCs in the presence of PTX/TPMPA/STRYCH (Aiv) in WT ooDS RGCs. GABA sIPSCs were isolated in the presence of STRYCH, GlyR sIPSCs were isolated in the presence of PTX/TPMPA, and all sIPSCs were eliminated in the presence of PTX/TPMPA/STRYCH. B) Normalized average glycinergic sIPSC of WT ooDS RGCs (black), ON α RGCs (grey), W3*Gla1*^{KD} (green) (See Chapter 3). C) WT ooDS RGC mean frequency (5.7 ± 0.4 events/sec) (Ci), rise time (3.2 ± 0.2 ms) (Cii), amplitude (61.4 ± 3.8 pA) (Ciii), and τ_{decay} (22.3 ± 0.6 ms) (Civ). D) Distribution of WT ooDS RGC glycinergic sIPSC τ_{decay} times. E) Cumulative distribution of glycinergic sIPSC τ_{decay} times in WT ooDS RGCs (black) and ON α RGCs (grey).

ooDS RGCs Express GlyR α 4-Positive Puncta

As an independent measure of subunit specific expression, we assessed GlyR α 4 positive puncta on the ooDS RGC dendrites and compared the density to an estimate of random puncta coincidence. The average ooDS GlyR α 4-positive puncta density was 0.15 ± 0.02 puncta $\cdot \mu\text{m}^{-1}$, which was significantly more than the random GlyR α 4-positive puncta density, which was 0.11 ± 0.01 puncta $\cdot \mu\text{m}^{-1}$ (Figure 4.3B,D $p < 0.0004$ (paired one-tailed T-test). When corrected for our estimate of randomly associated GlyR α 4-positive puncta, the corrected density of GlyR α 4 puncta expression on ooDS RGCs was 0.04 ± 0.01 puncta $\cdot \mu\text{m}^{-1}$ (Figure 4.3D). This corrected GlyR α 4-positive puncta value suggest positive expression of GlyR α 4 on ooDS RGCs. GlyR α 4 expression is absent in the *Gla4*^{-/-} retina (Nobles et al., 2012).

We also assessed GlyR α 2 positive puncta on the ooDS RGC dendrites and compared the density to an estimate of random puncta coincidence. The average ooDS RGC GlyR α 2-positive puncta density was 0.30 ± 0.09 puncta $\cdot \mu\text{m}^{-1}$, which was

similar to the random GlyR α 2-positive puncta density, which was 0.21 ± 0.06 puncta $\cdot \mu\text{m}^{-1}$ (Figure 4.3C,E, $p > 0.05$ (paired one-tailed T-test). When corrected for our estimate of randomly associated GlyR α 2-positive puncta, the corrected density of GlyR α 2 puncta expression on ooDS RGCs was 0.09 ± 0.08 puncta $\cdot \mu\text{m}^{-1}$ (Figure 4.3E). The similarity between the GlyR α 2-positive puncta and chance puncta coincidence suggests GlyR α 2 expression is absent on ooDS RGCs. GlyR α 2 expression is absent in the *Gla2*^{-/-} retina (Nobles et al., 2012).

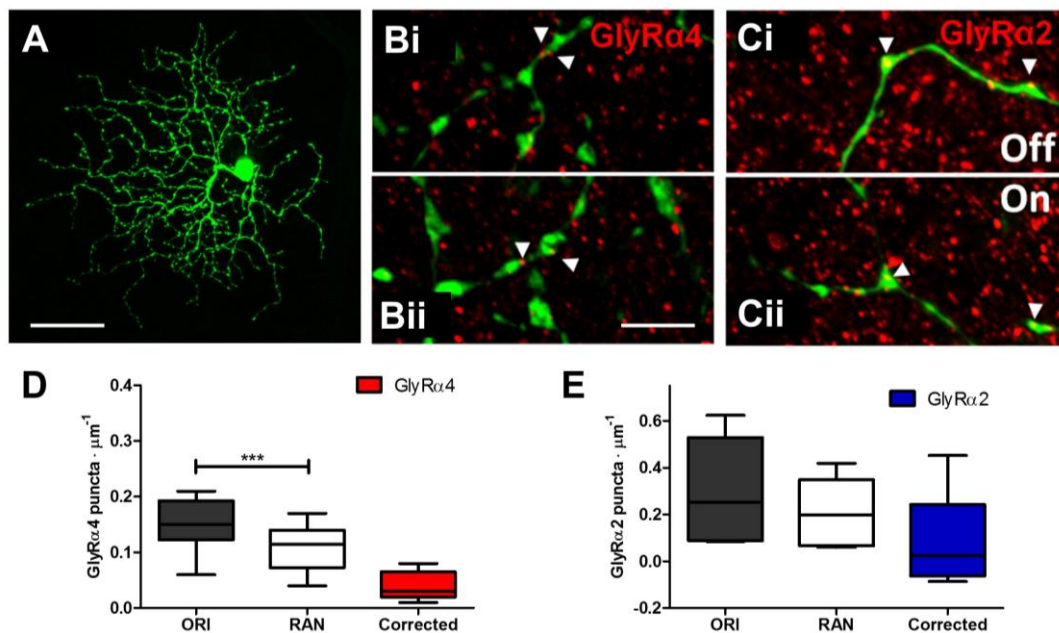


Figure 4.3. ooDS RGCs Express GlyR α 4 Puncta. (Images and data sourced from (C. Zhang, 2015). A) Whole mounted *En Face* image of ooDS RGC filled with neurobiotin (scale bar: $40\mu\text{m}$). B) Wholemount image of ooDS RGC dendrites (Bi – ON sublamina, Bii – OFF sublamina) stained for GlyR α 4 expression (red) (scale bar: $5\mu\text{m}$). White arrows indicate representative co-localization of GlyR α 4. C) Wholemount image of ooDS RGC dendrites (Ci – ON sublamina, Cii – OFF sublamina) stained for GlyR α 2 expression (red) (scale bar: $5\mu\text{m}$). White arrows indicate representative co-localization of GlyR α 2. D) Dendrites in WT ooDS RGCs have significantly more GlyR α 4 puncta density co-localization (μm^{-1}) than coincidence co-localization in the flipped (RAN) orientation (Wilcoxon Matched-pairs T-test, p value < 0.006). The corrected puncta density for GlyR α 4 puncta on ooDS RGCs is $0.04 \pm 0.01 \mu\text{m}^{-1}$ (4 cells, 10 dendritic areas). E) Dendrites in WT ooDS RGCs do not show significantly more GlyR α 2 puncta density co-localization (μm^{-1}) than coincidence co-localization in the flipped (RAN) orientation (Wilcoxon Matched-pairs T-test, p value < 0.563). The corrected

puncta density for GlyR α 2 puncta on ooDS RGCs is $0.09 \pm 0.08 \mu\text{m}^{-1}$ (3 cells, 6 dendritic areas)

*GlyR α 2-Mediated Synaptic Inputs Remain in *Glra4*^{-/-} ooDS RGCs*

To test the hypothesis that the ooDS RGCs express GlyR α 4, we recorded glycinergic sIPSCs in *Glra4*^{-/-} ooDS RGCs and found that the glycinergic sIPSC frequency was 5.8 ± 0.7 events/sec, which was similar to WT (Figure 4.4C; $p > 0.05$). In the presence of strychnine, all ooDS RGC glycinergic sIPSCs were eliminated in the *Glra4*^{-/-} indicating these were indeed GlyR-mediated. We characterized the glycinergic sIPSCs in the *Glra4*^{-/-} to determine what other GlyR α subunit is expressed and mediates these slow glycinergic synaptic currents. The *Glra4*^{-/-} ooDS glycinergic sIPSCs had a mean rise time of 3.4 ± 0.4 ms and were similar to WT (Figure 4.4D, $p > 0.05$). The ooDS RGC glycinergic sIPSC mean amplitude was 56.9 ± 8.0 pA, which was similar to WT (Figure 4.4E, $p > 0.05$). The glycinergic sIPSCs in the *Glra4*^{-/-} ooDS RGCs had a mean τ_{decay} of 23.5 ± 1.8 ms, which was also similar to WT (Figure 4.4F,G, $p > 0.05$). However, the τ_{decay} cumulative distribution of glycinergic sIPSCs of the *Glra4*^{-/-} ooDS RGCs was significantly different from WT and the curve was shifted to the right (Figure 4.4F, Kolmogorov–Smirnov test $p < 4.3e^{-5}$). Considering the GlyR α 4 puncta expression and the shift of the glycinergic sIPSC τ_{decay} curve indicate GlyR α 4 may be expressed on ooDS RGCs, but the similar sIPSC frequency and kinetics led us to hypothesize the majority of the glycinergic sIPSCs are mediated by GlyR α 2.

*Slow Glycinergic-Mediated sIPSCs Remain in the *Glra2*^{-/-} ooDS RGCs*

We tested the hypothesis that GlyR α 2 receptors mediate synaptic currents in ooDS RGCs, and recorded from these cells in *Gla2*^{-/-} retinas. Surprisingly, the frequency of glycinergic sIPSCs in *Gla2*^{-/-} ooDS RGCs was 6.3±0.4 events/sec and was similar to both WT and *Gla4*^{-/-} (Figure 4.4C; $p > 0.05$). In the presence of strychnine, the glycinergic sIPSCs were eliminated, demonstrating they are GlyR-mediated. The average rise time of the remaining glycinergic sIPSCs in the *Gla2*^{-/-} ooDS RGCs was 3.5±0.2 ms and was similar to both the WT and *Gla4*^{-/-} (Figure 4.4D, $p > 0.05$). The mean amplitude of the *Gla2*^{-/-} ooDS RGC glycinergic sIPSCs was 80.1±9.5 pA, and was similar to WT and *Gla4*^{-/-} (Figure 4.4E, $p > 0.05$). The average *Gla4*^{-/-} ooDS RGC glycinergic sIPSC τ_{decay} was 20.3±0.6 ms, which was also similar to WT and *Gla4*^{-/-} in the absence of GlyR α 2 (Figure 4.4F,G, $p > 0.05$). However, the cumulative glycinergic sIPSC τ_{decay} curve differed significantly from both WT and *Gla4*^{-/-} (Figure 4.4F, Kolmogorov–Smirnov test, $p < 0.02$ (*Gla2*^{-/-} vs. WT) and $p < 2.6e^{-04}$ (*Gla2*^{-/-} vs. *Gla4*^{-/-})). Considering the contention of eliminating GlyR α 2 or GlyR α 4 and observing no loss of glycinergic sIPSC frequency in ooDS RGCs, like we observe in other multi-subunit glycine receptor expression cells (see Chapter 3), we examined the glycinergic sIPSCs in a double KO model (*Gla4*^{-/-}/*Gla2*^{-/-}).

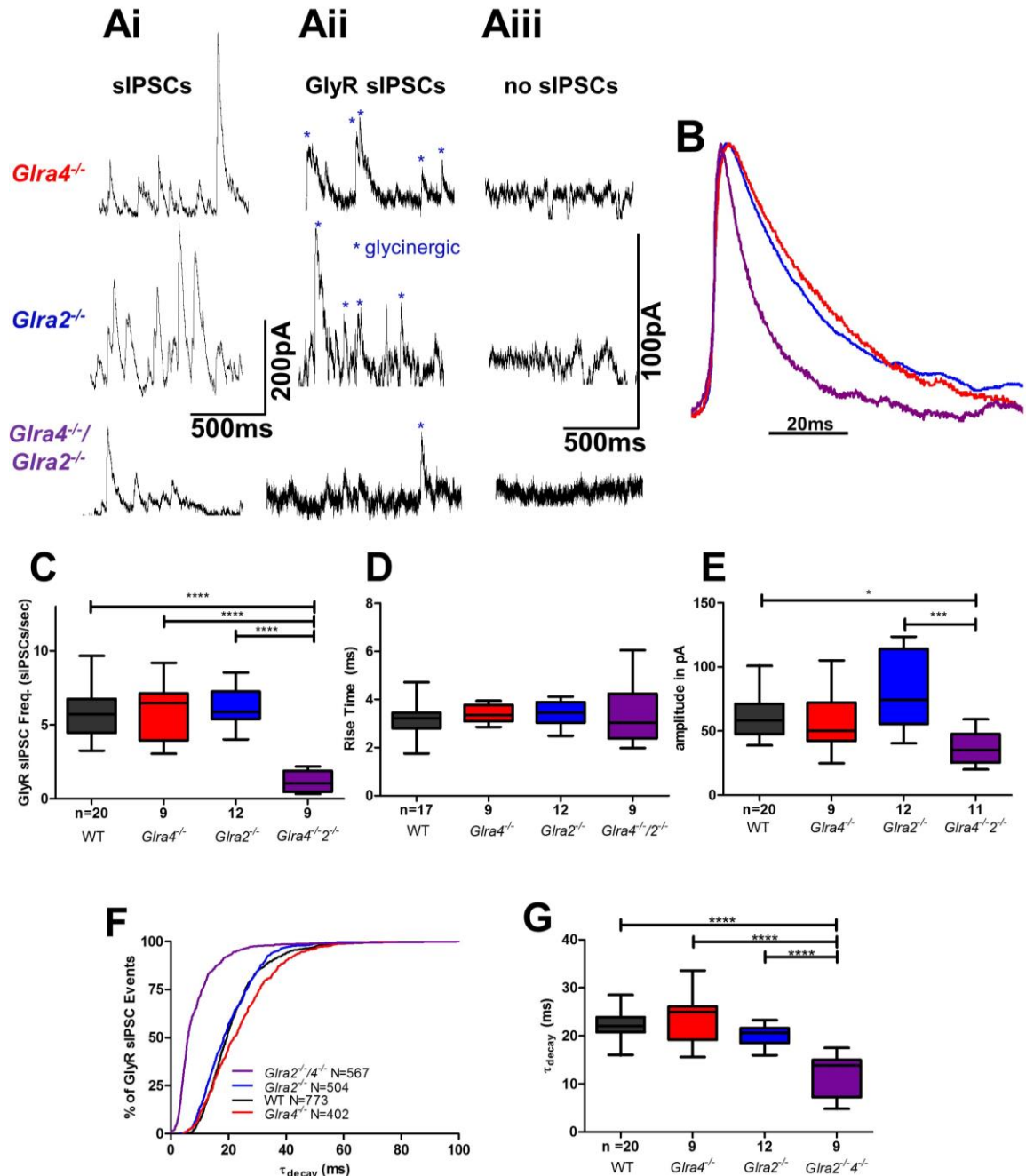


Figure 4.4. ooDS RGCs express both GlyR α 2 and GlyR α 4 A) Raw traces of sIPSCs (Ai), GlyR sIPSCs isolated in the presence of PTX/TPMPA (Aii), and eliminated sIPSCs in the presence of PTX/TPMPA/STRYCH (Aiii) in *Glra2*^{-/-}, *Glra4*^{-/-} and *Glra2*^{-/-}/*Glra4*^{-/-} ooDS RGCs. B) Average glycinergic sIPSC trace of *Glra4*^{-/-} (red), *Glra2*^{-/-} (Blue), and *Glra2*^{-/-}/*Glra4*^{-/-} ooDS RGCs C) Mean frequency (events/sec) of glycinergic sIPSCs in ooDS RGCs: WT (5.7±0.4), *Glra4*^{-/-} (5.8±0.7), *Glra2*^{-/-} (6.3±0.4), *Glra2*^{-/-}/*Glra4*^{-/-} (1.1±0.2). *Glra2*^{-/-}/*Glra4*^{-/-} GlyR sIPSC frequency is significantly less than WT or single KOs (One-way Analysis

of Variance, Bonferroni Post-Hoc test, **** p value < 0.0001). D) Average rise times of ooDS RGC glycinergic sIPSCs in WT (3.2 ± 0.2 ms), *Glra4*^{-/-} (3.4 ± 0.1 ms), *Glra2*^{-/-} (3.5 ± 0.2 ms), and *Glra2*^{-/-}/*Glra4*^{-/-} (3.4 ± 0.4 ms) are all similar (One-way Analysis of Variance, Bonferroni Post-Hoc test, p value > 0.05). E) Average amplitude of ooDS RGC glycinergic sIPSCs in: WT (61.4 ± 3.8 pA), *Glra4*^{-/-} (56.1 ± 9.0 pA), *Glra2*^{-/-} (93.4 ± 15.9 pA), and *Glra2*^{-/-}/*Glra4*^{-/-} (31.4 ± 4.7 pA). *Glra2*^{-/-}/*Glra4*^{-/-} was significantly less than both WT and *Glra2*^{-/-} (One-way Analysis of Variance, Bonferroni Post-Hoc test, * p value < 0.05, *** p value < 0.001). F) Cumulative distribution of GlyR sIPSC τ_{decay} in ooDS RGCs: WT (black), *Glra4*^{-/-} (red), *Glra2*^{-/-} (blue), *Glra2*^{-/-}/*Glra4*^{-/-} (purple). *Glra2*^{-/-}/*Glra4*^{-/-} GlyR sIPSC τ_{decay} is significantly faster than WT and both single KOs (Kolmogorov–Smirnov test). G) The mean τ_{decay} of ooDS RGC glycinergic sIPSCs was similar among: WT (22.3 ± 0.6 ms), *Glra4*^{-/-} (23.5 ± 1.8 ms), *Glra2*^{-/-} (20.3 ± 0.6 ms), and *Glra2*^{-/-}/*Glra4*^{-/-} (11.8 ± 1.5 ms) (One-way Analysis of Variance, Bonferroni Post-Hoc test, * p value > 0.05).

Glra4^{-/-}/*Glra2*^{-/-} Eliminates 80% of the Glycine-Mediated Synaptic Inputs in ooDS RGCs

To test the hypothesis that ooDS RGCs express both GlyR α 4 and GlyR α 2, we recorded glycinergic sIPSCs in these cells using *Glra4*^{-/-}/*Glra2*^{-/-}/TRHR mouse retinas. The *Glra4*^{-/-}/*Glra2*^{-/-} ooDS RGC frequency of glycinergic sIPSCs was 1.1 ± 0.2 events/sec, which was significantly less than WT, *Glra4*^{-/-} and *Glra2*^{-/-} (Figure 4.4C, p < 0.0001). This significant reduction in glycinergic sIPSC frequency indicates ooDS RGCs express both GlyR α 2 and GlyR α 4. However, some glycinergic sIPSCs remain in the *Glra4*^{-/-}/*Glra2*^{-/-} ooDS RGCs, and these were eliminated in the presence of strychnine (Figure 4.4Aiii). We examined the remaining glycinergic sIPSCs and found the average rise time of 3.4 ± 0.4 ms was similar to WT, *Glra2*^{-/-}, and *Glra4*^{-/-} (Figure 4.4D, p > 0.05). The average glycinergic sIPSC amplitude of ooDS RGCs in the *Glra4*^{-/-}/*Glra2*^{-/-} was 31.4 ± 4.7 pA, which was significantly less than both WT and *Glra2*^{-/-}, but similar to *Glra4*^{-/-} (Figure 4.4E, p < 0.001). The mean τ_{decay} of the remaining glycinergic sIPSCs in the *Glra4*^{-/-}/*Glra2*^{-/-}

ooDS RGCs was 11.8 ± 1.5 ms and significantly less than WT, *Glr4^{-/-}*, and *Glr2^{-/-}* (Figure 4.4G, $p < 0.0001$, One-way Analysis of Variance, Bonferroni Post-Hoc test). Similarly, the cumulative glycinergic sIPSC τ_{decay} curve differed significantly from WT, *Glr4^{-/-}*, and *Glr2^{-/-}* (Figure 4.4F, Kolmogorov–Smirnov test, $p < 8.08e^{-84}$). The characteristics of the remaining ooDS RGC glycinergic sIPSCs are most similar to GlyR α 3 currents that we recorded in F-mini RGCs in *Glr2^{-/-}* retinas, and in *Glr1_{KD}* infected W3 RGCs (see chapter 3) (Table 4.2). Based on these comparisons, we conclude that ooDS RGC glycinergic sIPSCs are primarily mediated by GlyR α 4 and GlyR α 2, with ~20% missing arising from GlyR α 3-mediated.

Table 4.2. GlyR α 3-Mediated sIPSC Currents.

RGC Type / Receptor / Model	Mean Rise Time (ms)	Mean Amplitude (pA)	Mean τ_{decay} (ms)
F-mini / GlyR α 3 / <i>Glr2^{-/-}</i>	2.0 ± 0.1	22.4 ± 3.0	7.8 ± 0.4
W3 / GlyR α 3 / <i>Glr1_{KD}</i>	2.5 ± 0.4	26.9 ± 3.1	10.1 ± 1.0
ooDS / GlyR α 3? / <i>Glr4^{-/-}/Glr2^{-/-}</i>	3.4 ± 0.4	31.4 ± 4.7	11.8 ± 1.5

rAAV-Mediated RNAi Reduces the GlyR-mediated sIPSC Frequency in rAAV-Glr4-shRNA Infected ooDS RGCs

There are several reasons why the frequency of glycinergic sIPSCs in *Glr4^{-/-}* or *Glr2^{-/-}* ooDS RGCs is similar to WT (Figure 4.4C). The frequency could be maintained if the global absence of one or the other glycine receptor enhances presynaptic glycine release onto the ooDS RGCs. There is also the possibility that expression of each of these receptors could be upregulated in the absence of the other, although we previously found no evidence for upregulation (Nobles et al., 2012). The WT GlyR receptor could be a heteromer containing both α 4 and α 2

subunits with a stoichiometry of (3 β :1 α 4:1 α 2). In this case, when either GlyR α 4 or GlyR α 2 expression was eliminated the remaining GlyR receptor would simply be composed of the typically observed GlyR2 α (3 β :2 α). There could be a fifth unknown glycine receptor alpha subunit, although this is unlikely because only four different α subunit genes are known from genetic screening.

To begin to distinguish among these possible scenarios, we eliminated expression of each receptor subunit selectively in only RGCs (as opposed to a global knockout) using an approach in which a retrogradely transported rAAV shRNA knocks down GlyR expression (C. Zhang et al., 2014). We first targeted double-labeled YPF positive ooDS RGCs with red nuclei in the rAAV-*Gira4*_{KD}-shRNA injected TRHR mice. In these infected cells expressing *Gira4*_{KD}-shRNA, the average frequency of glycinergic sIPSCs was 2.6 \pm 0.5 events/sec and was significantly reduced compared to WT (Figure 4.5B; $p < 0.0006$). This glycinergic sIPSC frequency represents a 55% reduction in glycinergic activity. Interestingly, the average rise time became slower at 4.6 \pm 0.3 ms than both WT and *Gira4*^{-/-} (Figure 4.5C, $p < 0.0001$). The mean amplitude of glycinergic sIPSCs in the *Gira4*_{KD}-shRNA was 28.5 \pm 3.7 pA and was significantly lower than both WT and *Gira4*^{-/-} (Figure 4.5D, $p < 0.0009$). The average τ_{decay} was 20.2 \pm 1.1 ms, which was similar to WT and *Gira4*^{-/-} (Figure 4.5F, $p > 0.05$). The cumulative distribution curve of the glycinergic sIPSC τ_{decay} of the *Gira4*_{KD}-shRNA infected ooDS RGCs was significantly different from both WT and *Gira4*^{-/-} (Figure 4.5E, Kolmogorov–Smirnov test, $p < 5.9e^{-11}$). A reduced frequency and amplitude in the *Gira4*_{KD}-shRNA infected ooDS RGCs suggests the synapses express fewer GlyRs overall. The

slow average τ_{decay} suggests that the majority of the remaining glycinergic sIPSCs are mediated by GlyR α 2. To evaluate the effectiveness of rAAV-*Gira4*_{KD}-shRNA, we then recorded glycinergic sIPSCs from ooDS RGCs in rAAV-*Gira4*_{KD}-shRNA in the *Gira2*^{-/-}/TRHR mouse model. We hypothesized the sIPSCs in this experiment would be similar to the *Gira4*^{-/-}/*Gira2*^{-/-} and have some remaining sIPSCs with a lower amplitude and a faster τ_{decay} .

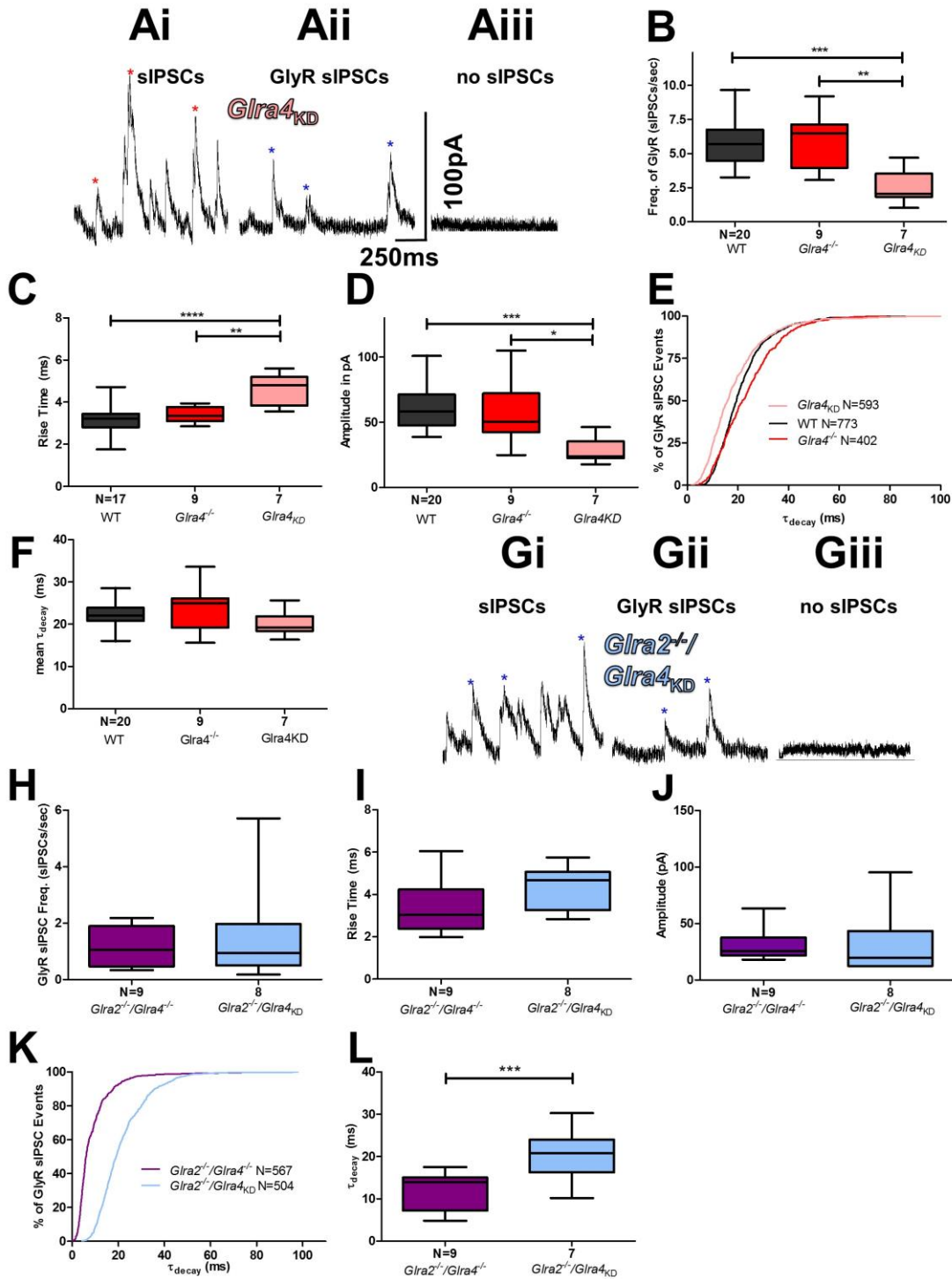


Figure 4.5. rAAV-*Glra4_{KD}*-shRNA reduces the frequency of glycinergic sIPSCs in oODS RGCs. A) Raw traces of rAAV-*Glra4_{KD}* infected oODS RGC glycinergic sIPSCs in cntl. bath (Ai), in the presence of PTX/TPMPA (Aii), and in PTX/TPMPA/STRYCH (Aiii). B) The mean frequency (events/sec) of glycinergic sIPSCs in oODS RGCs was significantly lower in *Glra4_{KD}*: WT (5.9 ± 0.4), *Glra4^{-/-}*

(5.8 ± 0.7), *Glr4_{KD}* (2.2 ± 0.4) (p value < 0.0025 One-Way Analysis of Variance, Bonferroni Post-Hoc test) **C**) Mean rise time (ms) of glycinergic sIPSCs in ooDS RGCs in WT (3.2 ± 0.4 ms), *Glr4^{-/-}* (3.4 ± 0.1 ms), and *Glr4_{KD}* (4.6 ± 0.3 ms). *Glr4_{KD}* is significantly higher than both WT and *Glr4^{-/-}* (p value < 0.001 One-Way Analysis of Variance, Bonferroni Post-Hoc test). **D**) The mean amplitude of ooDS RGC glycinergic sIPSCs was significantly less in *Glr4_{KD}*: WT (61.4 ± 3.8 pA), *Glr4^{-/-}* (56.1 ± 9.0 pA), and *Glr4_{KD}* (28.1 ± 4.3 pA) (p value < 0.0009 One-Way Analysis of Variance, Bonferroni Post-Hoc test). **E**) Cumulative distribution of GlyR sIPSC τ_{decay} in ooDS RGCs: WT (black), *Glr4^{-/-}* (red), rAAV-*Glr4_{KD}*-shRNA (pink). *Glr4_{KD}* τ_{decay} distribution is no different than WT or *Glr4^{-/-}* (Kolmogorov–Smirnov test). **F**) Mean glycinergic sIPSC τ_{decay} of WT, *Glr4^{-/-}*, and rAAV-*Glr4_{KD}*-shRNA infected ooDS RGCs were all similar (p > 0.05, One-Way Analysis of Variance, Bonferroni Post-Hoc test). **G**) Raw traces of *Glr2^{-/-}* + rAAV-*Glr4_{KD}* infected ooDS RGC glycinergic sIPSCs in cntl. bath (Gi) and in PTX/TPMPA (Gii), and in PTX/TPMPA/STRYCH (Giii). **H**) The mean frequency (events/sec) of glycinergic sIPSCs in ooDS RGCs was similar between: *Glr2^{-/-}/Glr4^{-/-}* (1.2 ± 0.2) and *Glr2^{-/-}* + rAAV-*Glr4_{KD}* infected ooDS RGCs (1.6 ± 0.6) (p > 0.05, One-Way Analysis of Variance, Bonferroni Post-Hoc test). **I**) Mean Rise time (ms) of glycinergic sIPSCs in ooDS RGCs in *Glr2^{-/-}/Glr4^{-/-}* (3.4 ± 0.4 ms) and *Glr2^{-/-}* + rAAV-*Glr4_{KD}* (4.3 ± 0.4 ms), was similar (p > 0.05, One-Way Analysis of Variance, Bonferroni Post-Hoc test). **J**) The mean amplitude of ooDS RGC glycinergic sIPSCs was similar between: *Glr2^{-/-}/Glr4^{-/-}* (31.4 ± 4.7 ms) and *Glr2^{-/-}* + rAAV-*Glr4_{KD}* (31.0 ± 10.1 ms) (p > 0.05, One-Way Analysis of Variance, Bonferroni Post-Hoc test). **K**) Cumulative distribution of GlyR sIPSC τ_{decay} in ooDS RGCs: *Glr2^{-/-}/Glr4^{-/-}* (purple) and *Glr2^{-/-}* + rAAV-*Glr4_{KD}* (light blue). The *Glr2^{-/-}* + rAAV-*Glr4_{KD}* glycinergic sIPSC τ_{decay} is significantly shifted to the right of *Glr2^{-/-}/Glr4^{-/-}* (Kolmogorov–Smirnov test). **L**) The mean glycinergic sIPSC τ_{decay} of *Glr2^{-/-}* + rAAV-*Glr4_{KD}* (20.3 ± 2.1 ms) is significantly slower than *Glr2^{-/-}/Glr4^{-/-}* (11.8 ± 1.5 ms) (p < 0.05, One-Way Analysis of Variance, Bonferroni Post-Hoc test).

rAAV-Mediated RNAi in Glr2^{-/-} ooDS RGCs Eliminates GlyR α 4-Mediated

sIPSCs in rAAV-Glr4-shRNA Infected ooDS RGCs

In *Glr2^{-/-}* ooDS RGCs infected with the *Glr4_{KD}*-shRNA, the frequency of glycinergic sIPSCs was 1.6 ± 0.7 events/sec, which was similar to the frequency recorded in *Glr2^{-/-}/Glr4^{-/-}* (Figure 5H, p > 0.05). The rise time of the infected ooDS RGCs was 4.5 ± 0.4 ms and similar to the rise time of the double knockout (Figure 5I, p > 0.05). The mean amplitude of the glycinergic sIPSCs in the *Glr4_{KD}*-shRNA

infected *Gla2*^{-/-} ooDS RGCs was 33.7±11.3 pA and was also similar to the *Gla2*^{-/-}/*Gla4*^{-/-} model (Figure 5J, $p > 0.05$). Surprisingly, the glycinergic sIPSC τ_{decay} cumulative distribution of the *Gla4*_{KD}-shRNA infected *Gla2*^{-/-} ooDS RGCs was significantly slower than the double knockout (Figure 5K, Kolmogorov–Smirnov test, $p < 6.8e^{-97}$). Correspondingly, the glycinergic sIPSC mean τ_{decay} of the *Gla4*_{KD}-shRNA infected *Gla2*^{-/-} ooDS RGCs was 21.7±1.8 ms and significantly slower than the *Gla4*^{-/-}/*Gla2*^{-/-} (4.5L, $p < 0.0007$). The glycinergic sIPSC frequency, rise time, and amplitude data suggest the *Gla4*_{KD}-shRNA infected *Gla2*^{-/-} ooDS RGCs are identical to *Gla4*^{-/-}/*Gla2*^{-/-} ooDS RGCs. In contrast, the glycinergic sIPSC τ_{decay} of the *Gla4*_{KD}-shRNA infected *Gla2*^{-/-} ooDS RGCs was significantly slower than *Gla4*^{-/-}/*Gla2*^{-/-} ooDS RGCs. The most likely explanation is that a developmental difference occurs when these RGCs lack glycinergic receptors from birth.

DISCUSSION

We demonstrated that WT ooDS RGCs receive synaptic glycinergic inputs and that these inputs are mediated by postsynaptic GlyRs with slow decay kinetics. Previous studies have shown that the α subunit of the GlyR is responsible for the decay kinetics of the synaptic inputs, the sIPSCs. Furthermore, those studies measured the sIPSC τ_{decay} of GlyR α 1 as ~3 ms, GlyR α 3 as ~ 10 ms, GlyR α 2 as ~27 ms, and GlyR α 4 as ~53 ms at room temperature or 25°C (Majumdar et al., 2007; Majumdar et al., 2009; Wassle et al., 2009). In our analysis of glycinergic sIPSCs we estimated both GlyR α 4 and GlyR α 2 receptors to have a faster τ_{decay}

time than the reported results due to the fact that our recording was at the mouse core body temperature of 36°C, which likely represents *in vivo* physiological GlyR kinetics. We then tested our hypothesis that WT ooDS RGCs express either GlyR α 4 or GlyR α 2 using immunohistochemistry and stained for GlyR α subunit specific-mediated puncta. Our findings confirmed GlyR α 4 is expressed on ooDS RGCs, but were inconclusive of their expression of GlyR α 2. Using *Glra4*^{-/-} (global knockout model) we recorded glycinergic sIPSCs in the ooDS RGCs and found the frequency, rise time, amplitude, and mean τ_{decay} similar to WT, and only the sIPSC cumulative distribution of τ_{decay} as an indication ooDS RGCs express GlyR α 4. We then recorded glycinergic sIPSCs in the *Glra2*^{-/-} and also found them to be similar to WT. Only when we recorded glycinergic sIPSCs from *Glra4*^{-/-}/*Glra2*^{-/-} did we see a significant reduction in sIPSC frequency, which demonstrated WT ooDS RGCs express both GlyR α 4 and GlyR α 2. We also measured the remaining sIPSCs and found their mean τ_{decay} to be indicative of GlyR α 3 ~10 ms. Further investigation is needed to verify that GlyR α 4 and GlyR α 2 expression is accompanied by the expression of GlyR α 3 or another GlyR.

Intrigued by the similarity of the glycinergic sIPSC analysis results of the single knockout model of ooDS RGC to the WT model, we recorded ooDS RGCs infected with an rAAV-*Glra4*_{KD}-shRNA and found the frequency of glycinergic sIPSCs was reduced. Additionally, we tested the same *Glra4*_{KD}-shRNA in *Glra2*^{-/-} to verify the effectiveness of the *Glra4*_{KD}-shRNA. We found that the *Glra2*^{-/-} + rAAV-*Glra4*_{KD}-shRNA infected ooDS RGCs had a similar frequency, amplitude, and rise time as the *Glra4*^{-/-}/*Glra2*^{-/-}. However, the mean τ_{decay} and the cumulative

distribution of the τ_{decay} was significantly slower. This is likely due to the imperfect efficiency of the *Glr4*_{KD}-shRNA as observed in Chapter 3 and in (C. Zhang et al., 2014). Our previous results from using an rAAV with shRNA to knockdown the expression of a GlyR were effective but some glycinergic sIPSCs remained (C. Zhang et al., 2014). It is likely some GlyR α 4 expression remains the *Glr2*^{-/-} + *Glr4*_{KD}-shRNA knockdown model, though low as mediated by the reduction in sIPSC frequency, remaining sIPSCs mediated by this expression may cause the τ_{decay} kinetics to be more similar to WT.

Synapse-Specific Expression of GlyR α 2 and GlyR α 4

In RGCs that co-express two or more GlyRs (F-mini, LED, HD, UHD, and J-RGC) the global knockout of a single GlyR α showed a reduction of glycinergic sIPSC frequency and the remaining sIPSCs demonstrated their standalone amplitude and kinetics (See Chapter 3). This result suggests different glycine receptor subtypes are expressed at different synapses in the same cell since a lower frequency of GlyR sIPSCs indicates less complete synaptic transmission due to the entire loss of receptors in a single synapse. However, evaluations of glycinergic sIPSCs in *Glr2*^{-/-} or *Glr4*^{-/-} in ooDS RGCs showed no change frequency or amplitude, which suggested two possibilities: 1) WT ooDS RGCs co-express GlyR α 4 and GlyR α 2 in different synapses, and global loss of one of these glycine receptors alters inhibition to their presynaptic amacrine cell. This change increases glycine release from the amacrine cells and a concomitant increase in GlyR sIPSC frequency in the ooDS RGCs, effectively masking the fewer number of GlyR synapses. 2) WT ooDS RGCs also co-express GlyR α 4 and GlyR α 2 in this

scenario, however, the loss of one glycine receptor subtype is compensated by the expression of the remaining glycine receptor expressed in the cell. Furthermore, it is conceivable the trafficking mechanisms for the two GlyRs could be the same, and traffic GlyR α 2 or GlyR α 4 interchangeably because these two GlyRs share a 91% homology (Matzenbach et al., 1994).

Scenario one is unlikely because we demonstrated drastic loss of glycinergic sIPSC activity in the *Gira4^{-/-}/Gira2^{-/-}* ooDS RGCs. Splice variants of the GlyR α 2 subunit have been found in the brain and spinal cord, making this scenario important to consider in future investigations (Miller et al., 2004; Oertel, Villmann, Kettenmann, Kirchhoff, & Becker, 2007). In the second scenario, the loss of a single glycine receptor could affect the downstream release properties of glycine vesicles onto ooDS RGCs, and mask the loss of GlyR expression by over-releasing glycine into synapses with the remaining GlyR. However, GlyR α 2, GlyR α 3, and GlyR α 1 are densely expressed throughout the IPL, yet GlyR α 4 is expressed only in the ON choline Acetyltransferase band in the IPL. (Buldyrev, Puthussery, & Taylor, 2012; Demb & Singer, 2012; Eggers & Lukasiewicz, 2006a; S. C. Lee et al., 2015; Manookin et al., 2008; Wassle et al., 2009; Weiss et al., 2008). As a result, to date, GlyR α 4 has only been found expressed in the ON SAC cells, which are synaptically connected to ooDS RGCs, but do not release glycine (S. C. Lee et al., 2015; Menger, Pow, & Wassle, 1998; Pow & Hendrickson, 1999). It is unlikely that both single knockouts would similarly affect the downstream AC-mediated glycine release onto ooDS RGCs because of the differential expression of GlyR α 2 and GlyR α 4. Nevertheless, the ON SACs may express both GlyR α 2

and GlyR α 4 (see Chapter 3), and the global loss of either GlyR may affect a serial inhibition connection, which influences glycine release onto the ooDS RGCs. And, GlyR α 4 and GlyR α 2 are kinetically similar. This scenario where glycine release is upregulated in the single knockout of either GlyR α 4 or GlyR α 2 is more likely to occur than the existence of a splice variant. However, the feasibility of both single KOs affecting glycine release onto the ooDS RGCs in a similar manner is not substantial.

In the third scenario, enough of the remaining GlyR mRNA in a single global knockout of another GlyR, is already present and it is translated and trafficked to the synapses, which would normally express the knocked out GlyR i.e. compensation for the loss of the knocked out GlyR. Or, compensation could occur via a more complex mechanism where there is gene overexpression of the remaining GlyR. We did successfully demonstrate this scenario is unlikely in our experiments using rAAV-*Gira4*KD-shRNA. In this experiment, the glycinergic sIPSC frequency was significantly reduced in rAAV-*Gira4*KD-shRNA infected WT ooDS RGCs. Also, the average GlyR turnover rate is about 20 hours, while in our rAAV injection experiments the rAAV-*Gira4*KD-shRNA was in the retina for up to a week before recording (Chow, Zuchowski, & Fetcho, 2017). However, this scenario is still the most feasible explanation for our findings because our experiments did not account for the upregulation or overexpression of the remaining GlyR in the single KO models that could have occurred during development. Our experiments should be recapitulated and account for the loss of a GlyR and the possible compensation of that loss during development. Furthermore, one could potentially

measure the rate of GlyR expression during development in a single KO model using qPCR.

CHAPTER V

DISCUSSION

I. GENERAL DISCUSSION

Studying the brain as a vision scientist gives one exposure to almost every facet of biomedical research. Researchers from almost every discipline can find a way to investigate the visual system. By using the tried and true methods of electrophysiology and immunohistochemistry, I successfully managed to add to the vast and quickly growing body of knowledge concerning vision. Though these methods continue to be the gold standard, vision research is expanding into realms likely never fathomed by the great vision scientists such as Barlow and Hill, Enroth-Cugell and Kuffler. The rapid development of technology and the mixing of disciplines has given vision researchers tools to parse out circuits, discover new cell types, and model the visual system for artificial intelligence. This field will likely continue to expand and will be fascinating to watch from the perspective of a scientist.

CHAPTER III Summary

We successfully identified much of the GlyR α subunit specific expression in a subset of RGCs, which together make up about 50% of the roughly 40,000 retinal ganglion cells found in a mouse retina. Collectively, these cells differentially

express all four different glycine receptor subtypes in the IPL. The α RGCs express GlyR α 1, the LED, HD, and UHD RGCs express both GlyR both GlyR α 3 and GlyR α 1, the F-mini RGCs express both GlyR α 2 and GlyR α 3, the J-RGCs express GlyR α 2, and the ON SACs likely express both GlyR α 4 and GlyR α 2. This is a comprehensive list of identified RGCs that collectively express each of the four GlyR α subunits. This list can now be exploited to investigate the individual roles of the different GlyRs within the retina. Furthermore, we developed an assay to investigate GlyR expression via a global knockout approach. This approach can be used to study other RGCs of interest and discover their GlyR subunit specific expression. Future research of retinal inhibitory circuits should evaluate the role of glycinergic inhibition at the level of the specific GlyR subunit as opposed to an all-or-none approach with disregard to subtle differences that avoid new discoveries.

Though our knockout approach was sufficient in the investigation of some of the RGC types, we employed a more powerful tool, the use of two different rAAV delivered shRNAs to knock down the expression of *Glr1* and *Glr4*. The knockdown experiments are superior to the global knock out experiments for many reasons: 1) Only glycine receptors expressed on infected RGCs are knocked down. Thus, with synapses and all glycine receptors of the upper circuitry intact, measurable changes are not masked or amplified by the loss of glycine receptors in other retinal cells. 2) In addition to studying glycine receptor function on retinal ganglion cells, knocking down glycine receptor expression also isolates the GABAergic receptors allowing for the study of their function. 3) rAAV delivered shRNAs allow for precise temporal control of the target gene so the injected animal

can mature into adulthood with all inhibitory circuitry and the synapses intact. Then, only the glycine receptors are knocked down, potentially preserving glycine release properties and the glycinergic synapses in amacrine cells and bipolar cells.

CHAPTER IV Summary

While identifying the expression or co-expression of glycine receptors on specific ganglion cells, a pattern emerged where the loss of a single glycine receptor always resulted in a decrease of GlyR activity. We observed this phenomenon by measuring the glycinergic sIPSC frequency in the ON α , ON τ , OFF α , OFF δ , UHD, LED, HD1, HD2, F-mini, J-RGCs, and the ON SACs. However, when measuring the frequency of glycinergic sIPSCs in the ooDS RGCs, the loss of a single receptor (either GlyR α 2 or GlyR α 4), did not result in a decrease of GlyR activity. It was not until the double knockout of both co-expressed GlyR α 2 and GlyR α 4 did a significant decrease in glycinergic sIPSC activity occur. In both single knockout examples, *Glr2*^{-/-} or *Glr4*^{-/-}, the remaining GlyR sIPSC frequency was unchanged from WT. The possible mechanisms which explain this abnormality are:

- 1) The presence of a splice variant of one of the GlyR α subunits, which have been found for GlyR α 2 and the GlyR β subunit (Miller et al., 2004; Oertel et al., 2007). However, the splice variants of GlyR α 2 are kinetically identical and their presence in the retina would be undetectable using our electrophysiological assay (Miller et al., 2004).

2) Another possibility is that both GlyR α 2 and GlyR α 4 are co-expressed in the ooDS RGCs. The global knockout of a single GlyR α subunit would result in an increase of the glycine release from amacrine cells onto the ooDS RGCs. The increase in glycine release would compensate for the loss of the single co-expressed GlyR and the typical observed decrease in frequency would effectively be masked. Since, we observed identical results in both *Gira2*^{-/-} and *Gira4*^{-/-}, compensation of glycine release from presynaptic ACs would likely be similar. However, we know the expression of GlyR α 2 and GlyR α 4 is differential. Furthermore, there is evidence of GlyR α 2 expression on narrow-field glycinergic amacrine cells. Yet, the only AC known to express GlyR α 4 is the wide-field starburst AC; which certainly connects synaptically with ooDS RGCs, but it does not release glycine. However, the ON SAC could be involved in a serial inhibition circuit with a glycinergic amacrine that releases glycine into the inhibitory synapses of the ooDS RGCs. If the ON SAC does express both GlyR α 4 and GlyR α 2, then altered GABA release in the proposed serial circuit resulting in either *Gira4*^{-/-} and *Gira2*^{-/-} could culminate in similar glycinergic sIPSC frequency.

3) The final scenario is also possible if ooDS RGCs co-express both GlyR α 2 and GlyR α 4. In a congenital knockout of a single GlyR α subunit, the remaining normally co-expressed GlyR expression is increased to compensate for the loss of the knocked out GlyR. In addition to the previous idea is that remaining endogenous expression was already high enough to compensate for the loss of the co-expressed GlyR. We observed no compensation in the knockdown model and furthermore, compensation of any GlyR in a single GlyR KO has not been

observed (Nobles et al., 2012). However, our knockdown model does not take into account the possibility of compensation of the remaining GlyR in the single GlyR KO during development. Further study is needed to verify this more plausible scenario including both a developmental study, and the measurement of mRNA expression of GlyRs in ooDS RGCs during development in WT and single KO models, and after the infection of an rAAV-*Gira4*_{KD}-shRNA.

After we identified the GlyR co-expression of GlyR α 2 and GlyR α 4 on ooDS RGCs, we set out to identify the mechanism in which these cells successfully maintain their glycinergic sIPSC frequency after a single GlyR knockout. We employed the rAAV delivered shRNA method to knock down the expression of GlyR α 4 and found glycinergic sIPSC frequency indeed decreased after the loss of the GlyR α 4, yet some glycinergic sIPSC activity remained, presumably mediated by GlyR α 2. This result suggests that any method of glycinergic sIPSC activity compensation occurs during or before synapse development, or is dependent on the loss of GlyR α 4 on presynaptic amacrine cells.

II. FURTHER DIRECTIONS

GlyR function is dependent on the release properties of the presynaptic amacrine cells. Using known labeled presynaptic amacrine cell and post-synaptic ganglion cell pairs could aptly reveal glycine receptor function. An example would be to explore the glycine release properties of the Vglut3 amacrine cell onto the W3B cells (specifically LED cells as opposed to the other cells labeled in the W3B line (HD1, HD2, or UHD cells) (T. Kim et al., 2015). The W3 cells express both GlyR α 1 and GlyR α 3 in different synapses. The Vglut3 amacrine cell may release

glycine onto only one receptor subtype. It is also possible that the co-expression of glycine receptors enables coordinated inhibitory kinetics, which would be impossible from single GlyR expression. I.e., the cooperation between co-expressed GlyR α 1 and GlyR α 3 on LED cells would be different from the individual expression of GlyR α 1 or GlyR α 3. If these co-expressing GlyRs have a harmonious function, then the tuning of the inhibitory signal is more acute than what can be created by the four individual receptors subtypes alone.

This idea of harmonious function among two co-expressed GlyRs has not been observed. Instead, the need for the variety of different GlyR decay kinetics is observed in two different types of cells of the VCN. The bushy cells and the T stellate cells of the VCN express different subunit specific GlyRs, which individually mediate the temporal inhibition differently (slow kinetic GlyRs increase the spike threshold improving spike precision in bushy cells while fast kinetic GlyRs mediate rapid inhibition that preserves the spike threshold and eliminates poorly timed spikes improving spike timing in T stellate cells (Xie & Manis, 2013)). Given the variety of visual response properties of the forty different retinal ganglion cell types, it should not be surprising that there is a need for four different subunit specific GlyRs. The different GlyRs likely play unique roles in modulating the different excitatory input into each different RGC type. For instance, the kinetically slow GlyR α 2 and GlyR α 4 likely improve spike precision in the ooDS, ON SAC and J-RGC cells in a similar manner to the bushy cells of the VCN. Then, kinetically faster GlyRs expressed on the W3 cells may match their inhibitory input with fast excitatory input, like the T stellate cells of the VCN, to not interfere with the

membrane potential, but instead improve excitatory spike timing output and inhibit poorly timed spikes.

REFERENCES

- Akrouh, A., & Kerschensteiner, D. (2015). Morphology and function of three VIP-expressing amacrine cell types in the mouse retina. *J Neurophysiol*, *114*(4), 2431-2438. doi:10.1152/jn.00526.2015
- Awatramani, G. B., Turecek, R., & Trussell, L. O. (2004). Inhibitory control at a synaptic relay. *J Neurosci*, *24*(11), 2643-2647. doi:10.1523/JNEUROSCI.5144-03.2004
- Baden, T., Berens, P., Franke, K., Roman Roson, M., Bethge, M., & Euler, T. (2016). The functional diversity of retinal ganglion cells in the mouse. *Nature*, *529*(7586), 345-350. doi:10.1038/nature16468
- Bae, J. A., Mu, S., Kim, J. S., Turner, N. L., Tartavull, I., Kemnitz, N., . . . Eyewirers. (2018). Digital Museum of Retinal Ganglion Cells with Dense Anatomy and Physiology. *Cell*, *173*(5), 1293-1306 e1219. doi:10.1016/j.cell.2018.04.040
- Beato, M. (2008). The time course of transmitter at glycinergic synapses onto motoneurons. *J Neurosci*, *28*(29), 7412-7425. doi:10.1523/JNEUROSCI.0581-08.2008
- Betz, H., & Laube, B. (2006). Glycine receptors: recent insights into their structural organization and functional diversity. *J Neurochem*, *97*(6), 1600-1610. doi:10.1111/j.1471-4159.2006.03908.x
- Bloomfield, S. A., & Dacheux, R. F. (2001). Rod vision: pathways and processing in the mammalian retina. *Prog Retin Eye Res*, *20*(3), 351-384.
- Bormann, J. (2000). The 'ABC' of GABA receptors. *Trends Pharmacol Sci*, *21*(1), 16-19.
- Bowmaker, J. K., & Dartnall, H. J. (1980). Visual pigments of rods and cones in a human retina. *J Physiol*, *298*, 501-511.
- Bracci, E., Ballerini, L., & Nistri, A. (1996). Spontaneous rhythmic bursts induced by pharmacological block of inhibition in lumbar motoneurons of the neonatal rat spinal cord. *J Neurophysiol*, *75*(2), 640-647. doi:10.1152/jn.1996.75.2.640
- Brink, P. R., Cronin, K., & Ramanam, S. V. (1996). Gap junctions in excitable cells. *J Bioenerg Biomembr*, *28*(4), 351-358.
- Buffelli, M., Burgess, R. W., Feng, G., Lobe, C. G., Lichtman, J. W., & Sanes, J. R. (2003). Genetic evidence that relative synaptic efficacy biases the outcome of synaptic competition. *Nature*, *424*(6947), 430-434. doi:10.1038/nature01844
- Buldyrev, I., Puthussery, T., & Taylor, W. R. (2012). Synaptic pathways that shape the excitatory drive in an OFF retinal ganglion cell. *J Neurophysiol*, *107*(7), 1795-1807. doi:10.1152/jn.00924.2011
- Byzov, A. L., & Shura-Bura, T. M. (1986). Electrical feedback mechanism in the processing of signals in the outer plexiform layer of the retina. *Vision Res*, *26*(1), 33-44.
- Caldwell, J. H., & Daw, N. W. (1978). Effects of picrotoxin and strychnine on rabbit retinal ganglion cells: changes in centre surround receptive fields. *J Physiol*, *276*, 299-310.

- Caldwell, J. H., Daw, N. W., & Wyatt, H. J. (1978). Effects of picrotoxin and strychnine on rabbit retinal ganglion cells: lateral interactions for cells with more complex receptive fields. *J Physiol*, 276, 277-298.
- Canteras, N. S., Ribeiro-Barbosa, E. R., Goto, M., Cipolla-Neto, J., & Swanson, L. W. (2011). The retinohypothalamic tract: comparison of axonal projection patterns from four major targets. *Brain Res Rev*, 65(2), 150-183. doi:10.1016/j.brainresrev.2010.09.006
- Cascio, M. (2006). Modulating inhibitory ligand-gated ion channels. *AAPS J*, 8(2), E353-361. doi:10.1208/aapsj080240
- Chapot, C. A., Euler, T., & Schubert, T. (2017). How do horizontal cells 'talk' to cone photoreceptors? Different levels of complexity at the cone-horizontal cell synapse. *J Physiol*, 595(16), 5495-5506. doi:10.1113/JP274177
- Chen, X., Hsueh, H. A., Greenberg, K., & Werblin, F. S. (2010). Three forms of spatial temporal feedforward inhibition are common to different ganglion cell types in rabbit retina. *J Neurophysiol*, 103(5), 2618-2632. doi:10.1152/jn.01109.2009
- Chow, D. M., Zuchowski, K. A., & Fetcho, J. R. (2017). In Vivo Measurement of Glycine Receptor Turnover and Synaptic Size Reveals Differences between Functional Classes of Motoneurons in Zebrafish. *Curr Biol*, 27(8), 1173-1183. doi:10.1016/j.cub.2017.03.032
- David-Watine, B., Goblet, C., de Saint Jan, D., Fucile, S., Devignot, V., Bregestovski, P., & Korn, H. (1999). Cloning, expression and electrophysiological characterization of glycine receptor alpha subunit from zebrafish. *Neuroscience*, 90(1), 303-317.
- Demb, J. B., & Singer, J. H. (2012). Intrinsic properties and functional circuitry of the All amacrine cell. *Vis Neurosci*, 29(1), 51-60. doi:10.1017/S0952523811000368
- Dowling, J. E., & Ripps, H. (1973). Effect of magnesium on horizontal cell activity in the skate retina. *Nature*, 242(5393), 101-103.
- Dutertre, S., Drwal, M., Laube, B., & Betz, H. (2012). Probing the pharmacological properties of distinct subunit interfaces within heteromeric glycine receptors reveals a functional betabeta agonist-binding site. *J Neurochem*, 122(1), 38-47. doi:10.1111/j.1471-4159.2012.07755.x
- Eggers, E. D., & Lukasiewicz, P. D. (2006a). GABA(A), GABA(C) and glycine receptor-mediated inhibition differentially affects light-evoked signalling from mouse retinal rod bipolar cells. *J Physiol*, 572(Pt 1), 215-225. doi:10.1113/jphysiol.2005.103648
- Eggers, E. D., & Lukasiewicz, P. D. (2006b). Receptor and transmitter release properties set the time course of retinal inhibition. *J Neurosci*, 26(37), 9413-9425. doi:10.1523/JNEUROSCI.2591-06.2006
- Eggers, E. D., McCall, M. A., & Lukasiewicz, P. D. (2007). Presynaptic inhibition differentially shapes transmission in distinct circuits in the mouse retina. *J Physiol*, 582(Pt 2), 569-582. doi:10.1113/jphysiol.2007.131763
- Ellis, E. M., Gauvain, G., Sivyer, B., & Murphy, G. J. (2016). Shared and distinct retinal input to the mouse superior colliculus and dorsal lateral geniculate nucleus. *J Neurophysiol*, 116(2), 602-610. doi:10.1152/jn.00227.2016
- Euler, T., Haverkamp, S., Schubert, T., & Baden, T. (2014). Retinal bipolar cells: elementary building blocks of vision. *Nat Rev Neurosci*, 15(8), 507-519.
- Fahrenfort, I., Steijaert, M., Sjoerdsma, T., Vickers, E., Ripps, H., van Asselt, J., . . . Kamermans, M. (2009). Hemichannel-mediated and pH-based feedback from horizontal cells to cones in the vertebrate retina. *PLoS One*, 4(6), e6090. doi:10.1371/journal.pone.0006090
- Farrow, K., Teixeira, M., Szikra, T., Viney, T. J., Balint, K., Yonehara, K., & Roska, B. (2013). Ambient illumination toggles a neuronal circuit switch in the retina and

- visual perception at cone threshold. *Neuron*, 78(2), 325-338.
doi:10.1016/j.neuron.2013.02.014
- Ferguson, L. R., Dominguez, J. M., 2nd, Balaiya, S., Grover, S., & Chalam, K. V. (2013). Retinal Thickness Normative Data in Wild-Type Mice Using Customized Miniature SD-OCT. *PLoS One*, 8(6), e67265. doi:10.1371/journal.pone.0067265
- Franke, K., & Baden, T. (2017). General features of inhibition in the inner retina. *J Physiol*, 595(16), 5507-5515. doi:10.1113/JP273648
- Franke, K., Berens, P., Schubert, T., Bethge, M., Euler, T., & Baden, T. (2017). Inhibition decorrelates visual feature representations in the inner retina. *Nature*, 542(7642), 439-444. doi:10.1038/nature21394
- Gamlin, C. R., Yu, W. Q., Wong, R. O. L., & Hoon, M. (2018). Assembly and maintenance of GABAergic and Glycinergic circuits in the mammalian nervous system. *Neural Dev*, 13(1), 12. doi:10.1186/s13064-018-0109-6
- Ghosh, K. K., Bujan, S., Haverkamp, S., Feigenspan, A., & Wässle, H. (2004). Types of bipolar cells in the mouse retina. *J Comp Neurol*, 469(1), 70-82. doi:10.1002/cne.10985
- Gill, S. B., Veruki, M. L., & Hartveit, E. (2006). Functional properties of spontaneous IPSCs and glycine receptors in rod amacrine (AII) cells in the rat retina. *J Physiol*, 575(Pt 3), 739-759. doi:10.1113/jphysiol.2006.112839
- Greene, M. J., Kim, J. S., Seung, H. S., & EyeWriters. (2016). Analogous Convergence of Sustained and Transient Inputs in Parallel On and Off Pathways for Retinal Motion Computation. *Cell Rep*, 14(8), 1892-1900. doi:10.1016/j.celrep.2016.02.001
- Grieger, J. C., Soltys, S. M., & Samulski, R. J. (2016). Production of Recombinant Adeno-associated Virus Vectors Using Suspension HEK293 Cells and Continuous Harvest of Vector From the Culture Media for GMP FIX and FLT1 Clinical Vector. *Mol Ther*, 24(2), 287-297. doi:10.1038/mt.2015.187
- Grimes, W. N., Zhang, J., Graydon, C. W., Kachar, B., & Diamond, J. S. (2010). Retinal parallel processors: more than 100 independent microcircuits operate within a single interneuron. *Neuron*, 65(6), 873-885. doi:10.1016/j.neuron.2010.02.028
- Grudzinska, J., Schemm, R., Haeger, S., Nicke, A., Schmalzing, G., Betz, H., & Laube, B. (2005). The beta subunit determines the ligand binding properties of synaptic glycine receptors. *Neuron*, 45(5), 727-739. doi:10.1016/j.neuron.2005.01.028
- Hartveit, E. (1999). Reciprocal synaptic interactions between rod bipolar cells and amacrine cells in the rat retina. *J Neurophysiol*, 81(6), 2923-2936. doi:10.1152/jn.1999.81.6.2923
- Harvey, R. J., Schmieden, V., Von Holst, A., Laube, B., Rohrer, H., & Betz, H. (2000). Glycine receptors containing the alpha4 subunit in the embryonic sympathetic nervous system, spinal cord and male genital ridge. *Eur J Neurosci*, 12(3), 994-1001.
- Haverkamp, S. (1995). Glycine Receptor Diversity in the Mammalian Retina. In H. Kolb, E. Fernandez, & R. Nelson (Eds.), *Webvision: The Organization of the Retina and Visual System*. Salt Lake City (UT).
- Haverkamp, S., Müller, U., Harvey, K., Harvey, R. J., Betz, H., & Wässle, H. (2003). Diversity of glycine receptors in the mouse retina: localization of the alpha3 subunit. *J Comp Neurol*, 465(4), 524-539. doi:10.1002/cne.10852
- Haverkamp, S., Müller, U., Zeilhofer, H. U., Harvey, R. J., & Wässle, H. (2004). Diversity of glycine receptors in the mouse retina: localization of the alpha2 subunit. *J Comp Neurol*, 477(4), 399-411. doi:10.1002/cne.20267
- Hecht, S., Schlaer, S., & Pirenne, M. H. (1941). Energy at the Threshold of Vision. *Science*, 93(2425), 585-587. doi:10.1126/science.93.2425.585

- Heinze, L., Harvey, R. J., Haverkamp, S., & Wassle, H. (2007). Diversity of glycine receptors in the mouse retina: localization of the alpha4 subunit. *J Comp Neurol*, *500*(4), 693-707. doi:10.1002/cne.21201
- Helmstaedter, M., Briggman, K. L., Turaga, S. C., Jain, V., Seung, H. S., & Denk, W. (2013). Connectomic reconstruction of the inner plexiform layer in the mouse retina. *Nature*, *500*(7461), 168-174. doi:10.1038/nature12346
- Hippenmeyer, S., Vrieseling, E., Sigrist, M., Portmann, T., Laengle, C., Ladle, D. R., & Arber, S. (2005). A developmental switch in the response of DRG neurons to ETS transcription factor signaling. *PLoS Biol*, *3*(5), e159. doi:10.1371/journal.pbio.0030159
- Hruskova, B., Trojanova, J., Kulik, A., Kralikova, M., Pysanenko, K., Bures, Z., . . . Turecek, R. (2012). Differential distribution of glycine receptor subtypes at the rat calyx of Held synapse. *J Neurosci*, *32*(47), 17012-17024. doi:10.1523/JNEUROSCI.1547-12.2012
- Ivanova, E., Muller, U., & Wassle, H. (2006). Characterization of the glycinergic input to bipolar cells of the mouse retina. *Eur J Neurosci*, *23*(2), 350-364. doi:10.1111/j.1460-9568.2005.04557.x
- Jacoby, J., & Schwartz, G. W. (2017). Three Small-Receptive-Field Ganglion Cells in the Mouse Retina Are Distinctly Tuned to Size, Speed, and Object Motion. *J Neurosci*, *37*(3), 610-625. doi:10.1523/JNEUROSCI.2804-16.2016
- Kamermans, M., Fahrenfort, I., Schultz, K., Janssen-Bienhold, U., Sjoerdsma, T., & Weiler, R. (2001). Hemichannel-mediated inhibition in the outer retina. *Science*, *292*(5519), 1178-1180. doi:10.1126/science.1060101
- Kamermans, M., & Werblin, F. (1992). GABA-mediated positive autofeedback loop controls horizontal cell kinetics in tiger salamander retina. *J Neurosci*, *12*(7), 2451-2463.
- Kandel, E. R., Schwartz, J. H., & Jessell, T. M. (2000). *Principles of neural science* (4th ed.). New York: McGraw-Hill, Health Professions Division.
- Keros, S., & Hablitz, J. J. (2005). Subtype-specific GABA transporter antagonists synergistically modulate phasic and tonic GABA conductances in rat neocortex. *J Neurophysiol*, *94*(3), 2073-2085. doi:10.1152/jn.00520.2005
- Kim, I. J., Zhang, Y., Meister, M., & Sanes, J. R. (2010). Laminar restriction of retinal ganglion cell dendrites and axons: subtype-specific developmental patterns revealed with transgenic markers. *J Neurosci*, *30*(4), 1452-1462. doi:10.1523/JNEUROSCI.4779-09.2010
- Kim, I. J., Zhang, Y., Yamagata, M., Meister, M., & Sanes, J. R. (2008). Molecular identification of a retinal cell type that responds to upward motion. *Nature*, *452*(7186), 478-482. doi:10.1038/nature06739
- Kim, T., Soto, F., & Kerschensteiner, D. (2015). An excitatory amacrine cell detects object motion and provides feature-selective input to ganglion cells in the mouse retina. *Elife*, *4*. doi:10.7554/eLife.08025
- Krieger, B., Qiao, M., Rousso, D. L., Sanes, J. R., & Meister, M. (2017). Four alpha ganglion cell types in mouse retina: Function, structure, and molecular signatures. *PLoS One*, *12*(7), e0180091. doi:10.1371/journal.pone.0180091
- Kuhse, J., Laube, B., Magalei, D., & Betz, H. (1993). Assembly of the inhibitory glycine receptor: identification of amino acid sequence motifs governing subunit stoichiometry. *Neuron*, *11*(6), 1049-1056.
- Kuo, S. P., Schwartz, G. W., & Rieke, F. (2016). Nonlinear Spatiotemporal Integration by Electrical and Chemical Synapses in the Retina. *Neuron*, *90*(2), 320-332. doi:10.1016/j.neuron.2016.03.012

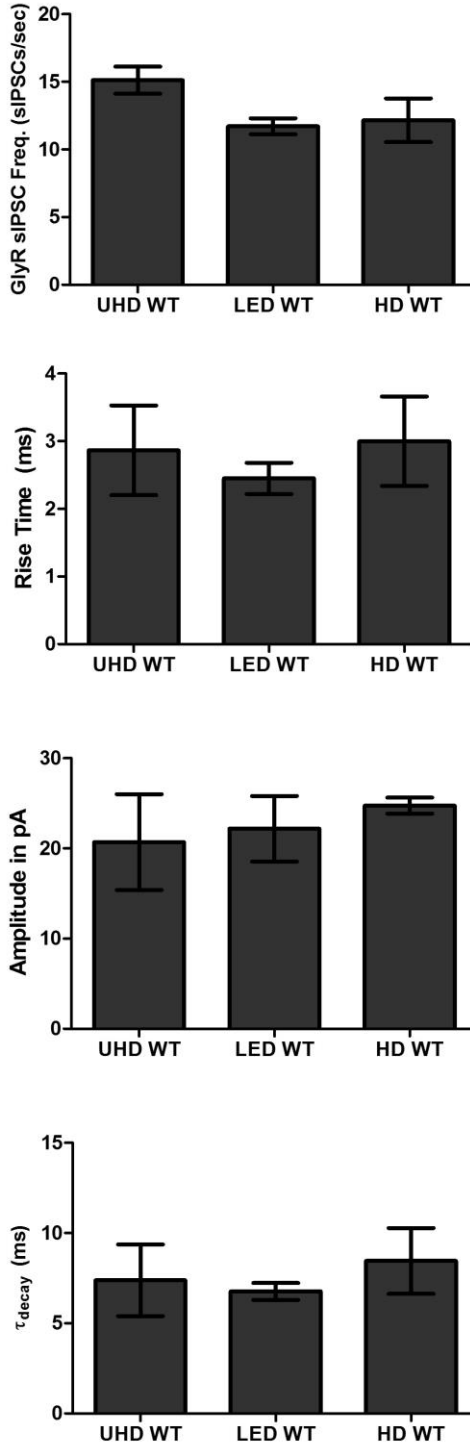
- Lamb, T. D. (2013). Evolution of phototransduction, vertebrate photoreceptors and retina. *Prog Retin Eye Res*, 36, 52-119. doi:10.1016/j.preteyeres.2013.06.001
- Leacock, S., Syed, P., James, V. M., Bode, A., Kawakami, K., Keramidas, A., . . . Harvey, R. J. (2018). Structure/Function Studies of the alpha4 Subunit Reveal Evolutionary Loss of a GlyR Subtype Involved in Startle and Escape Responses. *Front Mol Neurosci*, 11, 23. doi:10.3389/fnmol.2018.00023
- Lee, S., Chen, L., Chen, M., Ye, M., Seal, R. P., & Zhou, Z. J. (2014). An unconventional glutamatergic circuit in the retina formed by vGluT3 amacrine cells. *Neuron*, 84(4), 708-715. doi:10.1016/j.neuron.2014.10.021
- Lee, S. C., Meyer, A., Schubert, T., Huser, L., Dedek, K., & Haverkamp, S. (2015). Morphology and connectivity of the small bistratified A8 amacrine cell in the mouse retina. *J Comp Neurol*, 523(10), 1529-1547. doi:10.1002/cne.23752
- Legendre, P. (1999). Voltage dependence of the glycine receptor-channel kinetics in the zebrafish hindbrain. *J Neurophysiol*, 82(5), 2120-2129. doi:10.1152/jn.1999.82.5.2120
- Legendre, P. (2001). The glycinergic inhibitory synapse. *Cell Mol Life Sci*, 58(5-6), 760-793.
- Liu, J., & Sanes, J. R. (2017). Cellular and Molecular Analysis of Dendritic Morphogenesis in a Retinal Cell Type That Senses Color Contrast and Ventral Motion. *J Neurosci*, 37(50), 12247-12262. doi:10.1523/JNEUROSCI.2098-17.2017
- Lynch, J. W. (2004). Molecular structure and function of the glycine receptor chloride channel. *Physiol Rev*, 84(4), 1051-1095. doi:10.1152/physrev.00042.2003
- Lynch, J. W. (2009). Native glycine receptor subtypes and their physiological roles. *Neuropharmacology*, 56(1), 303-309. doi:10.1016/j.neuropharm.2008.07.034
- MacNeil, M. A., & Masland, R. H. (1998). Extreme diversity among amacrine cells: implications for function. *Neuron*, 20(5), 971-982.
- Majumdar, S., Heinze, L., Haverkamp, S., Ivanova, E., & Wässle, H. (2007). Glycine receptors of A-type ganglion cells of the mouse retina. *Vis Neurosci*, 24(4), 471-487. doi:10.1017/S0952523807070174
- Majumdar, S., Weiss, J., & Wässle, H. (2009). Glycinergic input of widefield, displaced amacrine cells of the mouse retina. *J Physiol*, 587(Pt 15), 3831-3849. doi:10.1113/jphysiol.2009.171207
- Maksay, G. (1996). From kinetics and thermodynamics of GABAA receptor binding to ionophore function. *Neurochem Int*, 29(4), 361-370.
- Manookin, M. B., Beaudoin, D. L., Ernst, Z. R., Flagel, L. J., & Demb, J. B. (2008). Disinhibition combines with excitation to extend the operating range of the OFF visual pathway in daylight. *J Neurosci*, 28(16), 4136-4150. doi:10.1523/JNEUROSCI.4274-07.2008
- Manzke, T., Niebert, M., Koch, U. R., Caley, A., Vogelgesang, S., Hulsmann, S., . . . Richter, D. W. (2010). Serotonin receptor 1A-modulated phosphorylation of glycine receptor alpha3 controls breathing in mice. *J Clin Invest*, 120(11), 4118-4128. doi:10.1172/JCI43029
- Masland, R. H. (2001). Neuronal diversity in the retina. *Curr Opin Neurobiol*, 11(4), 431-436.
- Masland, R. H. (2012). The neuronal organization of the retina. *Neuron*, 76(2), 266-280. doi:10.1016/j.neuron.2012.10.002
- Matzenbach, B., Maulet, Y., Sefton, L., Courtier, B., Avner, P., Guenet, J. L., & Betz, H. (1994). Structural analysis of mouse glycine receptor alpha subunit genes. Identification and chromosomal localization of a novel variant. *J Biol Chem*, 269(4), 2607-2612.

- McClements, M. E., & MacLaren, R. E. (2013). Gene therapy for retinal disease. *Transl Res*, 161(4), 241-254. doi:10.1016/j.trsl.2012.12.007
- Menger, N., Pow, D. V., & Wassle, H. (1998). Glycinergic amacrine cells of the rat retina. *J Comp Neurol*, 401(1), 34-46.
- Miller, P. S., Harvey, R. J., & Smart, T. G. (2004). Differential agonist sensitivity of glycine receptor alpha2 subunit splice variants. *Br J Pharmacol*, 143(1), 19-26. doi:10.1038/sj.bjp.0705875
- Moore-Dotson, J. M., Klein, J. S., Mazade, R. E., & Eggers, E. D. (2015). Different types of retinal inhibition have distinct neurotransmitter release properties. *J Neurophysiol*, 113(7), 2078-2090. doi:10.1152/jn.00447.2014
- Moore, L. A., & Trussell, L. O. (2017). Corelease of Inhibitory Neurotransmitters in the Mouse Auditory Midbrain. *J Neurosci*, 37(39), 9453-9464. doi:10.1523/JNEUROSCI.1125-17.2017
- Morgans, C. W. (2000). Neurotransmitter release at ribbon synapses in the retina. *Immunol Cell Biol*, 78(4), 442-446. doi:10.1046/j.1440-1711.2000.00923.x
- Murphy, G. J., & Rieke, F. (2006). Network variability limits stimulus-evoked spike timing precision in retinal ganglion cells. *Neuron*, 52(3), 511-524. doi:10.1016/j.neuron.2006.09.014
- Nobles, R. D., Zhang, C., Muller, U., Betz, H., & McCall, M. A. (2012). Selective glycine receptor alpha2 subunit control of crossover inhibition between the on and off retinal pathways. *J Neurosci*, 32(10), 3321-3332. doi:10.1523/JNEUROSCI.5341-11.2012
- O'Brien, B. J., Richardson, R. C., & Berson, D. M. (2003). Inhibitory network properties shaping the light evoked responses of cat alpha retinal ganglion cells. *Vis Neurosci*, 20(4), 351-361.
- Oertel, J., Villmann, C., Kettenmann, H., Kirchhoff, F., & Becker, C. M. (2007). A novel glycine receptor beta subunit splice variant predicts an unorthodox transmembrane topology. Assembly into heteromeric receptor complexes. *J Biol Chem*, 282(5), 2798-2807. doi:10.1074/jbc.M608941200
- Pang, J. J., Yang, Z., Jacoby, R. A., & Wu, S. M. (2018). Cone synapses in mammalian retinal rod bipolar cells. *J Comp Neurol*, 526(12), 1896-1909. doi:10.1002/cne.24456
- Park, S. J. H., Pottackal, J., Ke, J. B., Jun, N. Y., Rahmani, P., Kim, I. J., . . . Demb, J. B. (2018). Convergence and Divergence of CRH Amacrine Cells in Mouse Retinal Circuitry. *J Neurosci*, 38(15), 3753-3766. doi:10.1523/JNEUROSCI.2518-17.2018
- Paxinos, G., & Franklin, K. B. J. (2004). *The mouse brain in stereotaxic coordinates* (Compact 2nd ed.). Amsterdam ; Boston: Elsevier Academic Press.
- Pow, D. V., & Hendrickson, A. E. (1999). Distribution of the glycine transporter glyt-1 in mammalian and nonmammalian retinae. *Vis Neurosci*, 16(2), 231-239.
- Reid, C. A., & Lipinski, D. M. (2018). Small and Micro-Scale Recombinant Adeno-Associated Virus Production and Purification for Ocular Gene Therapy Applications. *Methods Mol Biol*, 1715, 19-31. doi:10.1007/978-1-4939-7522-8_2
- Rivlin-Etzion, M., Wei, W., & Feller, M. B. (2012). Visual stimulation reverses the directional preference of direction-selective retinal ganglion cells. *Neuron*, 76(3), 518-525. doi:10.1016/j.neuron.2012.08.041
- Rivlin-Etzion, M., Zhou, K., Wei, W., Elstrott, J., Nguyen, P. L., Barres, B. A., . . . Feller, M. B. (2011). Transgenic mice reveal unexpected diversity of on-off direction-selective retinal ganglion cell subtypes and brain structures involved in motion processing. *J Neurosci*, 31(24), 8760-8769. doi:10.1523/JNEUROSCI.0564-11.2011

- Rockhill, R. L., Daly, F. J., MacNeil, M. A., Brown, S. P., & Masland, R. H. (2002). The diversity of ganglion cells in a mammalian retina. *J Neurosci*, *22*(9), 3831-3843. doi:20026369
- Rossi, J., Balthasar, N., Olson, D., Scott, M., Berglund, E., Lee, C. E., . . . Elmquist, J. K. (2011). Melanocortin-4 receptors expressed by cholinergic neurons regulate energy balance and glucose homeostasis. *Cell Metab*, *13*(2), 195-204. doi:10.1016/j.cmet.2011.01.010
- Rouso, D. L., Qiao, M., Kagan, R. D., Yamagata, M., Palmiter, R. D., & Sanes, J. R. (2016). Two Pairs of ON and OFF Retinal Ganglion Cells Are Defined by Intersectional Patterns of Transcription Factor Expression. *Cell Rep*, *15*(9), 1930-1944. doi:10.1016/j.celrep.2016.04.069
- Russell, T. L., & Werblin, F. S. (2010). Retinal synaptic pathways underlying the response of the rabbit local edge detector. *J Neurophysiol*, *103*(5), 2757-2769. doi:10.1152/jn.00987.2009
- Sanes, J. R., & Masland, R. H. (2015). The types of retinal ganglion cells: current status and implications for neuronal classification. *Annu Rev Neurosci*, *38*, 221-246. doi:10.1146/annurev-neuro-071714-034120
- Sassoe-Pognetto, M., Wassle, H., & Grunert, U. (1994). Glycinergic synapses in the rod pathway of the rat retina: cone bipolar cells express the alpha 1 subunit of the glycine receptor. *J Neurosci*, *14*(8), 5131-5146.
- Singer, J. H., & Berger, A. J. (1999). Contribution of single-channel properties to the time course and amplitude variance of quantal glycine currents recorded in rat motoneurons. *J Neurophysiol*, *81*(4), 1608-1616. doi:10.1152/jn.1999.81.4.1608
- Smith, S. M., Chen, W., Vyleta, N. P., Williams, C., Lee, C. H., Phillips, C., & Andresen, M. C. (2012). Calcium regulation of spontaneous and asynchronous neurotransmitter release. *Cell Calcium*, *52*(3-4), 226-233. doi:10.1016/j.ceca.2012.06.001
- Sun, W., Li, N., & He, S. (2002). Large-scale morphological survey of mouse retinal ganglion cells. *J Comp Neurol*, *451*(2), 115-126. doi:10.1002/cne.10323
- Suryanarayanan, A., & Slaughter, M. M. (2006). Synaptic transmission mediated by internal calcium stores in rod photoreceptors. *J Neurosci*, *26*(6), 1759-1766. doi:10.1523/JNEUROSCI.3895-05.2006
- Tinsley, J. N., Molodtsov, M. I., Prevedel, R., Wartmann, D., Espigule-Pons, J., Lauwers, M., & Vaziri, A. (2016). Direct detection of a single photon by humans. *Nat Commun*, *7*, 12172. doi:10.1038/ncomms12172
- Trifonov, I. U. (1968). [Study of synaptic transmission between photoreceptor and horizontal cell by electric stimulations of the retina]. *Biofizika*, *13*(5), 809-817.
- van Wyk, M., Wassle, H., & Taylor, W. R. (2009). Receptive field properties of ON- and OFF-ganglion cells in the mouse retina. *Vis Neurosci*, *26*(3), 297-308. doi:10.1017/S0952523809990137
- Veruki, M. L., Gill, S. B., & Hartveit, E. (2007). Spontaneous IPSCs and glycine receptors with slow kinetics in wide-field amacrine cells in the mature rat retina. *J Physiol*, *581*(Pt 1), 203-219. doi:10.1113/jphysiol.2006.127316
- Wassle, H., Heinze, L., Ivanova, E., Majumdar, S., Weiss, J., Harvey, R. J., & Haverkamp, S. (2009). Glycinergic transmission in the Mammalian retina. *Front Mol Neurosci*, *2*, 6. doi:10.3389/neuro.02.006.2009
- Wei, W., & Feller, M. B. (2011). Organization and development of direction-selective circuits in the retina. *Trends Neurosci*, *34*(12), 638-645. doi:10.1016/j.tins.2011.08.002

- Wei, W., Hamby, A. M., Zhou, K., & Feller, M. B. (2011). Development of asymmetric inhibition underlying direction selectivity in the retina. *Nature*, *469*(7330), 402-406. doi:10.1038/nature09600
- Weiss, J., O'Sullivan, G. A., Heinze, L., Chen, H. X., Betz, H., & Wässle, H. (2008). Glycinergic input of small-field amacrine cells in the retinas of wildtype and glycine receptor deficient mice. *Mol Cell Neurosci*, *37*(1), 40-55. doi:10.1016/j.mcn.2007.08.012
- Werblin, F. S. (2010). Six different roles for crossover inhibition in the retina: correcting the nonlinearities of synaptic transmission. *Vis Neurosci*, *27*(1-2), 1-8. doi:10.1017/S0952523810000076
- Werblin, F. S. (2011). The retinal hypercircuit: a repeating synaptic interactive motif underlying visual function. *J Physiol*, *589*(Pt 15), 3691-3702. doi:10.1113/jphysiol.2011.210617
- Xie, R., & Manis, P. B. (2013). Target-specific IPSC kinetics promote temporal processing in auditory parallel pathways. *J Neurosci*, *33*(4), 1598-1614. doi:10.1523/JNEUROSCI.2541-12.2013
- Yamada, E. (1969). Some structural features of the fovea centralis in the human retina. *Arch Ophthalmol*, *82*(2), 151-159.
- Yang, X. L. (2004). Characterization of receptors for glutamate and GABA in retinal neurons. *Prog Neurobiol*, *73*(2), 127-150. doi:10.1016/j.pneurobio.2004.04.002
- Zhang, C. (2015). *Glycine Receptor Alpha Subunit (GlyR α) Specific Inhibition Contributes to Ganglion Cell Signaling in Mouse Retina*. (Ph.D. Dissertation), University of Louisville.
- Zhang, C., & McCall, M. A. (2012). Receptor targets of amacrine cells. *Vis Neurosci*, *29*(1), 11-29. doi:10.1017/S0952523812000028
- Zhang, C., Nobles, R. D., & McCall, M. A. (2015). GlyR α 2, not GlyR α 3, Modulates the Receptive Field Surround of OFF Retinal Ganglion Cells. *Vis Neurosci*. doi:10.1017/S0952523815000280
- Zhang, C., Rompani, S. B., Roska, B., & McCall, M. A. (2014). Adeno-associated virus-RNAi of GlyR α 1 and characterization of its synapse-specific inhibition in OFF alpha transient retinal ganglion cells. *J Neurophysiol*, *112*(12), 3125-3137. doi:10.1152/jn.00505.2014
- Zhang, Y., Dixon, C. L., Keramidas, A., & Lynch, J. W. (2015). Functional reconstitution of glycinergic synapses incorporating defined glycine receptor subunit combinations. *Neuropharmacology*, *89*, 391-397. doi:10.1016/j.neuropharm.2014.10.026

Supplemental Figure 1



Supplemental Figure 1. No difference observed among W3 RGC sIPSC characteristics

CURRICULUM VITAE

NAME: Ian Scot Pyle

ADDRESS: Kentucky Lion's Eye Center
University of Louisville School of Medicine
301 E. Muhammad Ali Blvd
Louisville, KY 40202

DOB: Indianapolis, Indiana – April 5, 1986

EDUCATION & TRAINING:

B.A., History
Hanover College
2004-08

M.Sc., Oral Biology
University of Louisville
2011-13

M.Sc., Anatomical Sciences and Neurobiology
University of Louisville
2013-2016

AWARDS: Dissertation Completion Award (2018)

The University of Louisville Graduate Student Council Travel Award
(2017)

The Association for Research in Vision and Ophthalmology (ARVO)
National Eye Institute Travel Grant Award (2017)

Sigma Xi Grants-in-Aid of Research (2015)

Integrated Programs in Biomedical Sciences Fellowship, University
of Louisville School of Medicine (August 2013 – August 2015)

PUBLICATIONS:

Fransen, J.W.; Pangeni, G.; **Pyle, I.S.**; McCall, M.A. "Functional changes in Tg P23H-1 rat retinal responses: differences between ON and OFF pathway transmission to the superior colliculus." (2015) J Neurophysiol: 114(4):2368-75

ABSTRACTS AND PRESENTATIONS:

Ian Pyle, Anne Carenbauer, S.G. Venkatesh, Douglas Darling.

"Molecular Mechanism of Regulated Exocrine Secretion"
Research!Louisville, October 2012. Louisville, KY

G. Pangeni, A. A. Thomas, **I. Pyle**, G. McGrady, G. Howell, S.W. John, M.A. McCall

"Retinal Ganglion Cell Spontaneous and Visually-Evoked Responses in the DBA/2J Mouse Model of Glaucoma" FASEB Retinal Neurobiology and Visual Processing, June 22-27, 2014. Saxtons River, VT

Pangeni, Gobinda, Fransen, James W., **Pyle, Ian S.**, McCall, Maureen A.

"Slow Onset and Protracted Decline in Visual Function in the P23H Rhodopsin Knock-in Mouse Model of Retinitis Pigmentosa" The Association for Research in Vision and Ophthalmology (ARVO), May 3-7, 2015 Denver, CO

Pyle, Ian S., McCall, Maureen A.

"Glycine Receptor Expression in the Developing Mammalian Retina" Cold Spring Harbor Laboratory (CSHL) Vision: A Platform for Linking Circuits, Behavior & Perception, July 6-21, 2015. Huntington, NY

Pyle, Ian S.; Zhang, Chi; McCall, Maureen A.

"Distinct Glycine Receptor Subunit Composition Across Retinal Ganglion Cell Types" ARVO May 7-11, 2017. Baltimore, MD

Nazarul Hasan, Jennifer Noel, **Ian Scot Pyle**, Gobinda Pangeni, Kathryn M Heath, Bart Gerard Borghuis, Maureen A. McCall. Ronald G. Gregg. "A dual function for LRIT3 – control of retinal photoreceptor synaptic morphology and depolarizing bipolar cell signaling" ARVO May 7-11, 2017. Baltimore, MD

McCall, M.A., **Pyle, I.**, Zhang, C., Sahu B., Lipinsky, D. & Gregg, R.G.

"Differential expression of Glycine Receptor α Subunits Across Identified Retinal Ganglion Cells" FASEB June 24-29, 2018. Olean, NY

Pyle, Ian S.

“Lab Introduction & Different Ganglion Cells Express Different Types of Glycine Receptors.” UofL Visual Sciences Retreat (VSR) September 26, 2018. Louisville, KY

CONFERENCES AND CONTINUING EDUCATION:

Federation of American Societies for Experimental Biology (FASEB),
Retinal Neurobiology and Visual Processing, Saxton’s River, VT, 2014

Cold Spring Harbor Laboratory (CSHL) Vision: A Platform for Linking
Circuits, Behavior & Perception. Huntington, NY, July 6-21, 2015

The Association for Research in Vision and Ophthalmology (ARVO),
Baltimore, MD, 2017

TEACHING EXPERIENCE:

Neuroanatomy, University of Louisville School of Medicine, T.A. Spring
2015